Strategies Employed by Enzymes to Generate and Stabilize Radical Intermediates: An Examination of Adenosylcobalamin- and Pyridoxal 5'-Phosphate-dependent Ornithine 4,5-Aminomutase

by

Caitlyn Makins

B.Sc., The University of British Columbia, 2010

A THESIS SUBMITTED IN PARTIAL FULFILLMENT OF
THE REQUIREMENTS FOR THE DEGREE OF

DOCTOR OF PHILOSOPHY

in

THE COLLEGE OF GRADUATE STUDIES

(Biochemistry and Molecular Biology)

THE UNIVERSITY OF BRITISH COLUMBIA

(Okanagan)

July 2014

Abstract

Enzymes that employ radical-based chemistry are able to catalyze a diverse array of energetically and chemically challenging reactions. Notably, their ability to break C–C, C–N, and C–H bonds makes them appealing targets for the development of biocatalysts. The research herein aims to investigate the strategies employed by radical enzymes in the generation, stabilization, and propagation of radical intermediates. Using adenosylcobalamin- and pyridoxal 5'-phosphate-dependent ornithine 4,5-aminomutase (OAM) as a model system, we have made several advances toward this end.

In Chapter 2, a combination of deuterium kinetic isotope effect, site-directed mutagenesis, modeling, and EPR studies were used to highlight structural differences between OAM and its structural homologue lysine 5,6-aminomutase (5,6-LAM) that contribute to their different mechanistic behaviours. Based on the obtained results, we propose that weaker substrate binding in 5,6-LAM compared to OAM accounts for the more promiscuous nature of 5,6-LAM, as well as its increased tendency to undergo radical-mediated suicide inactivation.

In Chapter 3, mutagenesis of a conserved glutamate residue, which forms electrostatic contact with the adenosyl ribose moiety of adenosylcobalamin in OAM and methylmalonyl-CoA mutase only upon substrate binding, reveals the contribution of electrostatics to homolysis of the Co–C bond. Electrostatic stabilization of the adenosyl group by the conserved glutamate residue was found to account for approximately half of the $10^{12\pm1}$-fold rate enhancement for homolysis achieved by the adenosylcobalamin-dependent enzymes. This mechanism for radical generation is conserved amongst the class I mutases and class III aminomutases and acts to prevent the enzymes from spurious radical generation in the absence of substrate.

In Chapters 4 and 5, spectroscopic techniques in combination with deuterium kinetic isotope effect studies were used to show that specific active site residues modulate radical catalysis in ornithine 4,5-aminomutase through their interactions with the pyridoxal 5'-phosphate cofactor. In particular, proton donors and acceptors to the Schiff base and pyridine nitrogen of pyridoxal 5'-phosphate decrease the barrier to isomerization and stabilize radical intermediates such as the proposed azacyclopropylcarbinyl radical.

Preface

Some of the results presented in Chapter 2 have been published and some figures have been reproduced with permission: Makins, C., Miros, F.N., Scrutton, N.S., and Wolthers, K.R. (2011) Role of histidine 225 in adenosylcobalamin-dependent ornithine 4,5-aminomutase, *Bioorganic Chemistry 40*, 39–47. EPR samples were prepared by Caitlyn Makins and run by Dr. Charles J. Walsby at Simon Fraser University.

A version of Chapter 3 has been published and some of the figures have been reproduced with permission: Makins, C., Pickering, A.V., Mariani, C., and Wolthers, K.R. (2013) Mutagenesis of a Conserved Glutamate Reveals the Contribution of Electrostatic Energy to Adenosylcobalamin Co-C Bond Homolysis in Ornithine 4,5-Aminomutase and Methylmalonyl-CoA Mutase, *Biochemistry 52*, 878–888 (© 2013 American Chemical Society). Alex V. Pickering, an undergraduate researcher in the Wolthers group, conducted the fluorescence binding assays for methylmalonyl-CoA presented in section 3.9.

The work presented in Chapter 4, along with some of the results from Chapter 2, has been prepared as a manuscript to be submitted for publication. Makins, C., Whitelaw, D.A., Walsby, C.J., and Wolthers, K.R. (2014) Isotope Effects for Deuterium Transfer in Adenosylcobalamin-dependent Ornithine 4,5-aminomutase Provide Mechanistic Insight into the Role of Tyr187, *manuscript prepared for Biochemistry.* EPR samples were prepared by Caitlyn Makins and run by Dr. Charles J. Walsby at Simon Fraser University.

Some of the results presented in Chapter 5 have been published and some figures have been reproduced with permission: Makins, C., Miros, F.N., Scrutton, N.S., and Wolthers, K.R. (2011) Role of histidine 225 in adenosylcobalamin-dependent ornithine 4,5-aminomutase, *Bioorganic Chemistry 40*, 39–47.

Table of Contents

List of Tables

List of Figures

List of Abbreviations

$\Delta G^{\ddagger}$	Activation energy barrier
$\Delta\Delta G^{\ddagger}$	Change in activation energy barrier height
5,6-LAM	Lysine 5,6-aminomutase
3',4'-anAdoMet	S-3',4'-anhydroadenosyl-L-methionine
AdoCbl	Adenosylcobalamin
Ado•	5'-deoxyadenosyl radical
AdoH	5'-deoxyadenosine
CHES	N-cyclohexyl-2-aminoethanesulfonic acid
Da	Dalton
dH_2O	Deionized water
$^{D}k_{cat}$	Deuterium primary kinetic isotope effect on k_{cat}
$^{D}k_{cat}/K_m$	Deuterium primary kinetic isotope effect on k_{cat}/K_m
D-orn	D-ornithine
DL-orn	DL-ornithine
DL-orn-d_6	DL-ornithine-3,3,4,4,5,5-d_6
DABA	DL-2,4-diaminobutyric acid
DABA-d_5	D-2,4-diaminobutyric-2,3,3,4,4-d_5 acid
DAP	2,4-diaminopentanoic acid
DAPDH	2,4-diaminopentanoic acid dehydrogenase
DFT	Density Functional Theory
DMB	Dimethylbenzimidazole
EDTA	Ethylenediaminetetraacetic acid
EPPS	4-(2-hydroxyethyl)piperazine-1-propanesulfonic acid
EPR	Electron Paramagnetic Resonance
GM	Glutamate mutase
HEPES	4-(2-hydroxyethyl)-1-piperazine-N'-2-ethanesulfonic acid
IPTG	isopropyl-β-D-1-thiogalactopyranoside
KIE	Kinetic Isotope Effects
LB	Luria-Bertani Broth

LUMO	Lowest unoccupied molecular orbital
MCM	Methylmalonyl-CoA mutase
MES	2-morpholinoethanesulfonic acid
N-MePLP	N-methyl pyridoxal 5'-phosphate
NAD^+	β-nicotinamide adenine dinucleotide
Ni-NTA	Ni^{2+}-nitrilotriacetic acid
OAM	Ornithine 4,5-aminomutase
OR	Ornithine racemase
PCET	Proton-coupled electron transfer
PCR	Polymerase chain reaction
PDB	Protein Data Bank
PLP	Pyridoxal 5'-phosphate
PMSF	Phenylmethanesulfonylfluoride
RNR	Ribonucleotide reductase
SAM	S-adenosyl-L-methionine
SDS-PAGE	Sodium dodecyl sulfate polyacrylamide gel electrophoresis
TB	Terrific Broth
TIM	Triosephosphate isomerase
TRIS	2-amino-2-hydroxymethyl-propane-1,3-diol

Acknowledgements

I would like to thank my amazing and very organized (although she doesn't think so) supervisor, Dr. Kirsten R. Wolthers, for her guidance and support throughout the years. I could not have asked for a better supervisor. I would also like to extend a big thank you to Dr. David B. Jack, who has been a mentor to me since my third year of undergraduate studies. I thank the other members of my committee, Dr. James A. Bailey and Dr. W. Stephen McNeil, for their guidance and helpful discussions about experimental design and cobalamin chemistry. I am grateful to my friends Dr. Eric Dennis and Yann André for their assistance with organic synthesis. I would also like to thank Dr. Paul Shipley for his help with sample preparation and ^{1}H-NMR spectroscopy, and Dr. Charles J. Walsby for running my EPR samples. I owe a special thank you to my lab mate, Douglas Whitelaw, for his endless willingness to help me with my tediously long kinetic assays and anaerobic experiments in the glovebox. I extend my thanks to the Natural Sciences and Engineering Council of Canada for funding my research.

Finally I wish to thank my friends and family for all of their support. Mom, Ashley, and Matt, I could not have made it through this without you.

This thesis is dedicated

to

the three musketeers

Chapter 1 : Introduction

Asymmetric synthesis, or the production of enantiomerically pure compounds, is currently a rapidly growing field in chemistry. The products of asymmetric synthesis reactions, such as chiral amines, diamines, and α- and β-amino acids, are typically used as precursors for a number of target molecules including pharmaceuticals, agrochemicals, specialty chemicals and even biofuels.[1-3] The importance of having an enantiomerically pure product is demonstrated in the administration of chiral drug molecules. Biological processes are inherently stereoselective; therefore one enantiomer of a drug may be more active in the body, while the other is not only less active but potentially harmful. A number of drugs are currently administered as racemic mixtures with no serious side effects; however, low activity of one enantiomer in the mixture potentially increases the required dosage.[4, 5] Naproxen is a prime example of a drug that cannot be administered as a racemic mixture. The (S)-enantiomer of naproxen is about 30 times more active than the (R)-enantiomer, acting as a powerful painkiller. (R)-naproxen is not only less effective as a painkiller but is also highly toxic to the liver and its administration would be detrimental.[4] The two enantiomers clearly show different pharmacokinetic and pharmacodynamics properties within the body, highlighting the importance of chirality in the synthesis and administration of drugs. In this case, initial production of only the one enantiomer of interest, rather than trying to remove the unwanted (R)-enantiomer after the fact, would be ideal.

Asymmetric synthesis is inherently challenging given that bench-top reactions tend to produce racemic mixtures, as opposed to enantiomerically pure products. As such, synthetic chemists often employ complicated, multistep processes requiring harsh reaction conditions and the use of metallo- and organocatalysts, which must themselves be synthesized and are often toxic, in attempts to produce regioselective compounds enriched in one stereoisomer.[6] Given the large number of steps required for many of these reactions, both yields and chemical purity are often low and scaled-up versions of the reactions become rather inefficient, rendering them expensive, environmentally unfriendly and non-ideal for industrial applications. As an alternative to the use of metallo- and organocatalysts, a recent trend in asymmetric synthesis is the development and use of enzymes, known as biocatalysts, to carry out these types of reactions. Advanced DNA technologies and bioinformatics tools,

along with an increasing number of available protein structures, have allowed researchers to employ techniques such as directed evolution, computer modeling, and rational design to selectively engineer and modify naturally occurring enzymes to accept different substrates and produce desired compounds, rather than their natural products.[7] For example, a rhodium-catalyzed asymmetric enamine hydrogenation reaction, used to produce the antidiabetic compound sitagliptin, was recently replaced with a more efficient biocatalytic process involving a pyridoxal 5'-phosphate-dependent transaminase.[8] Given that most enzymes have a high substrate specificity, operate under mild physiological conditions, carry out reactions that are already both regio- and stereoselective, and generally exhibit a high turnover rate, it is not surprising that biocatalysts are gaining the attention of synthetic chemists.

Developing enzymes as biocatalysts is not without its challenges. As mentioned previously, enzymes usually display high specificity, accepting only a narrow range of substrates.[9] A good biocatalyst, however, would be able to accept a number of different substrates, maintain high activity, retain regio- and stereoselectivity for each substrate, and itself remain stable under a variety of experimental conditions. As such, a certain amount of active site manipulation and tailoring, involving more than one mutation, is often necessary in order to meet these criteria. This requires a detailed knowledge of both the structure and mechanism of action of the selected enzyme, including which residues are involved in substrate binding, as well as others that are absolutely necessary for catalysis to occur. Once these factors are known, researchers can begin to determine whether an enzyme or a particular class of enzymes is worth pursuing for the biocatalytic synthesis of a specific product.

Enzymes that employ radical-based mechanisms are able to catalyze a diverse range of chemically and energetically challenging reactions involving cleavage of C–C, C–N, and C–H bonds, which makes them particularly appealing targets for their development as biocatalysts. With advances in radical detection methods, such as time-resolved EPR, and the use of bioinformatics tools, the number of enzymes shown or hypothesized to employ radical-based mechanisms has increased dramatically in recent years. Based on the presence of a conserved CxxxCxxC motif, it is currently estimated that there are more than 2800 radical S-adenosyl-L-methionine-dependent enzymes, only a handful of which have thus far been isolated and characterized.[10, 11] In order to develop these enzymes as biocatalysts, an

understanding of how these enzymes generate, stabilize, and control the trajectory of their radical intermediates is of fundamental importance.

The research herein aims to expand on our knowledge of the strategies employed by radical enzymes in the generation and stabilization of high-energy radical intermediates. The thesis focuses on ornithine 4,5-aminomutase (OAM), an adenosylcobalamin- and pyridoxal 5'-phosphate (PLP)-dependent radical enzyme. As such, the following introductory chapter will discuss in detail the class of adenosylcobalamin-dependent isomerases, which includes OAM, as well as the role of the PLP cofactor in traditional PLP-dependent enzymes and its unique role in the aminomutases. A brief overview of radical enzymes in general is also provided.

1.1 Radical Enzymes

1.1.1 The History of Radical Enzymes

The first protein-based radical was discovered in the enzyme ribonucleotide reductase (RNR) isolated from *Eschericia coli* in 1973.[12, 13] RNR participates in DNA synthesis by converting ribonucleoside diphosphates into deoxyribonucleotides through reduction of the 2'-hydroxyl group (Figure 1.1).[12, 14] The active form of ribonucleotide reductase is an $\alpha_2\beta_2$ heterodimer comprising two loosely associated subunits, referred to as proteins R1 and R2.[15] Protein R1 binds the ribonucleoside diphosphate substrates, however it is unable to reduce the substrates in the absence of protein R2.[12, 14] The crystal structure of protein R2 (a homodimer) revealed a diiron center coordinated within a four-helix bundle in each monomer.[16] Surprisingly, EPR spectroscopy revealed a signal characteristic of an organic free radical rather than a metallo-paramagnetic species. The organic radical signal was, however, found to be dependent on the presence of iron within the protein, suggesting that the metal center was involved in generation of the radical species.[12, 14] Isotopic substitution[17, 18] and site-directed mutagenesis[19] experiments discovered that the stable radical was located on a tyrosine residue (Tyr122), which is about 5.3 Å away from the diiron center and therefore does not directly coordinate to the iron atoms.[15] The precise

mechanism by which the tyrosyl radical is generated is still unclear but is thought to involve molecular oxygen, which coordinates to the diiron center.

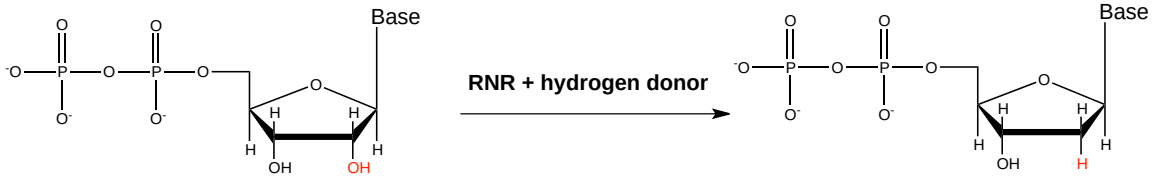

Figure 1.1 Reduction of ribonucleoside diphosphates to deoxyribonucleotides by ribonucleotide reductase. The 2'-hydroxyl (left, red) is reduced through a mechanism initiated by a transient thiyl radical (Cys439).

The tyrosyl radical from protein R2 is essential to catalysis in RNR as reduction of tyrosyl 122 leads to inactivation of the enzyme.[20] The crystal structure of protein R2 shows that Tyr122 is buried within the protein approximately 10 Å from the surface, and in fact a model of protein R2 in association with protein R1 indicates that the tyrosyl radical exists approximately 35 Å away from the actual active site.[15, 21] Thus, a specific pathway must be involved in transferring the radical from Tyr122 in protein R2 over to the active site in protein R1. This is quite an amazing feat given that radicals are highly reactive species and must therefore be tightly controlled in order to avoid spurious side reactions.

Elucidation of the proposed radical transfer pathway in RNR is complicated by the fact that a crystal structure for the associated R1 and R2 subunits is unavailable. Sequence alignment of RNRs from different species shows that several highly conserved residues, which could be involved in the pathway, exist in both proteins R1 and R2.[21, 22] These residues include W48, D84, H118, Y122, D237, Y356, C439, Y730, and Y731.[22] The exact pathway for radical propagation through R2 to R1 is still under investigation but the mechanism is thought to involve long-range proton-coupled electron transfer (PCET).[23] Once the radical reaches the R1 subunit, it is believed that a transient thiyl radical (Cys439) abstracts a hydrogen atom from C-3' of the ribonucleoside diphosphate substrate thereby initiating the reductive mechanism.[23, 24]

Since the initial discovery and characterization of the stable tyrosyl radical (Y122•) in RNR, a number of other enzymes have been shown to utilize both transient and stable

protein-derived radicals in their catalytic mechanisms. In 1989, EPR studies of pyruvate formate lyase from *E. coli*, which participates in the anaerobic degradation pathway of glucose by converting pyruvate to formate, showed the presence of a stable glycyl radical.[25] Around the same time it was discovered that when *E. coli* cells were grown under anaerobic conditions they expressed an RNR enzyme that was distinct from the RNR previously isolated under aerobic conditions. In fact, while the aerobic RNR required oxygen for catalytic activity, the anaerobically expressed RNR was inactivated by its presence.[26, 27] Moreover, anaerobic RNR was found to be dependent on the same activation factors as pyruvate formate lyase, which subsequently lead to the detection of a glycyl radical, rather than a tyrosyl radical, in the enzyme.[28-30] A third class of RNR, which catalyzes adenosylcobalamin (AdoCbl)-dependent nucleotide reduction, was also isolated from *Lactobacillus leichmannii*. The EPR spectrum of this enzyme revealed an organic radical that was coupled to the central cobalt ion (Co^{2+}) of the cobalamin cofactor.[31] Similarities in the mechanisms of nucleotide reduction catalyzed by the aerobic RNR from *E. coli* and the RNR from *L. leichmannii*, along with mutagenesis studies, indicated that the organic radical was likely a stable thiyl radical.[32] Indeed, deuteration of a specific cysteine residue (C408) within the active site resulted in perturbations to the EPR spectrum, which confirmed that the organic radical interacting with the cobalt nucleus was a thiyl radical originating from Cys408.[31] Thus, the participation of protein-derived radicals in the catalytic mechanisms of several enzymes was firmly established within a few years.

1.1.2 Strategies for Radical Generation

With the identification of multiple protein-derived radicals, it has become apparent that radical enzymes employ several different strategies for generating the initial radical species. The tyrosyl radical of aerobic RNR is generated through an oxygen-dependent mechanism involving the diferric center.[12-14] The tyrosyl radical found in galactose oxidase, an enzyme that oxidizes primary alcohols to aldehydes, is generated following donation of an electron to a copper ion to which the tyrosine residue is coordinated.[33, 34] The class Ib RNRs utilize a dimanganese (rather than diferric) center to generate a tyrosyl radical.[35] Based on these and numerous other examples, the requirement of a metal cofactor, such as Fe, Cu, Co,

or Mn, for the generation of transient and stable radicals is a common theme amongst the known radical enzymes.

Interestingly, no metal center was found in pyruvate formate lyase or anaerobic RNR. Instead, generation of the stable glycyl radical in both enzymes was found to be dependent on an interaction with a specific activating enzyme.[36] These activating enzymes were, however, found to be dependent on the presence of an iron-sulfur center and S-adenosyl-L-methionine (SAM), thereby suggesting that in addition to the metal center SAM was also somehow involved in radical generation.[27, 28, 36, 37] In each case, formation of the protein-based radical by the activating enzyme occurred with concomitant irreversible cleavage of SAM into 5'-deoxyadenosine and methionine.[36] It was postulated that a 5'-deoxyadenosyl radical, generated by interaction between SAM and the iron-sulfur cluster within the activating enzyme, was responsible for generating the protein-based radical through hydrogen atom abstraction.[38, 39] Evidence for the existence of this putative high-energy radical intermediate was provided by EPR studies of the SAM-dependent enzyme lysine 2,3-aminomutase, in which SAM was replaced by the coenzyme analogue S-3',4'-anhydroadenosyl-L-methionine (3',4'-anAdoMet).[40, 41] While the 5'-deoxyadenosyl radical is too unstable to be observed spectroscopically, the structure of 3',4'-anAdoMet (Figure 1.2) allowed for formation of a more stable allylic radical, which was detectable by EPR spectroscopy. In addition to observation of the allylic radical, substitution of the glycine residue in PFL with deuterium labeled glycine resulted in deuteration of the methyl group of 5'-deoxyadenosine, indicating that the 5'-deoxyadenosyl moiety was involved in hydrogen abstraction.[38]

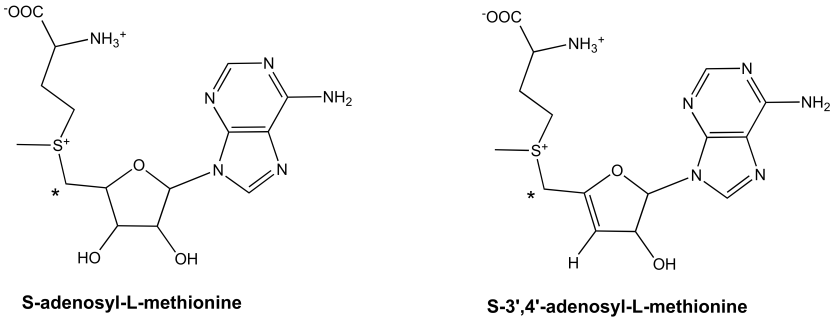

Figure 1.2 Structure of S-adenosyl-L-methionine and the analogue S-3',4'-adenosyl-L-methionine. Donation of an electron from a [4Fe-4S] cluster to the sulfonium ion results in homolytic cleavage of the C5'–S bond to produce the 5'-deoxyadenosyl radical. Use of the S-3',4'-adenosyl-L-methionine analogue results in formation of an allylic radical, which is sufficiently stable to be detected spectroscopically.

As mentioned previously, the radical SAM-dependent enzymes share a conserved CxxxCxxC motif and are also dependent on the presence of an iron-sulfur cluster for activity.[10, 11] Spectroscopic techniques, including EPR, Raman, and Mössbauer spectroscopy, as well as the crystal structures of several SAM-dependent enzymes, have indicated that the iron-sulfur cluster exists in a $[4Fe\text{-}4S]^{2+}$ or $[4Fe\text{-}4S]^{+}$ form, and that three of the irons are coordinated to the three cysteine residues of the conserved motif (Figure 1.3).[42-44] The fourth unique iron site becomes coordinated to the carboxylate and amino groups of the SAM cofactor.[43] The current proposed mechanism is that the $[4Fe\text{-}4S]^{+}$ cluster donates an electron to the sulfonium ion, which reduces the strength of the C–S bond of SAM allowing it to undergo homolytic cleavage to form the 5'-deoxyadenosyl radical.

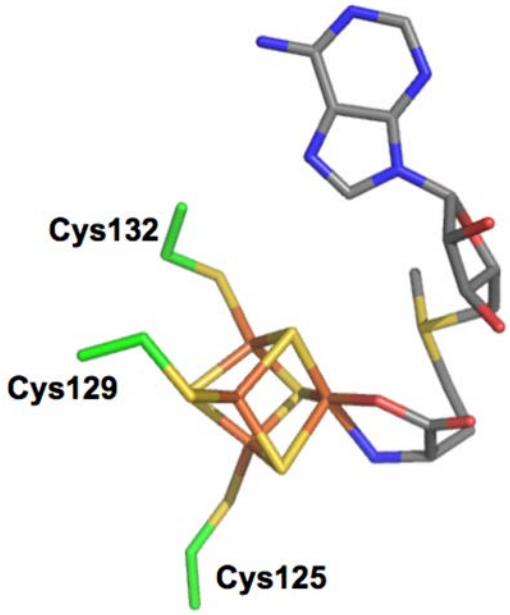

Figure 1.3 Active site of lysine 2,3-aminomutase showing S-adenosyl-L-methionine coordinated to the [4Fe-4S] cluster (PDB entry 2A5H). Upon substrate binding, $[4Fe\text{-}4S]^{+}$ donates an electron to the sulfonium ion, resulting in homolytic cleavage of the C–S bond to generate the 5'-deoxyadenosyl radical.

As detailed in the following section, the adenosyl radical, generated by reductive cleavage of the SAM cofactor, is generated through a distinct mechanism in the coenzyme B_{12}-dependent isomerases.

1.2 Coenzyme B_{12}-dependent Isomerases

1.2.1 Subclasses of Coenzyme B_{12}-dependent isomerases

The complexity of the adenosylcobalamin (AdoCbl) or coenzyme B_{12}-dependent isomerases has intrigued researchers since the elucidation of the vitamin B_{12} (cyanocobalamin) crystal structure in 1956.[45, 46] This crystal structure showed for the first time the presence of a carbon-metal bond, something that was not previously thought to exist. The AdoCbl-dependent isomerases make up the largest subfamily of B_{12}-dependent enzymes and are found almost exclusively in bacteria where they play a role in preparing substrates for subsequent breakdown in various fermentation pathways.[47] An exception is methylmalonyl-CoA mutase (MCM), which is found in both bacteria and mammals. In mammals, MCM plays a critical role in the catabolism of branched-chain amino acids, cholesterol, and odd-chain fatty acids into succinyl-CoA, which can then enter the citric acid cycle for ATP production.[48, 49] The characteristic isomerization reaction catalyzed by these enzymes is a 1,2-rearrangement whereby a hydrogen atom and a variable substituent, X, are interchanged between adjacent carbon atoms (Figure 1.4). Depending on the specific enzyme, X can be an –OH, $–NH_2$, or a carbon-containing fragment.[46, 47, 50]

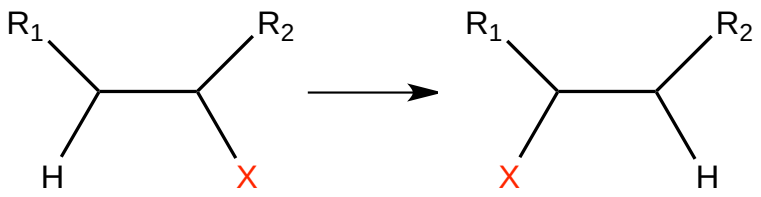

Figure 1.4 Characteristic isomerization reaction catalyzed by AdoCbl-dependent isomerases. A hydrogen atom and a variable substituent, X, are interchanged between vicinal carbon atoms of the substrate. The variable substituent is an –OH, $–NH_2$, or a carbon-containing fragment.

Although sharing very little sequence homology, the AdoCbl-dependent isomerases share core structural motifs. Each enzyme consists of a Rossmann-like domain, which houses the AdoCbl cofactor, and an $(\alpha/\beta)_8$ triosephosphate isomerase (TIM) barrel domain, which binds the incoming substrate (Figure 1.5). Based on the mode of cofactor binding, the identity of the migrating group, and whether any additional cofactors are required, the AdoCbl-dependent isomerases have been divided into three subclasses: the class I mutases, the class II eliminases, and the class III aminomutases. The class I mutases, such as MCM and glutamate mutase (GM), catalyze reversible carbon skeleton rearrangements.[51, 52] The class II eliminases, such as diol dehydratase (DD) and ethanolamine ammonia lyase (EAL), catalyze a 1,2-rearrangement involving the migration of an –OH or $–NH_2$ group, rather than a carbon-containing fragment. In class II eliminases, the rearrangements are followed by the irreversible formation of an aldehyde and elimination of either H_2O or NH_3. Moreover, an additional potassium ion cofactor is required for the rearrangement to occur.[53] Ornithine 4,5-aminomutase (OAM) and lysine 5,6-aminomutase (5,6-LAM) are currently the only known enzymes belonging to the third subclass of AdoCbl-dependent isomerases, which requires the presence of an additional cofactor, pyridoxal 5'-phosphate (PLP), to carry out a 1,2-amino shift.

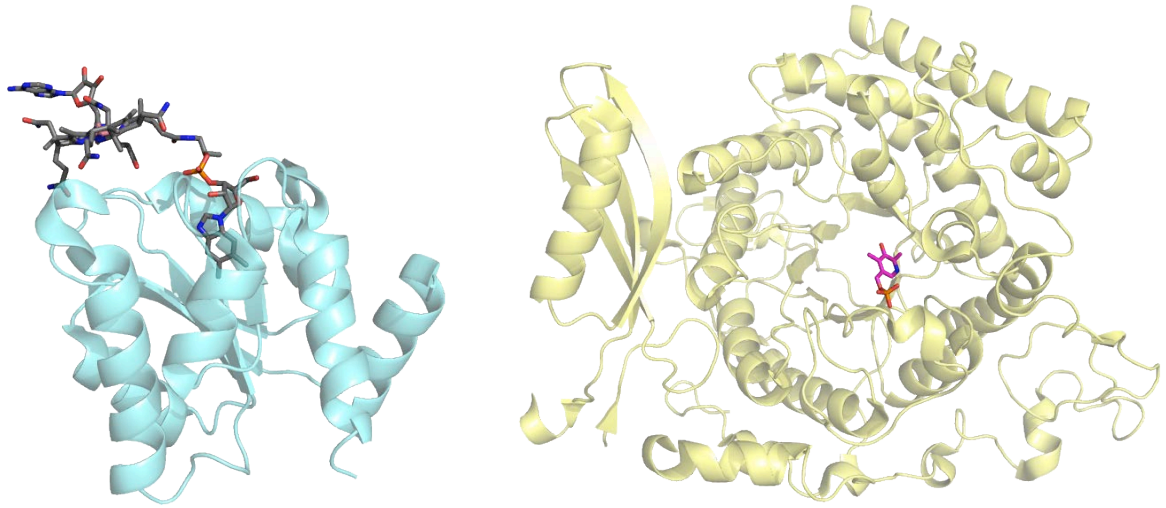

Figure 1.5 The core structural motifs shared by the AdoCbl-dependent isomerases. These include a Rossmann-like domain (Left), which binds the AdoCbl cofactor (gray), and a TIM-barrel domain (Right), which is the site of substrate binding.

1.2.2 Structure and Function of Coenzyme B_{12}

Adenosylcobalamin, or coenzyme B_{12} ($C_{72}H_{100}CoN_{18}O_{17}P$), is a large complex organometallic cofactor (Figure 1.6), having a molecular weight of 1579.58 g/mol. A central cobalt ion is coordinated equatorially to four nitrogen atoms donated by pyrroles, labeled A–D, within a corrin macrocycle. A 5'-deoxyadenosyl (Ado) group is coordinated to the cobalt ion in the upper axial position, forming one of the few instances of a carbon-metallic bond in nature. It is this Co–C bond and its catalytic role in enzymes that has piqued the interest of researchers for the past few decades. In solution, the lower axial ligand is a nitrogen atom from an intramolecular 5,6-dimethylbenzimidazole (DMB) base, often referred to as a nucleotide tail, which extends from ring D of the corrin macrocycle.[47] This unique built-in axial ligand is not seen in other tetrapyrrolic cofactors, such as hemes. A number of additional side chains, including methyl, acetamide, and propionamide groups, extend off of the four pyrrole rings adding to the complexity and size of the cofactor. These side chains form numerous hydrogen bonding interactions with amino acid residues, anchoring the cofactor tightly within the protein.[46, 47, 54] Spectroscopic and structural studies have shown that once AdoCbl is bound to the enzyme, the imidazole group of a histidine residue within the protein itself sometimes replaces the lower axial DMB ligand, such that the DMB adopts an extended conformation and is buried within a hydrophobic pocket of the Rossmann-like domain. The class I mutases and class III aminomutases, which contain a conserved DXHXXG sequence, bind the cofactor in this “base-off / His-on” conformation,[55-57] while the class II eliminases lack the conserved sequence and bind the cofactor in the “base-on / His-off” mode (Figure 1.7).[58]

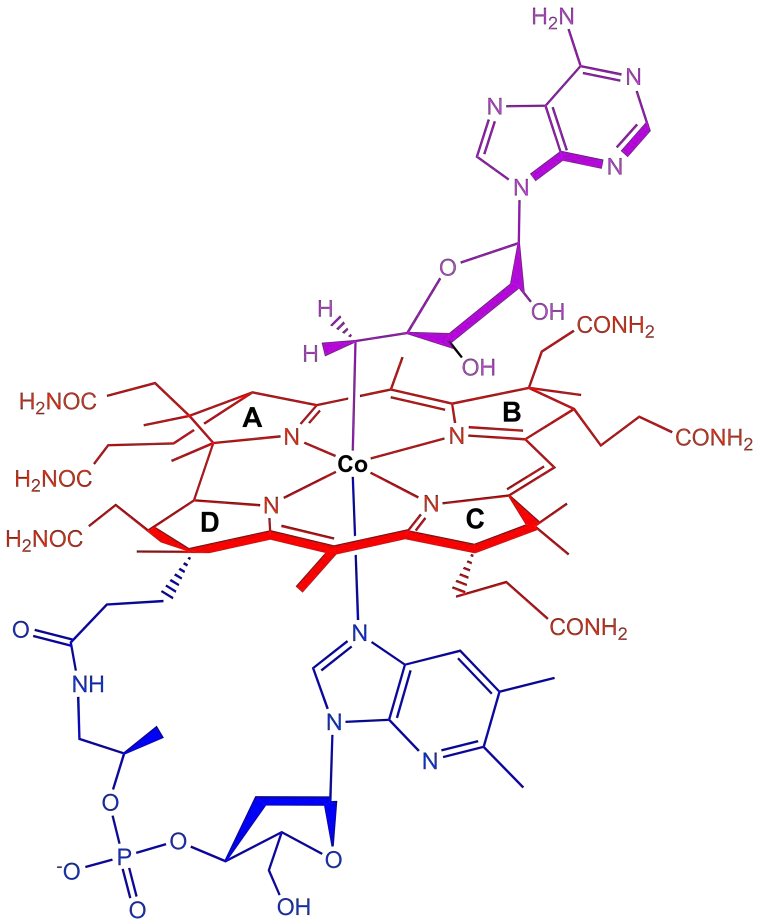

Figure 1.6 Solution structure of the adenosylcobalamin cofactor. A nitrogen atom from the intramolecular DMB base (blue) coordinates to the central cobalt in the lower axial position. An adenosyl moiety (purple) is coordinated in the upper axial position. The corrin ring (red) donates the equatorial nitrogens from pyrrole rings A–D.

The resting state of AdoCbl finds the cofactor in a six-coordinate, octahedral geometry, with cobalt existing in a low-spin d^6 Co(III) oxidation state. In this form, the cofactor is referred to as cob(III)alamin. During catalytic turnover, the Co–C bond undergoes homolytic cleavage forming a low-spin d^7 Co(II) ion and a 5'-deoxyadenosyl radical (Ado•), which then initiates the rearrangement mechanism, and leaves the cofactor in a five-coordinate state referred to as cob(II)alamin. The Co–C bond is later re-formed through geminate recombination, thus regenerating the AdoCbl cofactor for the next round of catalysis. In this way, AdoCbl acts as the source of radicals for this class of enzymes.

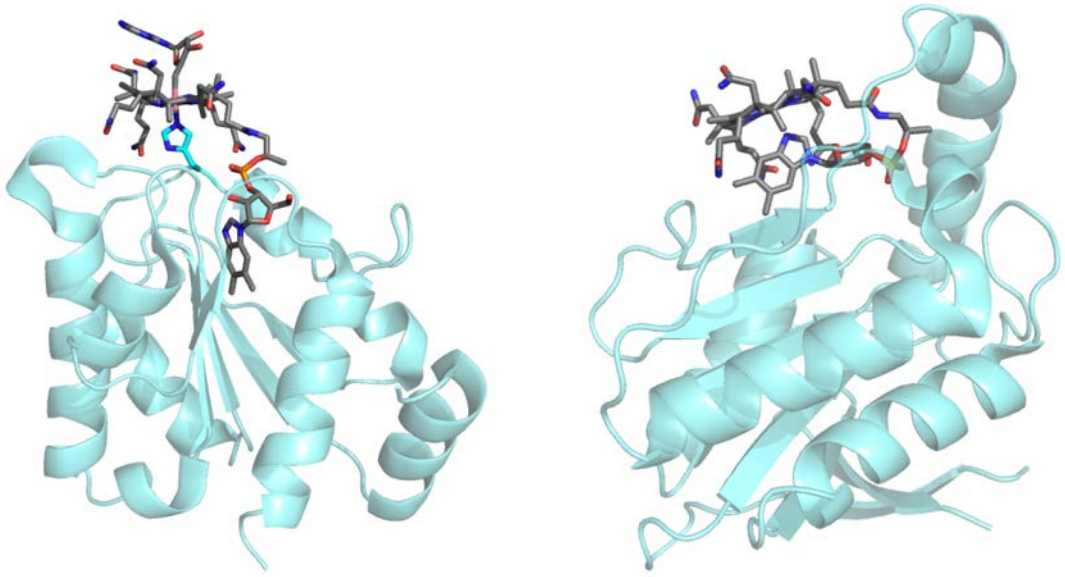

Figure 1.7 Conformational states of enzyme-bound adenosylcobalamin. AdoCbl adopts one of two conformational states within the AdoCbl-dependent isomerases. In the "base-off / His-on" state (Left) the dimethylbenzimidazole base, which extends off of pyrrole ring D, adopts an extended conformation and a histidine residue from the enzyme coordinates to the cofactor in the lower axial position. In the "base-on / His-off" state (Right) the dimethylbenzimidazole base remains coordinated to the cobalt center in the lower axial position.

1.2.3 General Catalytic Scheme

The same general reaction scheme can be applied to all AdoCbl-dependent isomerases (Figure 1.8). Upon substrate binding, the Co–C bond of the AdoCbl cofactor undergoes homolytic cleavage forming cob(II)alamin and a 5'-deoxyadenosyl radical (Ado•). The latter highly reactive species then abstracts a hydrogen atom from the substrate to form 5'-deoxyadenosine (AdoH) and a carbon-centered substrate radical intermediate. The substrate radical then undergoes a 1,2-rearrangement to form a product-like radical intermediate. Reabstraction of a hydrogen atom from AdoH by the product-like radical regenerates the adenosyl radical. The catalytic cycle is completed by product release and recombination of Ado• with cob(II)alamin to re-form the Co–C bond.

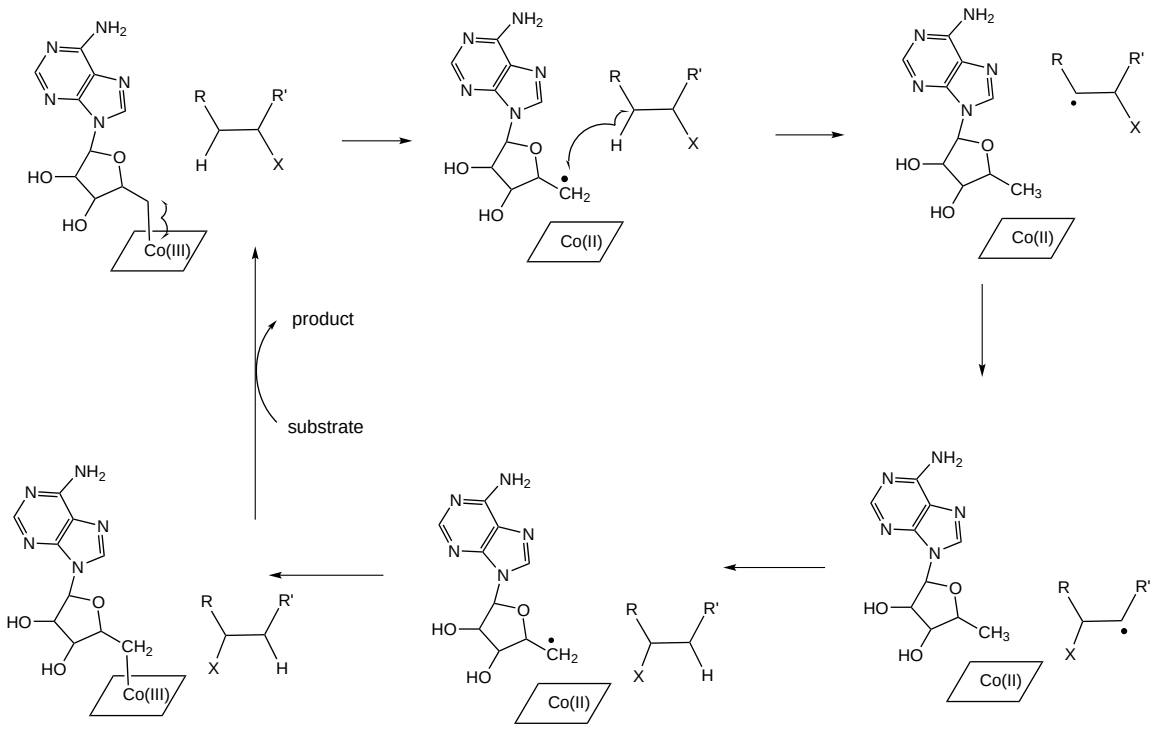

Figure 1.8 Generalized catalytic cycle for 1,2-rearrangements catalyzed by AdoCbl-dependent isomerases. Substrate binding induces Co–C bond homolysis forming cob(II)alalmin and a 5'-deoxyadenosyl radical (Ado•). The Ado• abstracts a hydrogen atom from the substrate to form a substrate-radical intermediate and 5'-deoxyadenosine (AdoH). Isomerization leads to a product-like radical intermediate, which then re-abstracts hydrogen from AdoH. Release of product and re-formation of the Co–C bond complete the cycle.[59]

1.2.4 Activation of the Co–C bond towards adenosyl radical formation

Adenosylcobalamin-requiring enzymes are one of the model systems that have been used by experimental and computational chemists to examine the basis for enzymatic catalytic rate enhancement.[51, 54, 60-62] In aqueous solution, homolysis of the AdoCbl Co–C bond occurs slowly at a rate of ~10^{-9} s^{-1} at 25 ºC, corresponding to an activation energy ($\Delta G^{\ddagger}$) of ~130 kJ/mol. The equilibrium constant has been estimated to be ~ 7.9 x 10^{-18} M, greatly favoring the intact form of the cofactor. In contrast, AdoCbl-dependent enzymes turn over at

rates of ~2–300 s^{-1}, where bond homolysis is not even the rate-limiting step.[54, 60, 63] Stopped-flow spectroscopy reveals that the rate constant for Co–C bond homolysis in MCM and OAM is >600 s^{-1}, and the equilibrium constant is close to one.[59, 64-66] Thus, these enzymes are able to greatly reduce the energy barrier to homolysis and ensure that the bond breaking process is reversible. Pre-steady-state kinetic experiments with glutamate mutase (GM) and MCM have shown that Co–C bond homolysis is coupled to hydrogen atom abstraction, such that reaction with their respective deuterium-labeled substrates causes a decrease in the observed rates of homolysis.[66, 67] There is, however, debate about whether Co–C bond homolysis and abstraction of hydrogen from the substrate follow a stepwise or concerted pathway.[68, 69] If the reference reaction is based on the rate of homolysis of AdoCbl in solution (10^{-9} s^{-1} at 25 ºC), then the $\Delta\Delta G^{\ddagger}$ is ~73 kJ/mol.[70] If the concerted pathway is invoked, the $\Delta\Delta G^{\ddagger}$ is ~40 kJ/mol.[60]

Kinetic, structural, and theoretical studies of AdoCbl-dependent isomerases have led to several different proposals for the origin of this ~$10^{12\pm1}$-fold rate acceleration of Co–C bond homolysis.[54, 60, 71] The strain hypothesis suggests that the enzyme distorts the geometry of the cofactor, leading to a substantial weakening of the Co–C bond. Originally, it was proposed that the enzyme compresses the Co–N_{Im} bond, leading to an upward folding of the corrin ring and to strain on the Co–C bond,[72] but this idea has not been supported through resonance Raman spectroscopy[73, 74] or the crystal structures of AdoCbl-dependent enzymes.[75-78] A modified version of the strain hypothesis centers on the distortion of the Co–C5'-C4' bond angle that results from the adenosyl group being under increased steric strain in the active site. There are those, however, that argue that enzymes are inherently too flexible to allow for significant strain.[60] Two theoretical studies suggested that the catalytic effects originate from specific interactions between residues in the active site and the polar ribose group, but the studies disagree on the degree to which electrostatic versus strain energy weakens the Co–C bond.[54, 60] The origin of this discrepancy stems from differences in the computational methods employed by the investigators, as well as difficulties in separating the various energy contributions experimentally.

1.2.5 Radical Stabilization and Control of Radical Trajectories

The highly reactive nature of radical intermediates necessitates that their generation and trajectories be tightly regulated to avoid spurious side reactions. In addition, radical enzymes have had to develop strategies for lowering the high-energy barriers associated with their proposed rearrangement mechanisms. As mentioned previously, the class II eliminases require the presence of an additional potassium ion cofactor in order for catalysis to occur.[53] Studies have shown that in diol dehydratase the potassium ion interacts with the hydroxyl groups of the substrate, along with five other ligands donated by the protein, to form a hepta-coordinate environment around the potassium ion (Figure 1.9).[71, 79] The presence of the potassium ion within the active site of diol dehydratase (DD) increases the binding affinity of the adenosylcobalamin cofactor for the enzyme, resulting in a 2500-fold activation of the Co–C bond, which then undergoes homolysis following substrate binding.[53] Modeling studies based on the crystal structure of DD reconstituted with adeninylpentylcobalamin suggest that once the adenosyl radical is formed the ribose moiety of the adenosyl group actually rotates about the N-glycosidic bond, thereby moving the C5'-centered radical from > 10 Å away (based on EPR simulations)[80] to within 2 Å of the substrate.[81] Once the substrate radical forms, the hydroxyl group is thought to migrate from C2 to C1 to form a 1,1 gem-diol intermediate, which is then dehydrated to form the final aldehyde product. Computational studies have indicated that a glutamate residue (E170) and a histidine residue (H143) within the DD active site are important for stabilizing the intermediates of the pathway. The histidine residue partially protonates the migrating hydroxyl group, while the glutamate residue partially deprotonates the spectator hydroxyl group, thus lowering the migration barrier so that the rearrangement can take place.[82]

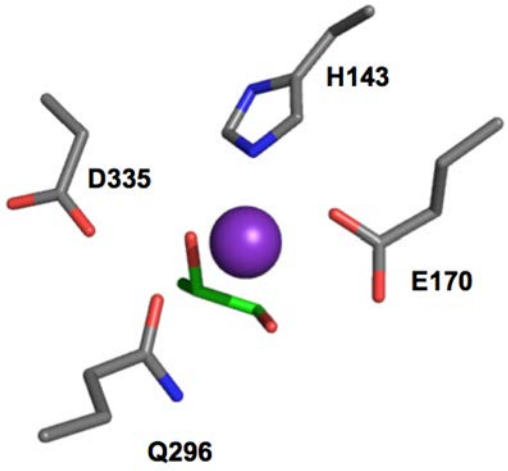

Figure 1.9 Coordination environment of the potassium ion in adenosylcobalamin-dependent diol dehydratase (PDB entry 1UC4). In addition to interacting with the hydroxyl groups of the substrate (green), the potassium ion (purple) is coordinated to several residues (gray) within the active site.

In comparison to the eliminases, the class I mutases do not require the presence of any additional cofactors, but they have developed similar strategies for controlling and stabilizing their radical intermediates. The crystal structure of glutamate mutase (1I9C) reveals electron density suggesting that the ribose ring of the 5'-deoxyadenosyl moiety exists in two distinct conformations. It is thought that pseudorotation of the ribose ring from a $C_{2'}$-*endo* to a $C_{3'}$-*endo* conformation (Figure 1.10) moves the C5'-centered radical closer to the substrate for hydrogen atom abstraction.[83] The ensuing radical rearrangement mechanism of glutamate mutase is proposed to occur via a fragmentation/recombination pathway, as evidenced by detection of the glycyl radical and acrylate intermediates.[84, 85] Computational studies have indicated that three arginine residues and a glutamate residue respectively serve to neutralize the carboxylate and amino groups of the substrate, thereby reducing the migration barrier for the rearrangement step in GM.[85] Based on these and the results for DD, it appears that active site residues in the AdoCbl-dependent isomerases play an integral role in stabilizing radical intermediates.

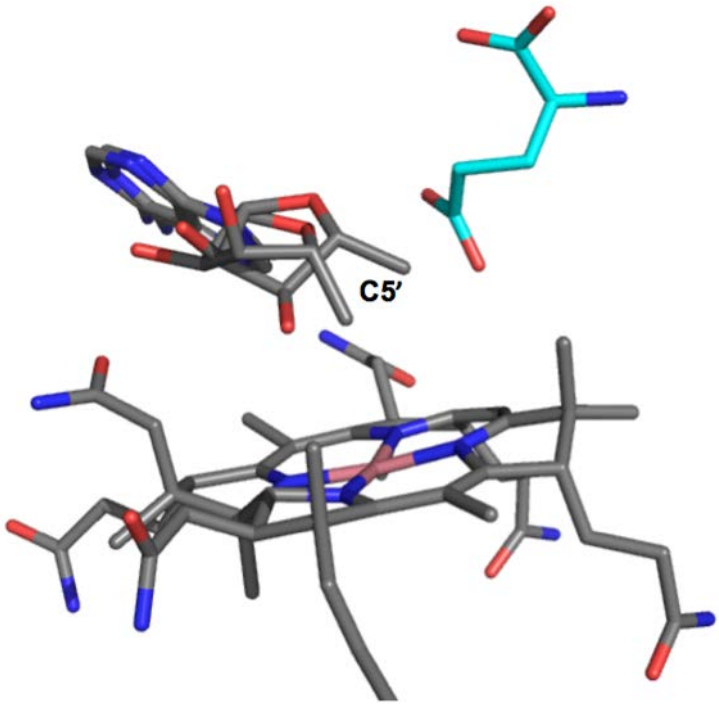

Figure 1.10 Pseudorotation of the ribose ring of the 5'-deoxyadenosyl moiety in glutamase mutase upon substrate binding. The crystal structure of GM (PDB entry 1I9C) shows two distinct conformations of the ribose ring: the C2'-*endo* conformation, in which the C5'-carbon is farther away from the substrate, and the C3'-*endo* conformation, in which the C5'-carbon is in close proximity to the substrate, allowing for hydrogen atom abstraction.

1.3 Class III Aminomutases

1.3.1 Structure and function of AdoCbl-dependent aminomutases

Ornithine 4,5-aminomutase (OAM) and lysine 5,6-aminomutase (5,6-LAM) are currently the only known AdoCbl-dependent isomerases that utilize an additional cofactor, pyridoxal 5'-phosphate (PLP), for catalysis. Both enzymes function in the catabolism of amino acids in several species of anaerobic bacteria, most notably *Clostridia.*[86] Specifically, OAM participates in the second step of the oxidative fermentation pathway of L-ornithine (Figure 1.11). In the first step of the pathway, L-ornithine is converted to D-ornithine by ornithine racemase. OAM then interconverts D-ornithine to 2,4-diaminopentanoate (DAP). In

the third step, DAP dehydrogenase (DAPDH) catalyzes the NAD^+-dependent oxidation of DAP to 2-amino-4-ketopentanoate, which is then further catabolized to acetate and alanine. In contrast to OAM, which is highly substrate-specific for D-ornithine, 5,6-LAM shows more substrate promiscuity as it is able to transform D- or L-lysine into D- or L-2,5-diaminohexanoate, as well as L-β-lysine into 3,5-diaminohexanoate.[87, 88]

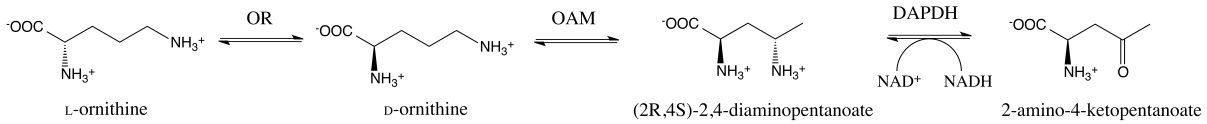

Figure 1.11 Oxidative fermentation pathway of L-ornithine. L-ornithine is first converted to D-ornithine by ornithine racemase (OR). D-ornithine is then interconverted to 2,4-diaminopentanoate by ornithine 4,5-aminomutase (OAM). In the third step of the pathway, 2,4-diaminopentanoate is oxidized to 2-amino-4-ketopentanoate in a NAD^+-dependent reaction catalyzed by 2,4-diaminopentanoate dehydrogenase (DAPDH). The final breakdown products include acetate and alanine.

Ornithine 4,5-aminomutase, isolated from *Clostridium sticklandii*, exists as an $\alpha_2\beta_2$ heterodimer comprised of two strongly associating subunits, OraE (82.9 kDa) and OraS (12.8 kDa).[89] Each OraE subunit comprises a TIM barrel domain and a Rossmann-like domain. A domain swap occurs in the heterodimer, whereby the Rossmann-like domain of one OraE subunit associates with the TIM barrel domain of a second OraE subunit and vice versa, such that two identical active sites are formed (Figure 1.12).[76] 5,6-LAM is also an $\alpha_2\beta_2$ heterodimer; however, unlike OAM the TIM barrel and Rossmann-like domains are found on separate α- (55 kDa) and β- (30 kDa) subunits (Figure 1.13). The α- and β-subunits display 28 and 35% sequence identity and 39 and 47% sequence similarity, respectively, to the OraE subunit of OAM.[90]

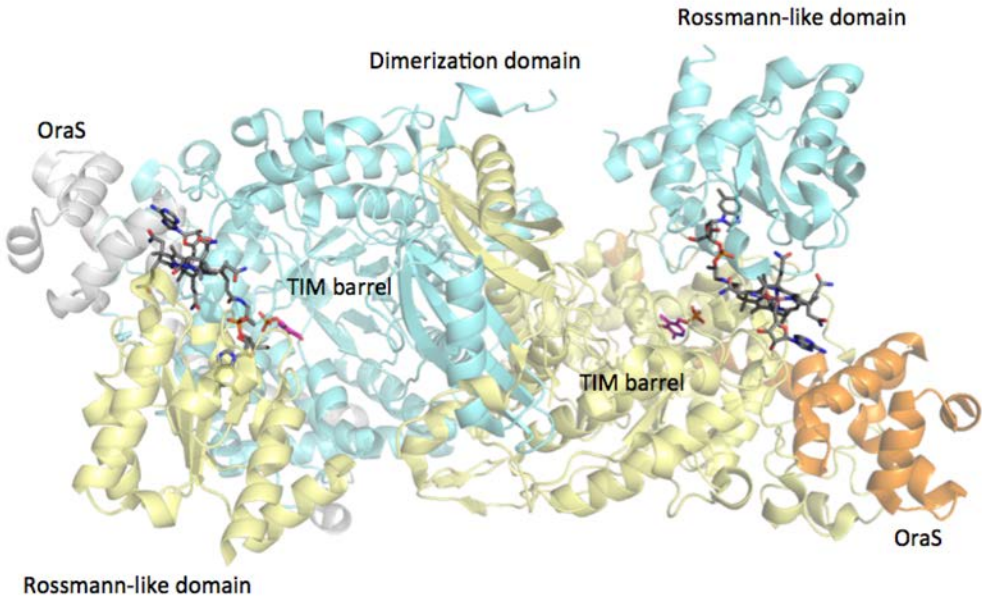

Figure 1.12 Quaternary structure of substrate-free ornithine 4,5-aminomutase with bound AdoCbl and PLP cofactors (PDB entry 3KP1). OAM is an $\alpha_2\beta_2$ heterodimer comprised of two strongly associating subunits, OraE (blue and yellow) and OraS (orange and gray). The Rossmann-like domain of one OraE subunit associates with the TIM barrel domain of the second OraE subunit, and vice versa, to form two identical active sites.

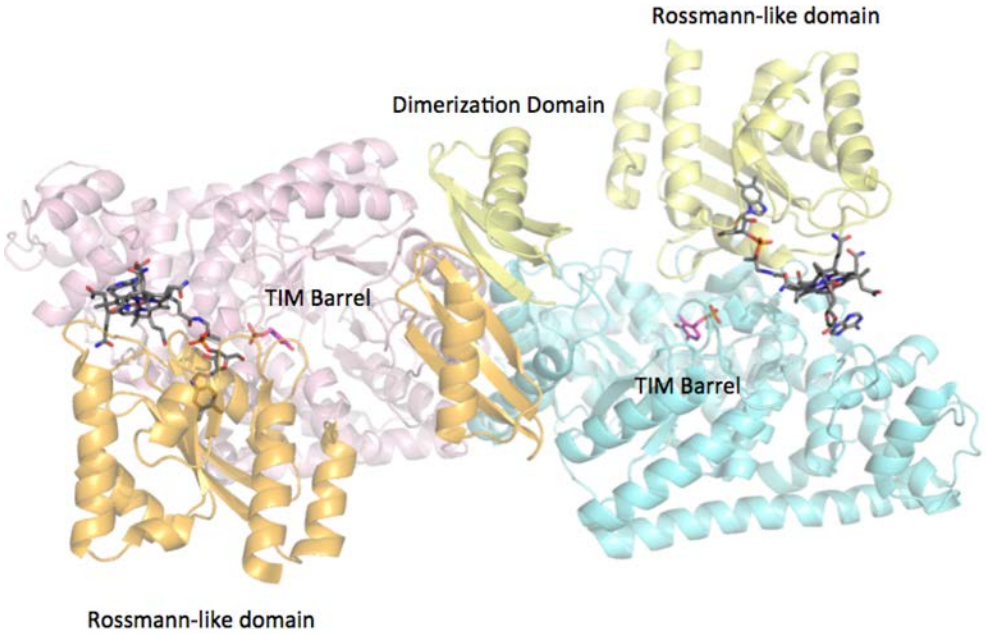

Figure 1.13 Crystal structure of lysine 5,6-aminomutase (PDB entry 1XRS). 5,6-LAM exists as an $\alpha_2\beta_2$-heterodimer. The α subunit (pink and cyan) comprises the TIM barrel domain, while the β subunit (yellow and orange) comprises the Rossmann-like domain.

Structural and spectroscopic studies reveal that substrate binding induces structural rearrangements in the protein scaffold.[64, 75, 91] Recent computational studies of OAM show that the Rossmann-like domain undergoes an ~52° rotation and ~14 Å translation upon binding of the substrate. In the substrate-free form of OAM, the Rossmann-like domain is tilted toward the edge of the TIM barrel, exposing the 5'-deoxyadenosyl moiety of AdoCbl to the solvent (Figure 1.15).[76] The PLP cofactor, noncovalently bound to the TIM barrel active site, forms an internal aldimine with a lysine (Lys144β in 5,6-LAM and Lys629 in OAM) originating from the Rossmann-like domain (Figure 1.14). This protein–cofactor covalent link effectively locks the enzyme into an edge-on conformation (Figure 1.15), separating the PLP and 5'-deoxyadenosyl moiety by ~ 23 Å in the pre-catalytic state, thereby protecting the enzymes from spurious radical generation in the absence of substrate. The incoming substrate displaces the internal aldimine, forming an external aldimine link via its migrating amino group. This first step of the catalytic cycle is anticipated to free the Rossmann-like domain to rotate toward the TIM barrel to form the top-on conformation, as observed in the crystal structures of the class I mutases (Figure 1.15).[77, 78] Positioning of AdoCbl into the active site triggers Co–C bond homolysis.

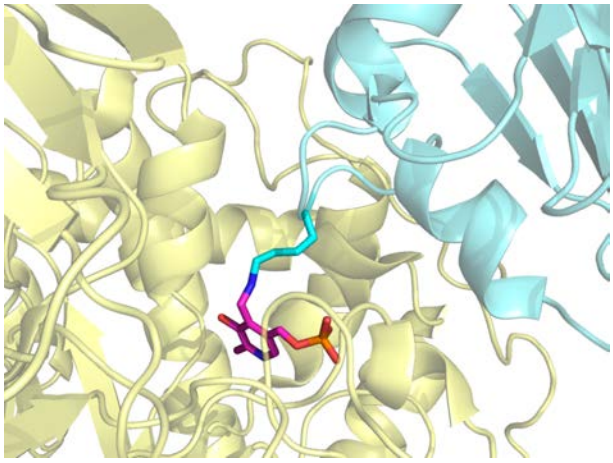

Figure 1.14 Internal aldimine linkage in OAM (PDB entry 3KP1). Substrate-free form of OAM showing the PLP cofactor, housed within the TIM barrel domain (yellow ribbons), covalently linked to the Rossmann-like domain (cyan ribbons) through the terminal amino group of Lys629.

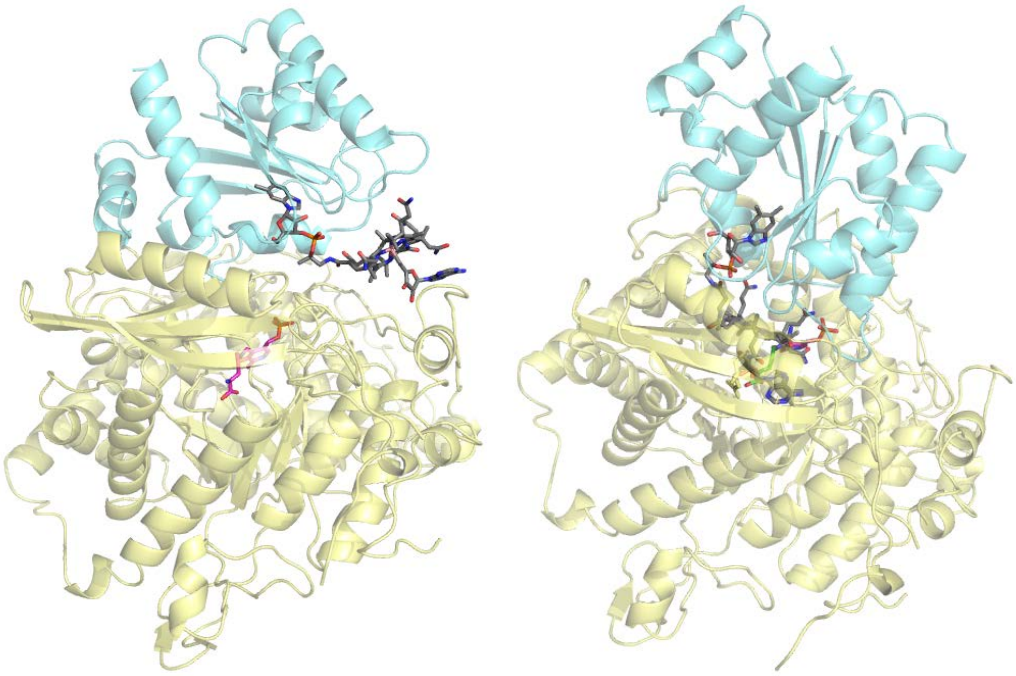

Figure 1.15 Open conformation and modeled closed conformation of OAM. OAM exists in an edge-on conformation prior to substrate binding (left), which effectively expels the AdoCbl cofactor from the active site, and separates the AdoCbl and PLP cofactors by ~23 Å. Upon substrate binding, the internal aldimine linkage is replaced by a new covalent bond between PLP and the terminal amino group of the substrate, allowing the Rossmann-like domain to move into a top-on conformation (right).[76]

1.3.2 Proposed Catalytic Mechanism

The proposed catalytic mechanism for the AdoCbl-dependent aminomutases (Figure 1.16) is based on S-adenosyl-L-methionine- and PLP-dependent lysine 2,3-aminomutase, which catalyzes a similar 1,2-amino group migration.[92-95] Substrate binding results in transimination, whereby the aldimine linkage between PLP and the internal lysine residue is replaced by an external aldimine linkage between PLP and the terminal amino group of the substrate. Breakage of the internal aldimine linkage frees the Rossmann-like domain to rotate and position itself directly over the TIM barrel domain in a conformation similar to that captured in the crystal structures of glutamate mutase and methylmalonyl-CoA mutase.[76-78] This top-on conformation establishes new noncovalent interactions between the adenosyl moiety and active site residues, which are thought to contribute to homolysis of the AdoCbl

Co–C bond resulting in formation of cob(II)alamin and a 5'-deoxyadenosyl radical (Ado•).[59, 60] The Ado• abstracts a hydrogen atom from the substrate to form a substrate radical intermediate and 5'-deoxyadenosine (AdoH). The substrate radical then isomerizes into a product-like radical via a proposed azacyclopropycarbinyl radical intermediate. Reabstraction of a hydrogen atom from AdoH by the product-like radical regenerates the adenosyl radical. The catalytic cycle is completed by product release and recombination of Ado• with cob(II)alamin to re-form the Co–C bond.

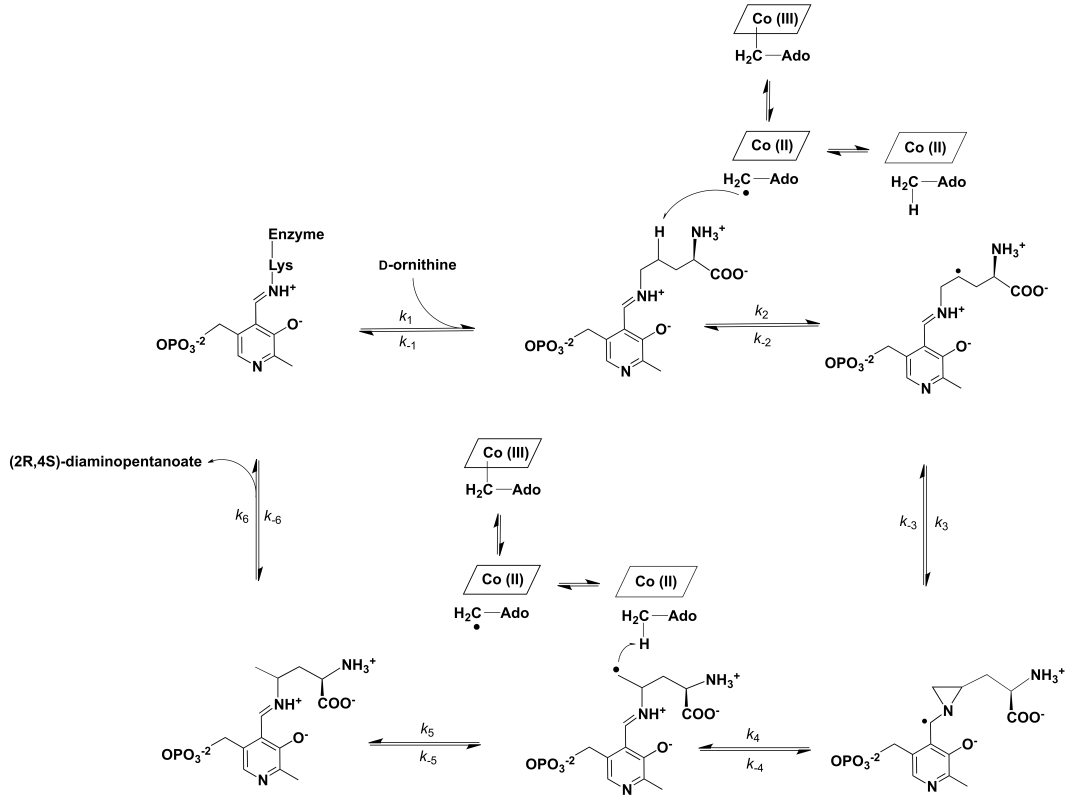

Figure 1.16 Proposed catalytic mechanism for ornithine 4,5-aminomutase. Binding of substrate results in transimination, whereby the internal aldimine linkage between PLP and Lys629 is replaced by an external aldimine linkage between PLP and the terminal amino group of D-ornithine. Conformational changes upon substrate binding induce homolysis of the AdoCbl Co–C bond, resulting in formation of cob(II)alamin and a 5'-deoxyadenosyl radical (Ado•). Ado• abstracts the C4 hydrogen from D-ornithine to form a substrate radical intermediate and 5'-deoxyadenosine. The substrate radical then isomerizes into a product-like radical via an azacyclopropylcarbinyl radical intermediate. Reabstraction of a hydrogen atom from 5'-deoxyadenosine by the product-like radical regenerates the adenosyl radical. Product release and recombination of Ado• with cob(II)alamin to reform the Co–C bond complete the catalytic cycle.

1.3.3 The Role of Pyridoxal 5'-Phosphate

Apart from its role in anchoring the substrate within the active site, computational studies indicate that the PLP cofactor plays a much larger role in AdoCbl-dependent aminomutase catalysis. It has been suggested that the PLP cofactor lowers the barrier to intramolecular isomerization by introducing unsaturation into the migrating amino group, thus allowing the reaction to proceed via a cyclic intermediate, which is stabilized through captodative effects.[96] These captodative effects originate from the electron-withdrawing capability of the pyridine ring and the electron-donating capability of the nitrogen lone pair adjacent to the radical center.[96] Simulations in which the pyridine nitrogen was protonated revealed that PLP was able to further reduce the barrier to ring closure, as well as stabilize the cyclic intermediate to a greater degree than the non-cyclized substrate- or product-like radical intermediates. It was suggested that this overstabilization could lead to inactivation of the enzyme, and that protonation of the imino group by the nearby phenolic oxygen was required to prevent the cyclic intermediate from becoming trapped in a local energy minimum.[96] Even though PLP plays a stabilizing role, none of the proposed radical intermediates nor the cob(II)alamin species have been observed spectroscopically in the reactions of OAM or 5,6-LAM with their physiological substrates, indicating that these intermediates are relatively unstable with very short lifetimes.[64, 97]

The role of PLP in stabilizing high-energy radical intermediates in the aminomutases is unique. The cofactor typically facilitates catalysis in traditional PLP-dependent enzymes by stabilizing an α-carbanion intermediate. The structure of PLP (Figure 1.17) allows the negative charge on the α-carbon to become delocalized through the conjugated π-system of the Schiff base and the pyridine ring. As such, the cofactor is often referred to as being an electron-sink. Protonation of the pyridine nitrogen further increases the electrophilicity of the pyridine ring, and has been shown to participate in controlling the reaction specificity of PLP-dependent enzymes.[98] The protonation state of the imino nitrogen plays a similar role.[99]

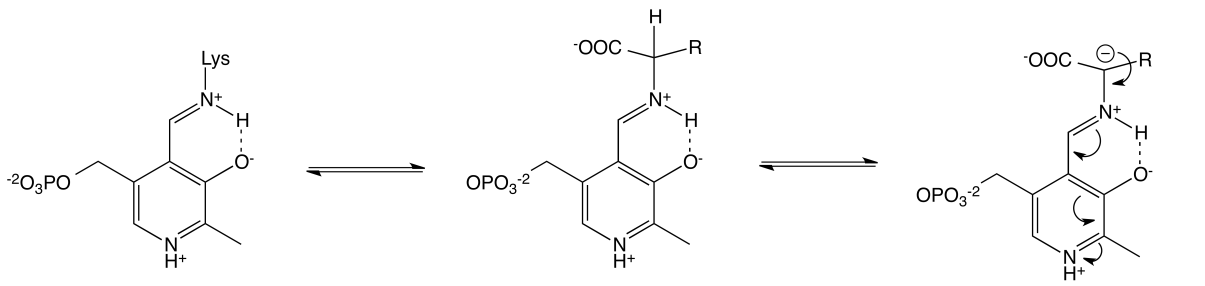

Figure 1.17 Traditional role of PLP as an electron-sink. Initially, PLP forms a Schiff base with a lysine residue from the protein, referred to as the internal aldimine state. The lysine residue is displaced by the incoming substrate, which forms a Schiff base with the PLP to form an external aldimine species. The structure of the PLP cofactor allows it to stabilize the carbanion intermediate that forms during catalysis in the PLP-dependent enzymes.

1.4 Research Objectives

The main goal of this thesis was to further our current understanding of the strategies employed by enzymes to ensure controlled radical initiation and propagation of the ensuing high-energy radical intermediates. As such, in Chapter 2 we used a combination of kinetic isotope effects, mutagenesis, modeling studies, and EPR spectroscopy to uncover features of the OAM catalytic mechanism and active site organization that differentiate it from its homologue, the more catalytically promiscuous lysine 5,6-aminomutase. In Chapter 3, we sought to examine the contribution of electrostatics to activation of the Co–C bond in the class I mutases and the class III aminomutases by mutating a conserved glutamate residue, which interacts with the adenosyl moiety of the adenosylcobalamin cofactor. Chapters 4 and 5 investigated the role of residues proximal to the pyridoxal 5'-phosphate cofactor, as they are in a position to modulate radical catalysis through their interactions with PLP. In particular, their effect on the protonation state of the imino and pyridine nitrogens of the PLP cofactor was examined.

Chapter 2 : Mechanistic Differences between Ornithine 4,5-aminomutase and Lysine 5,6-aminomutase Revealed through Deuterium Kinetic Isotope Effects and Modeling Studies

2.1 Chapter Summary

Adenosylcobalamin-dependent ornithine 4,5-aminomutase (OAM) and lysine 5,6-aminomutase (5,6-LAM) utilize pyridoxal 5'-phosphate to facilitate radical-based 1,2-amino shifts. Despite being structural homologues, OAM and 5,6-LAM exhibit marked differences in both their kinetic behaviour and substrate specificity. OAM is highly substrate-specific for D-ornithine, which it converts to 2,4-diaminopentanoate. In contrast, 5,6-LAM shows more substrate promiscuity as it is able to convert D- or L-lysine into D- or L-2,5-diaminohexanoate, as well as L-β-lysine into 3,5-diaminohexanoate.[100] 5,6-LAM also undergoes rapid suicide inactivation at a 10-fold higher rate than that observed in OAM.[101] Here we have employed deuterium kinetic isotope effect studies of OAM, and modeling studies of the 5,6-LAM active site, to account for these differences. Wild-type OAM displayed $^{D}k_{cat}$ and $^{D}k_{cat}/K_{m}$ values of 7.6 ± 0.5 and 2.5 ± 0.4, respectively, upon reaction with DL-ornithine-3,3,4,4,5,5-d_6. The lower value of $^{D}k_{cat}/K_{m}$ relative to $^{D}k_{cat}$ suggests that the substrate has a tight binding affinity and therefore a slow rate of release from the active site. In contrast, a kinetic isotope effect was not observed on the rate constant associated with Co–C bond homolysis, as this step is likely gated by the formation of the external aldimine. Modeling of D-lysine and L-β-lysine into the 5,6-LAM active site reveals that there are fewer and weaker interactions between the substrate and the protein compared to OAM. In addition, simulations of the OAM EPR spectrum indicate that the distance between the persistent organic radical and the cob(II)alamin center is ~6.7 Å, and therefore smaller than the ~10.5 Å distance observed in 5,6-LAM.[91, 102] These results suggest that substrate binding is weaker in 5,6-LAM compared to OAM, which could account for the more promiscuous nature of 5,6-LAM, as well as its increased tendency to undergo radical-mediated suicide inactivation. The relationship between the OAM and 5,6-LAM active sites, their substrate specificity, and ability to control enzyme-mediated radical chemistry is discussed.

2.2 Purification and steady-state characterization of OAM

2.2.1 Purification of Ornithine 4,5-Aminomutase (OAM)

The OraE and OraS genes associated with ornithine 4,5-aminomutase were previously cloned from *Clostridium sticklandii* genomic DNA and inserted into the pET23d vector, thus attaching a hexahistidine tag to the C-terminus of the enzyme. The plasmid was designated pETOAMH2.[64] Following co-expression in *E. coli*, the OraE and OraS gene products were purified by Ni-NTA affinity chromatography and anion exchange chromatography. As shown in Figure 2.1, protein bands corresponding to the OraE and OraS subunits are observed at 83 and 13 kDa, respectively.

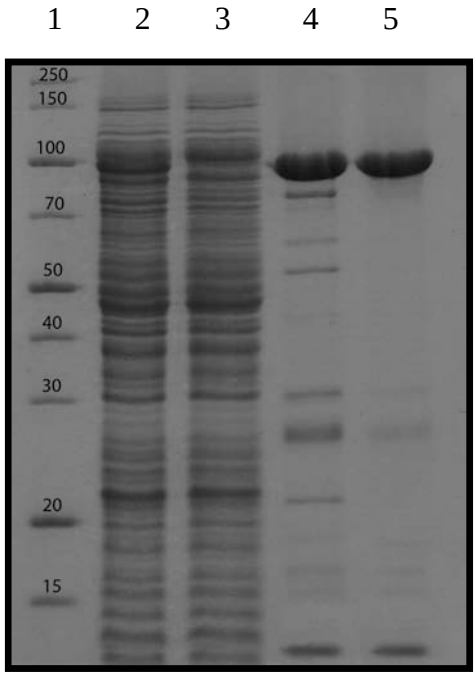

Figure 2.1 Purification of OAM. SDS 14 % polyacrylamide gel showing purification of ornithine 4,5-aminomutase by Ni-NTA affinity and anion exchange chromatography. Lane 1, protein molecular weight markers in kDa; Lane 2, crude extract from Rosetta(DE3)pLysS cells over-expressing OAM; Lane 3. Flow-through from Ni-NTA column; Lane 4, Ni-NTA eluate from first purification step; Lane 5, Q-sepharose eluate from second purification step.

2.2.2 Purification of Diaminopentanoate dehydrogenase (DAPDH)

In order to measure the steady-state turnover of OAM, we developed a continuous UV-visible spectrophotometric assay utilizing a coupling enzyme. As mentioned previously, OAM participates in the second step of the anaerobic oxidative degradation pathway of L-ornithine. The product of the OAM reaction, 2,4-diaminopentanoate (DAP), is then converted into 2-amino-4-ketopentanoate by DAPDH in the third step of the pathway. During the oxidation of DAP, NAD^+ is concomitantly reduced to NADH which absorbs at 340 nm allowing its production to be followed spectrally. As such, we cloned the gene for DAPDH from *Clostridium difficile* genomic DNA. The high level of DAPDH amino acid sequence similarity (84%) between the two *Clostridia* species suggests that the enzyme from *C. difficile* can substitute for the *C. sticklandii* counterpart in measuring OAM turnover. Following heterologous bacterial expression, DAPDH bearing a C-terminal hexahistidine tag was purified to homogeneity using Ni-NTA affinity chromatography followed by Q-sepharose anion exchange chromatography (Figure 2.2). The apparent molecular weight of the enzyme (41 kDa) determined from SDS-PAGE closely matches the predicted molecular weight of 40,551 Da for a hexahistidine tagged protein.

2.2.3 Purification of Ornithine Racemase

Ornithine racemase, the first enzyme in the anaerobic oxidative degradation pathway of L-ornithine, converts L-ornithine to D-ornithine.[103] DL-ornithine-3,3,4,4,5,5-d_6 was enzymatically produced from L-ornithine-3,3,4,4,5,5-d_6 using ornithine racemase cloned from *C. difficile* genomic DNA. Ornithine racemase, bearing a C-terminal hexahistidine tag, was heterologously expressed in *E. coli* and purified to homogeneity via Ni-NTA affinity chromatography followed by anion exchange chromatography. The apparent molecular weight (42 kDa), as determined by SDS-PAGE, closely matches the predicted molecular weight of 41,772 kDa for a hexahistidine-tagged OR (Figure 2.3).

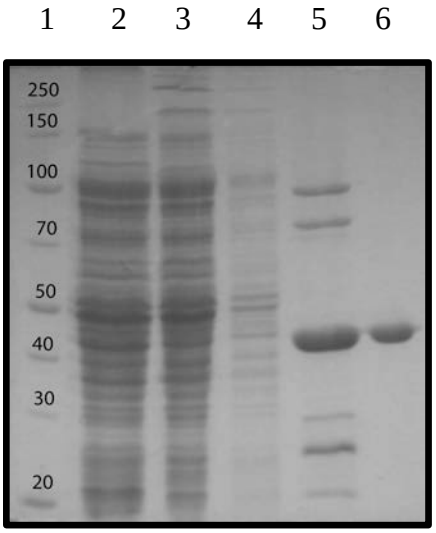

Figure 2.2 Purification of DAPDH. SDS 10 % polyacrylamide gel showing purification of (2R,4S)-2,4-diaminopentanoate dehydrogenase by Ni-NTA affinity and anion exchange chromatography. Lane 1, protein molecular weight markers in kDa; Lane 2, crude extract from DADPH over-expressing Rosetta(DE3)pLysS cells; Lane 3. Flow-through from Ni-NTA column; Lane 4, wash with 50 mM Tris pH 7.5, 0.5 M NaCl, 20 mM imidazole; Lane 5, Ni-NTA eluate from first purification step; Lane 6, Q-sepharose eluate from second purification step.

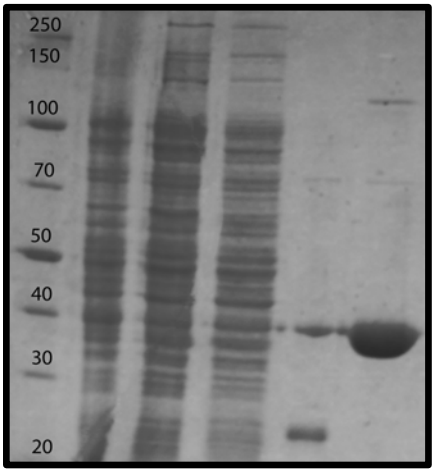

Figure 2.3 Purification of ornithine racemase. SDS 10 % polyacrylamide gel showing purification of ornithine racemase (OR) from *Clostridium difficile* by Ni-NTA affinity chromatography followed by Q-sepharose anion-exchange chromatography. Lane 1, protein molecular weight markers in kDa; Lane 2, crude extract from Rosetta(DE3)pLysS cells over-expressing OR; Lane 3, flow-through from initial Ni-NTA column; Lane 4, wash with 50 mM Tris pH 7.5, 0.5 M NaCl, 20 mM imidazole; Lane 5, Ni-NTA eluate from first purification step; Lane 6, Q-sepharose eluate from second purification step.

2.2.4 Determination of the equilibrium constant for OAM

The equilibrium constant for the conversion of D-ornithine to 2,4-diaminopentanoate was determined to gain insight into the nature of the first irreversible step in the mechanism of OAM. Reaction of D-ornithine with OAM results in a shift of the terminal amino group from C5 to C4 to produce 2,4-diaminopentanoate. The two hydrogen atoms on C5 of D-ornithine appear as a triplet at 3.02 ppm, J = 7.4 Hz in a ^{1}H-NMR spectrum, while the three hydrogen atoms on C5 of the product 2,4-diaminopentanoate appear as a doublet at 1.33 ppm, J = 6.6 Hz (Figure 2.4). Using the relative integrals of these peaks, the equilibrium constant for OAM was determined to be 1.7, indicating that the reaction is freely reversible, with a slight preference for product formation. As such, the first irreversible step is likely product release under substrate-limiting conditions.

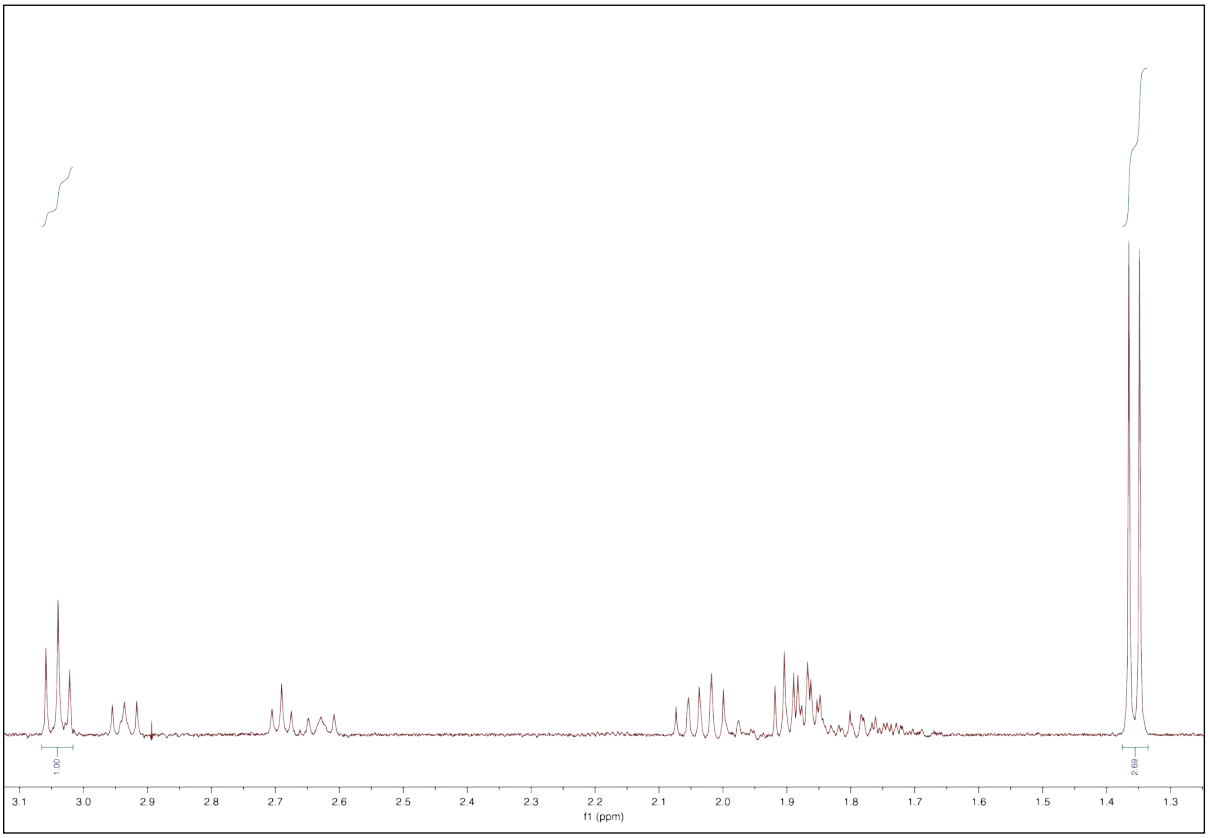

Figure 2.4 ^{1}H-NMR spectrum of the reaction of ornithine 4,5-aminomutase with D-ornithine at equilibrium. The triplet at 3.02 ppm represents the two hydrogen atoms on C5 of the substrate D-ornithine, while the doublet at 1.33 ppm represents the three hydrogen atoms on C5 of the product 2,4-diaminopentanoate.

2.2.5 Deuterium kinetic isotope effects for OAM

The coupled-enzyme assay was designed to measure the activity of OAM. Under the assay conditions used, a lag phase characteristic of coupled-enzyme assays was observed. This lag phase is consistent with the turnover rate of DAPDH being limited by the rate of OAM turnover (Figure 2.5). Thus, the absorbance increase at 340 nm, corresponding to the reduction of NAD^+ to NADH, is representative of the turnover rate of OAM. Macroscopic kinetic parameters for wild-type OAM were determined by measuring the initial velocity as a function of substrate concentration (Figure 2.6). The data were fit to the Michaelis-Menten equation (Eq. 2.1 in section 2.10.7).

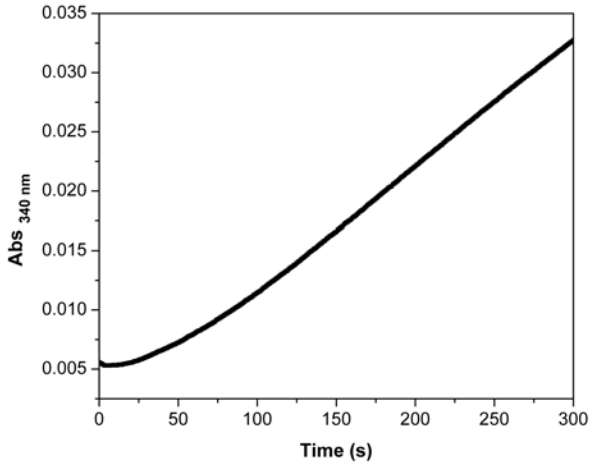

Figure 2.5 Coupled-enzyme spectrophotometric assay for monitoring OAM turnover. Sample absorbance data collected at 340 nm for wild-type OAM with 2.5 mM D-ornithine during the coupled-enzyme assay with DAPDH. The initial velocity of the reaction was determined from the linear portion of the curve between 150 and 210 seconds, following the initial lag phase.

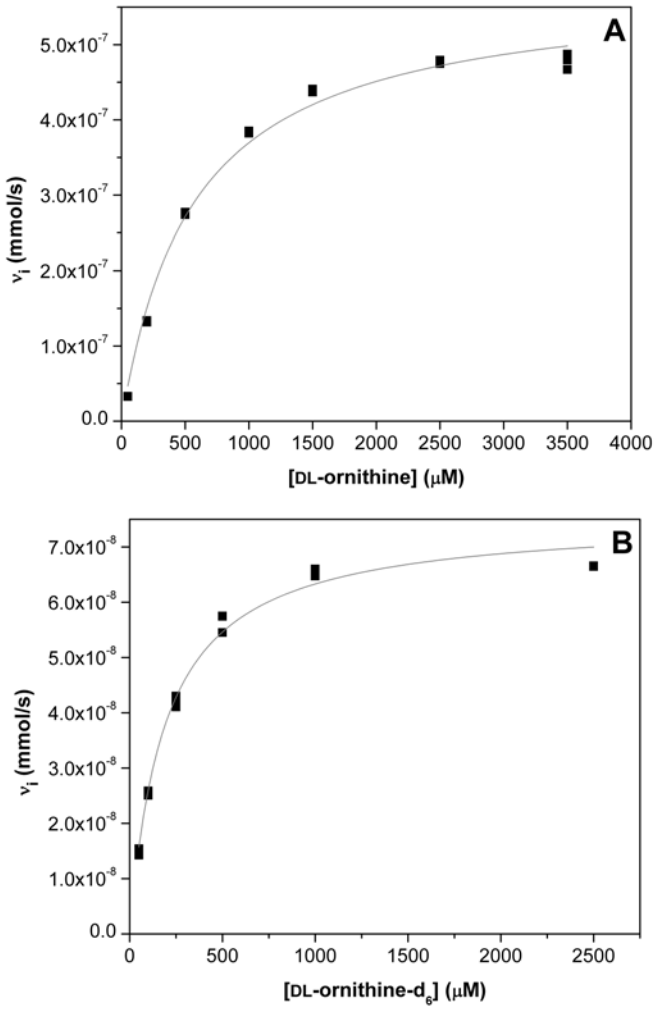

Figure 2.6 Determination of steady-state kinetic parameters for wild-type OAM. A plot of initial velocity, v_i, versus substrate concentration was generated for wild-type OAM with (A) DL-ornithine and (B) DL-ornithine-3,3,4,4,5,5-d_6. Data were collected in triplicate and the data were fit to the Michaelis-Menten equation (Eq. 2.1) using non-linear least-squares regression analysis using the computer program Origin 8.0 to determine macroscopic kinetic parameters, which are listed in Table 2.1.

The kinetic parameters for wild-type OAM with D-ornithine, DL-ornithine, and DL-ornithine-3,3,4,4,5,5-d_6 are summarized in Table 2.1. Wild-type OAM was found to display a k_{cat} value of 2.9 ± 0.1 s^{-1} with both D-ornithine and DL-ornithine, similar to that previously reported.[89] The observed K_m values were 190 ± 13 μM and 567 ± 45 μM for D-ornithine and DL-ornithine, respectively. The difference in the value of K_m for the two substrates is attributed to the fact that OAM is inactive towards the L-isomer. Given the structural

similarity to D-ornithine, the L-isomer likely acts as a competitive inhibitor and thus the addition of a saturating amount of DL-ornithine achieves the same turnover rate as the D-isomer but increases the apparent K_m value. Both k_{cat} and K_m were reduced with DL-ornithine-3,3,4,4,5,5-d_6, resulting in a $^{D}k_{cat}$ value of 7.6 ± 0.5 and a $^{D}k_{cat}/K_m$ value of 2.5 ± 0.4 ($^{D}k_{cat}$ and $^{D}k_{cat}/K_m$ are primary deuterium kinetic isotope effects; they are the ratio of the macroscopic kinetic parameters for the proteated substrate and the deuterated substrate). The kinetic isotope effect (KIE) on k_{cat} suggests that hydrogen atom abstraction is at least partially rate-limiting in the mechanism of ornithine 4,5-aminomutase.

Table 2.1 Summary of steady-state kinetic parameters for wild-type OAM with substrates D-ornithine, DL-ornithine, and DL-ornithine-3,3,4,4,5,5-d_6.

Substrate	k_{cat} (s^{-1})	K_m (μM)	k_{cat}/K_m ($M^{-1}s^{-1}$)
D-ornithine	2.9 ± 0.1	190 ± 13	$15 \times 10^3 \pm 1.2 \times 10^3$
DL-ornithine	2.9 ± 0.1	570 ± 45	5100 ± 410
DL-ornithine-d_6	0.38 ± 0.01	190 ± 11	2000 ± 170

2.3 Anaerobic UV-visible spectroscopy

HoloOAM (wild-type OAM with PLP and AdoCbl) exhibits a characteristic UV-visible binding spectrum with prominent contributions from both the PLP (416 nm) and AdoCbl (528 nm) cofactors,[64] as shown in Figure 2.7. The binding of the physiological substrate D-ornithine results in an initial transimination event to form the external aldimine species (Figure 2.7A). This is observed spectrally as a decrease in absorbance at 416 nm and the formation of an absorbance peak at 425 nm. Substrate binding also induces homolysis as demonstrated by a small absorbance decrease at 528 nm. The substrate analogue, DL-2,4-diaminobutyrate (DABA), produces similar changes to the UV-visible spectrum upon

binding to OAM (Figure 2.7B). However, in contrast to D-ornithine, the addition of DABA induces a greater percentage of the holoenzyme to undergo homolysis, as evidenced by the larger decrease in absorbance at 528 nm, and results in the formation of a discrete peak at 470 nm.[64] The absorbance increase at 470 nm is attributed to the accumulation of the cob(II)alamin intermediate, which suggests that docking of DABA leads to the formation of an overstabilized radical species (see Discussion in section 2.9 for further explanation).[64] The same build-up of cob(II)alamin is not spectrally observed during turnover with D-ornithine.

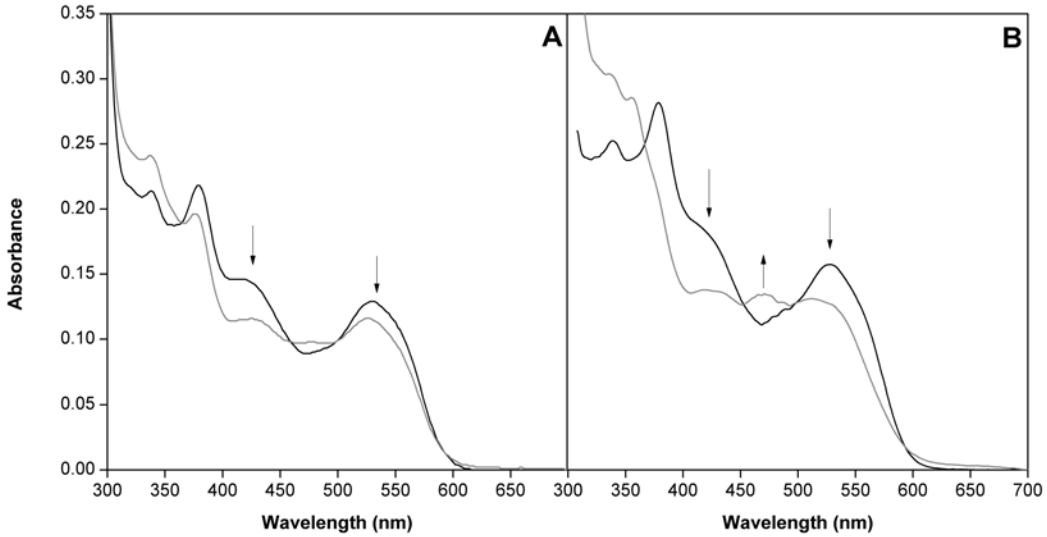

Figure 2.7 Changes in the UV-visible absorbance spectra of wild-type OAM upon binding of D-ornithine and DL-2,4-diaminobutyrate. The holoenzyme reaction mixture contained 15 μM apoOAM, 15 μM PLP, and 15 μM AdoCbl in 100 mM NH_4^+EPPS buffer, pH 8.5. Spectral changes for OAM were recorded before (black line) and after (gray line) the addition of (A) 2.5 mM D-ornithine and (B) 2.5 mM DL-2,4-diaminobutyrate under anaerobic conditions. The decreases in absorbance at 416 nm and 528 nm reflect formation of the external aldimine and homolysis of the Co–C bond, respectively. The absorbance peak that forms at 470 nm upon addition of DABA in panel B represents accumulation of cob(II)alamin.

2.4 Stopped-flow determination of pre-steady-state rate constants for transimination and Co–C bond homolysis

The observed rate constants for transimination and homolysis, monitored via stopped-flow spectroscopy, are on the same order of magnitude (~500 s^{-1})[64] and therefore much faster

than the observed turnover rate of OAM (2.9 s^{-1}). A monoexponential fit of the absorbance traces at 416 nm (1–20 ms) produced a rate constant of 464 ± 36 s^{-1} for the formation of the external aldimine upon binding of the inhibitor DL-2,4-diaminobutyrate (Figure 2.8A). The observed rate constant for Co–C bond homolysis upon rapid mixing of the holoenzyme with DABA was 489 ± 40 s^{-1} (Figure 2.8B).

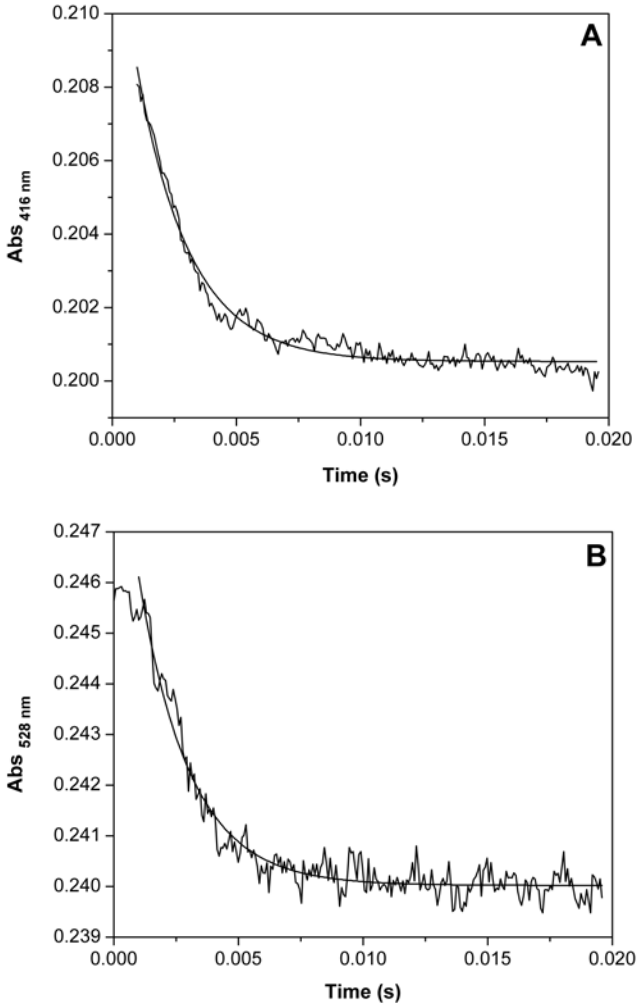

Figure 2.8 Stopped-flow absorbance changes following transimination and Co–C bond homolysis in OAM. Formation of (A) the external aldimine and (B) homolysis of the Co–C bond were followed at 416 nm and 528 nm, respectively. The absorbance changes were monitored over 20 ms following rapid mixing of 50 μM holoOAM with 5 mM DL-2,4-diaminobutyrate. An average of 8–10 traces were fit to a monoexponential equation to obtain the observed rate constants for transimination (464 ± 36 s^{-1}) and homolysis (489 ± 40 s^{-1}).

Pre-steady-state kinetic experiments with glutamate mutase and methylmalonyl-CoA mutase have shown that Co–C bond homolysis is coupled to hydrogen atom abstraction, such that reaction with their respective deuterium-labeled substrates causes a decrease in the observed rates of homolysis.[65, 66] Reaction of holoOAM with D-2,4-diaminobutyrate-2,3,3,4,4-d_5 ($1140 \pm 150\ s^{-1}$), however, yielded no discernable difference in the rate constant for Co–C bond homolysis from that observed upon reaction with protiated DL-2,4-diaminobutyrate ($980 \pm 88\ s^{-1}$) (Figure 2.9).

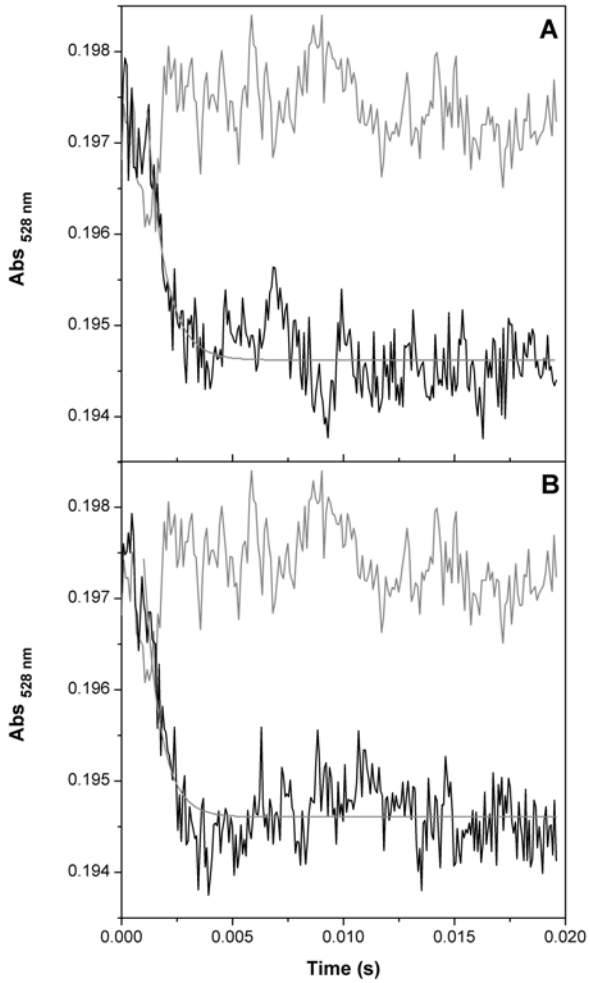

Figure 2.9 Stopped-flow absorbance changes following homolysis in wild-type OAM. Homolysis of the Co–C bond was monitored at 528 nm over 20 ms following rapid mixing of 50 μM holoOAM with 5 mM DL-2,4-diaminobutyric acid (A) and DL-2,4-diaminobutyric-2,3,3,4,4-d_5 acid (B). In both cases, 9 traces were averaged and fit to a single-exponential equation. The observed rate constant for homolysis in wild-type OAM was similar for DABA ($980 \pm 88\ s^{-1}$) and DABA-d_5 ($1140 \pm 150\ s^{-1}$). Blank traces where holoOAM was rapidly mixed against buffer are shown in gray.

2.5 EPR spectroscopy

An EPR signal is not observed upon reaction of native OAM with the natural substrate D-ornithine, consistent with the anaerobic UV-visible spectrum, due to the shortened lifetime of the radical intermediates. However, the enzyme has been shown to exhibit an EPR signal with the substrate analogue DL-2,4-diaminobutyrate, due to the inhibitor's ability to form a persistent radical in the active site (see Section 2.9.2 for further details).[64] The EPR spectrum of WT-OAM with DABA shows a major peak with a $g_{\perp}$ value of 2.11, along with a hyperfine splitting pattern further up field due to coupling between the unpaired electron of the organic radical and the cobalt nucleus[64] (Figure 2.10). A similar EPR spectrum was also observed for glutamate mutase.[104] The shifted $g_{\perp}$ value for cob(II)alamin, and the fact that only one triplet species is observed (as opposed to two), suggests that the lone pair on the cob(II)alamin is strongly exchange-coupled to the organic radical. Simulations of the glutamate mutase EPR spectrum indicate that the distance between the two paramagnetic centers is ~ 7 Å. Given that OAM elicits a similar EPR spectrum, it is likely that the distance between the cob(II)alamin and the DABA-PLP radical is also ~ 7 Å.

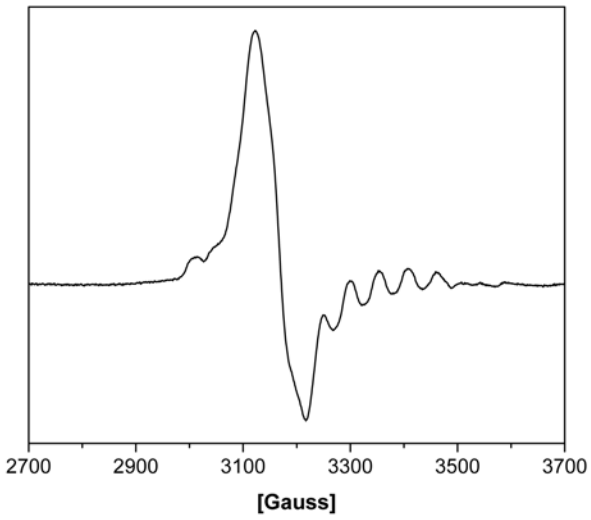

Figure 2.10 EPR spectrum of holoOAM mixed with DL-2,4-diaminobutyrate. An equimolar mixture (600 μM) of apoOAM, PLP, and AdoCbl was prepared. After the addition of 5 mM DL-2,4-diaminobutyrate the sample was loaded into an EPR tube and flash frozen in liquid nitrogen, as described in section 2.10.12. The observed signal is that of cob(II)alamin strongly exchange-coupled to the DABA-PLP organic radical, indicating that the two paramagnetic centers are 7 Å apart.

2.6 Aerobic inactivation of OAM

In the presence of both the natural substrate D-ornithine (Figure 2.11A) and the substrate analogue DL-2,4-diaminobutyrate (Figure 2.11B), wild-type OAM undergoes suicide inactivation under aerobic conditions whereby the cob(II)alamin center is intercepted by molecular oxygen resulting in a build-up of cob(III)alamin (absorbance increase at 358 nm).[64] During turnover with D-ornithine, the rate constant for cob(III)alamin formation is 0.4 min^{-1} for wild-type OAM (Figure 2.12). The rate increases ~4-fold in the presence of the inhibitor DABA (1.6 min^{-1}).

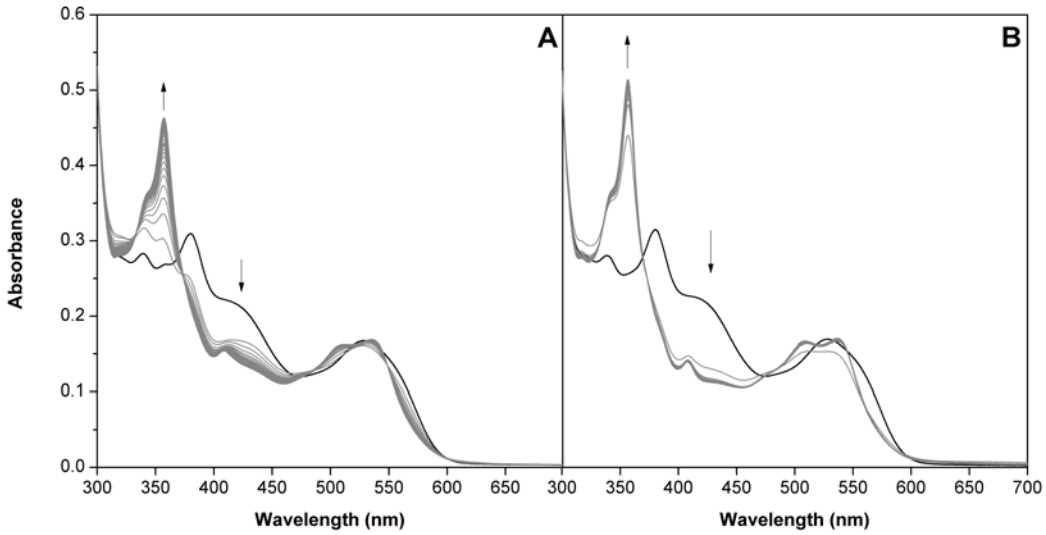

Figure 2.11 Aerobic UV-visible spectrum of wild-type OAM. The holoenzyme solution contained 15 μM OAM, 15 μM PLP, and 15 μM AdoCbl in 100 mM NH_4^+EPPS pH 8.5. Spectral changes for wild-type OAM were recorded prior to the addition of substrate (black lines) and then every minute for 30 minutes (gray lines) following the addition of 2.5 mM D-ornithine (A) and 2.5 mM DL-2,4-diaminobutyrate (B). The rapid absorbance increase at 358 nm represents the build-up of cob(III)alamin as the cob(II)alamin center is intercepted by molecular oxygen. The decrease in absorbance at 416 nm reflects formation of the external aldimine.

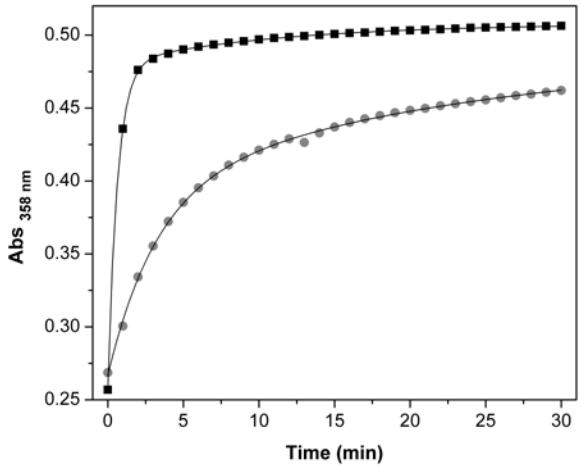

Figure 2.12 Aerobic formation of cob(III)alamin by wild-type OAM. The rate of cob(III)alamin formation upon reaction with D-ornithine (gray circles) is 0.4 min^{-1}. The rate of inactivation with DL-2,4-diaminobutyrate (black squares) increases 4-fold (1.6 min^{-1}). Data were fit to a double exponential equation to determine the observed rates for cob(III)alamin formation.

2.7 5,6-LAM active site modeling

While crystal structures of OAM in both substrate-free and substrate-bound forms are available, only a resting-state crystal structure is available for 5,6-LAM.[75] In order to compare the substrate binding sites of OAM and 5,6-LAM, D-lysine and L-β-lysine were modeled into the 5,6-LAM active site using the AutoDock software package. One hundred structures were generated for each simulation and clustered by conformational similarity (rmsd within 2.0 Å). Structures were ranked from lowest to highest energy within each cluster. Each cluster was ranked based on its lowest energy structure (Figure 2.13). In order for a structure to be considered a viable fit, the PLP portion of the ligand had to overlay with the original PLP cofactor in the substrate-free structure of 5,6-LAM.

The PLP-D-lysine simulation generated 31 distinct conformational clusters. The largest cluster consists of 20 structures and also contains the lowest energy structure. Analysis of this lowest energy structure reveals that the PLP portion of the ligand superimposes almost exactly with the original PLP cofactor, thereby retaining the numerous interactions between the enzyme and the phosphate group of PLP. The D-lysine portion of the ligand interacts primarily with two residues: Lys370 interacts with the α-carboxylate group,

while Asp298 interacts with the α-amino group (Figure 2.14A). Analogous interactions are observed in OAM. Arg297 in OAM replaces Lys370 of 5,6-LAM, while Glu81 replaces Asp298 (Figure 2.15). Similar results were obtained for the PLP-L-β-lysine simulation, which generated 25 distinct conformational clusters. The lowest energy cluster contained 40 structures including the lowest energy structure. This lowest energy structure retains all of the interactions observed with the PLP-D-lysine structure (Figure 2.14B).

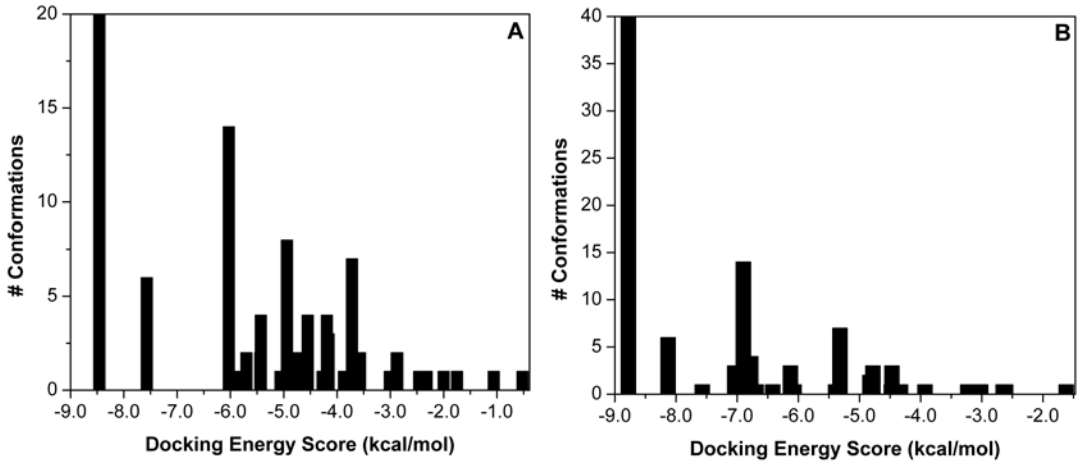

Figure 2.13 Histograms of the 100 conformations generated in the (A) D-lysine-PLP and (B) L-β-lysine-PLP simulations carried out in AutoDock version 4.2.5.1. Conformations are organized into clusters based on an rmsd of 2.0 Å or less. Clusters are ranked by the lowest energy conformation existing in each cluster.

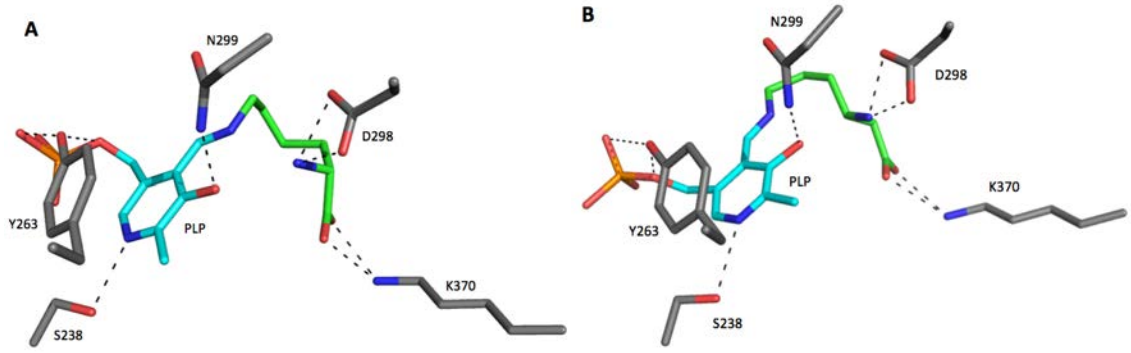

Figure 2.14 Model of the 5,6-LAM active site with bound substrate. 5,6-LAM with substrates D-lysine (A) and L-β-lysine (B) in the active site forming interactions with residues Lys370 and Asp298.

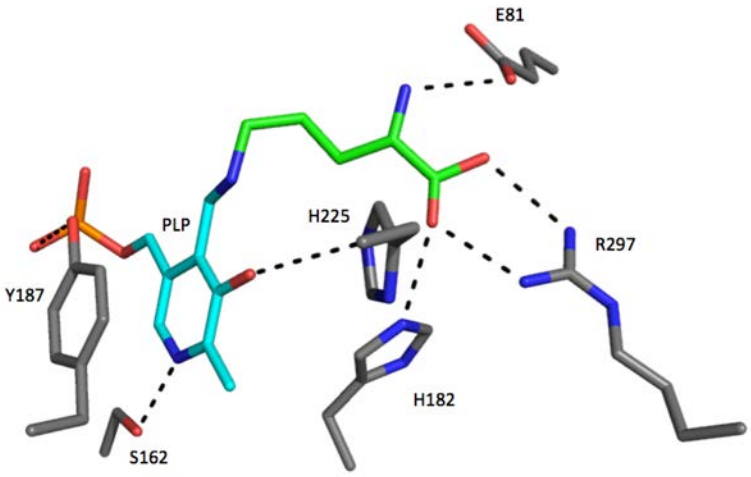

Figure 2.15 Active site of ornithine 4,5-aminomutase complexed with the natural substrate D-ornithine (PDB entry 3KOZ). The substrate (green) forms a covalent Schiff base linkage with the imine nitrogen of the PLP cofactor (cyan). Selected active site residues interacting with the substrate and PLP cofactor are shown in gray. In particular, Tyr187 forms a π-stacking interaction with the pyridine ring of PLP, the guanidinium side-chain of Arg297 forms a salt bridge with the α-carboxylate group of the substrate, and residues His225, His 182, Asn226, Glu81, and Ser162 provide additional hydrogen-bonding interactions with the substrate and cofactor.

2.8 Attempts to increase substrate promiscuity in OAM

To evaluate the potential for the development of OAM as a biocatalyst, attempts were made to broaden the range of substrates that the enzyme is able to accept. The substrate-bound crystal structure of OAM reveals that Arg297 forms a bidentate ionic interaction with the α-carboxylate of the substrate (Figure 2.15). The modeling studies indicate that this interaction is replaced by a single salt bridge between Lys370 and the α-carboxylate of the substrate in 5,6-LAM. Wild-type OAM is unable to accept D-lysine, which is one carbon longer than D-ornithine, as a substrate. This could be attributed to the presence of Arg297, which is one carbon longer than the analogous lysine residue in 5,6-LAM. As such, Arg297 likely controls substrate length in OAM. Here we have mutated Arg297 to a lysine residue to examine its role in OAM catalysis.

Aerobic spectral studies with R297K reveal that formation of the external aldimine species is impaired in the variant, as evidenced by the absorbance changes at 416 nm (Figure 2.16). In the case of D-ornithine (Figure 2.16A), the absorbance increases at 416 nm unlike the wild-type enzyme, which shows a strong absorbance decrease at 416 nm (Figure 2.11A). In contrast, upon binding of DL-2,4-diaminobutyrate (Figure 2.16B) the absorbance still decreases at 416 nm, albeit to a lesser degree than observed in the native enzyme (Figure 2.11B). A small amount of cob(III)alamin is formed (increase at 358 nm) upon reaction with D-ornithine and DL-2,4-diaminobutyrate, indicating that the enzyme is still able to cleave the Co–C bond of the adenosylcobalamin cofactor even though no homolysis is detected spectrally.

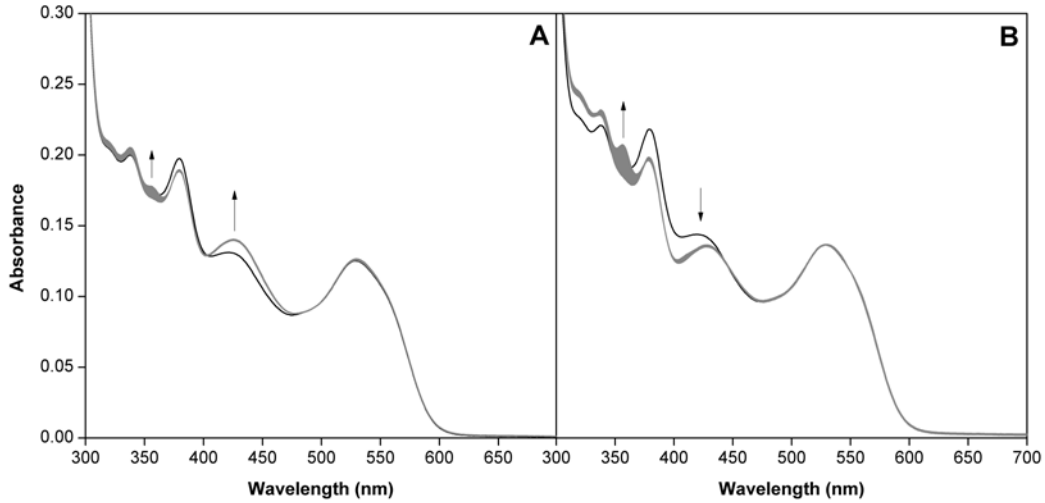

Figure 2.16 Aerobic binding spectra for OAM R297K variant. The holoenzyme solution contained 15 μM OAM, 15 μM PLP, and 15 μM AdoCbl in 100 mM NH_4^+EPPS pH 8.5. Spectral changes were recorded before (black lines) and after (gray lines) the addition of 2.5 mM D-ornithine (A) and DL-2,4-diaminobutyrate (B). Spectra were recorded every minute for 60 minutes.

The R297K variant was also reacted with D-lysine to assess whether the active site of OAM is now large enough to accept the longer substrate. As seen in Figure 2.17, the R297K variant exhibits a similar UV-visible binding spectrum with D-lysine to that with D-ornithine, suggesting that R297K may be able to bind D-lysine. The absorbance at 416 nm initially

increases (as with D-ornithine), but then slowly decreases with time. There is no build-up of cob(III)alamin even after 60 minutes indicating that while the enzyme may be able to bind the new substrate to some extent, it remains unable to induce homolysis of the Co–C bond and therefore the formation of any radical intermediates.

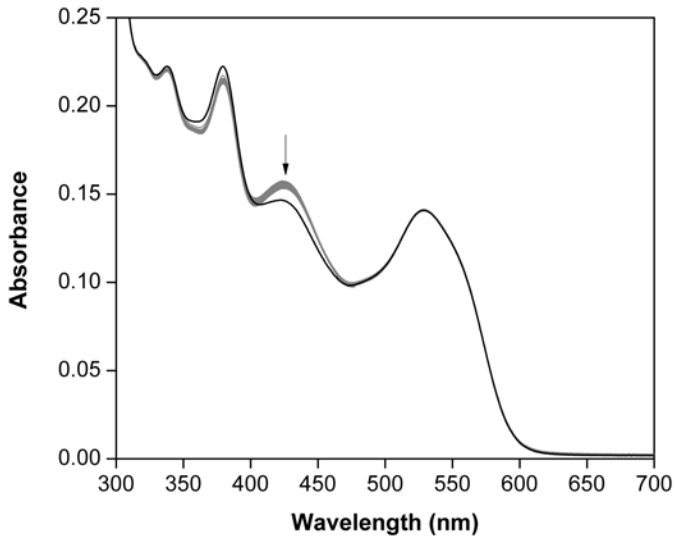

Figure 2.17 Aerobic binding spectrum for OAM R297K with D-lysine. The holoenzyme solution contained 15 μM OAM, 15 μM PLP, and 15 μM AdoCbl in 100 mM NH_4^+EPPS pH 8.5. Spectral changes were recorded before (black line) and after (gray lines) the addition of 2.5 mM D-lysine. Spectra were recorded every minute for 60 minutes. Substrate binding results in an initial increase in absorbance at 416 nm, followed by a slow decrease.

The crystal structure of OAM also reveals that Glu81 forms a salt bridge with the α-amino group of the substrate. The modeling studies suggest that this residue is important for substrate binding given that a similar salt bridge interaction is formed in 5,6-LAM between Asp298 and the substrate. Conservative replacement of Glu81 in OAM with a glutamine results in a significant loss of OAM activity (4500-fold). The UV-visible binding spectra upon addition of D-ornithine (Figure 2.18A) and DL-2,4-diaminobutyrate (Figure 2.18B) indicate that substrate binding is also impaired in this variant, as the absorbance decrease at 416 nm is much smaller than that of the native enzyme. Additionally, there is no cob(III)alamin build-up as evidenced by the lack of an absorbance increase at 358 nm,

indicating that generation of the cob(II)alamin intermediate through homolysis of the Co–C bond is also greatly impaired.

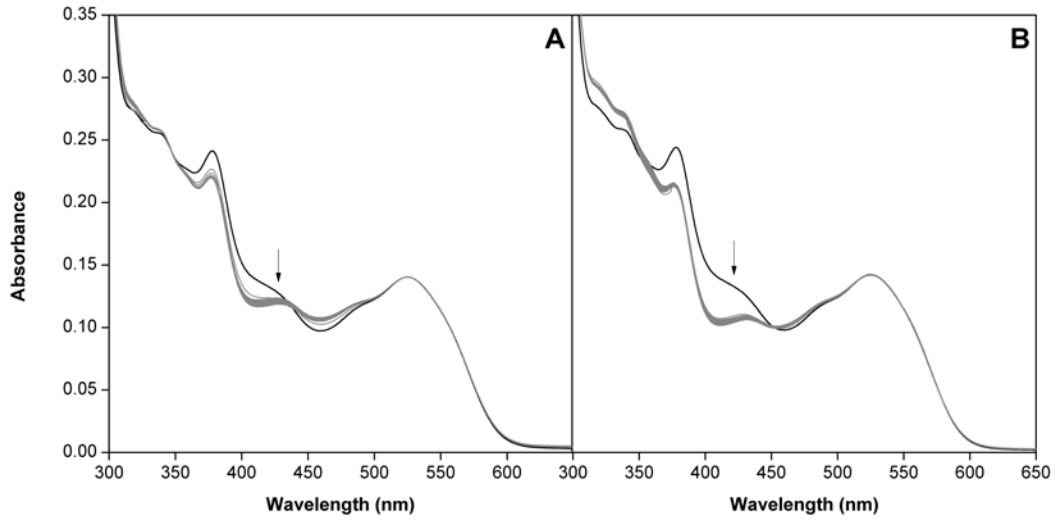

Figure 2.18 Aerobic binding spectra for OAM E81Q variant. The holoenzyme solution contained 15 μM OAM, 15 μM PLP, and 15 μM AdoCbl in 100 mM NH_4^+EPPS pH 8.5. Spectral changes were recorded before (black lines) and every minute for 60 mintues after (gray lines) the addition of 2.5 mM D-ornithine (A) and DL-2,4-diaminobutyrate (B). Formation of the external aldimine is represented by the absorbance decrease at 416 nm. No absorbance increase is observed at 358 nm, indicating a lack of cob(III)alamin build-up.

To further probe the role of both Glu81 and the α-amino group of the substrate in OAM catalysis, wild-type OAM was reacted with 5-aminovaleric acid. The substrate analogue 5-aminovaleric acid lacks the α-amino group but is otherwise identical to the natural substrate D-ornithine. The UV-visible binding spectrum of wild-type OAM with 5-aminovaleric acid (Figure 2.19) differs from that of the E81Q variant with D-ornithine (Figure 2.18A). An even smaller decrease in absorbance at 416 nm is observed; indicating that formation of the external aldimine is dependent on the presence of the α-amino group. Even though less of the external aldimine species is formed compared to E81Q, the wild-type enzyme exhibits a build-up of cob(III)alamin in the presence of 5-aminovaleric acid, indicating that radical intermediates are present even though no Co–C bond homolysis is detected in the UV-visible binding spectrum.

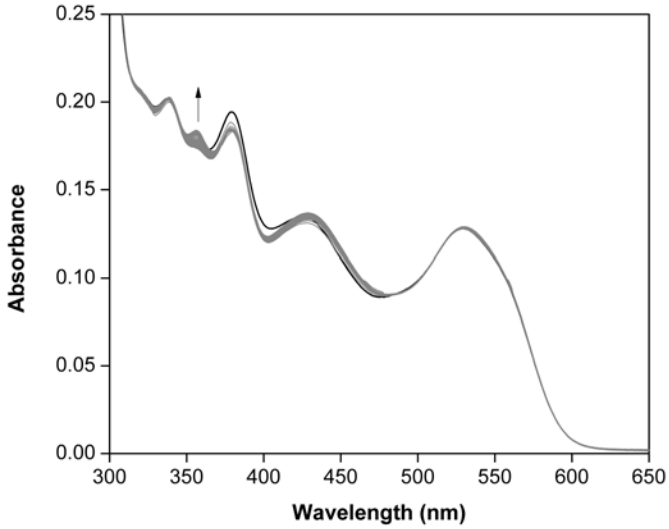

Figure 2.19 Aerobic binding spectra for wild-type OAM with substrate 5-aminovaleric acid. The holoenzyme mixture contained equimolar amounts of OAM, PLP, and AdoCbl in 100 mM NH_4^+EPPS pH 8.5. Spectra were recorded before (black line) and after (gray lines) the addition of 2.5 mM 5-aminovaleric acid. Spectra were recorded every minute for 60 minutes. A slow increase in absorbance is observed at 358 nm, representing formation of cob(III)alamin.

2.9 Discussion

2.9.1 Co–C bond homolysis is gated by transimination

The requirement of pyridoxal 5'-phosphate distinguishes the class III aminomutases from the structurally similar class I mutases. Structural rearrangements are observed in both subclasses upon substrate binding, followed by homolysis of the Co–C bond and abstraction of a hydrogen atom to generate a substrate radical intermediate. In the case of OAM and 5,6-LAM, substrate binding first involves a transimination event whereby the substrate forms a covalent Schiff base linkage with the PLP cofactor (Figure 1.16). The rate constants for homolysis in the class I mutases (GM, MCM), as well as the class II eliminases (ethanolamine ammonia lyase), are estimated via stopped-flow to be >600 s^{-1} at 25 ºC, as the event is mostly complete within the dead-time of the instrument.[64-66, 105] The ability to spectrally follow more of the absorbance decrease outside of the dead-time suggests that the homolysis event is comparatively slower in OAM.[64] KIE experiments with glutamate mutase

and methylmalonyl-CoA mutase have shown that Co–C bond homolysis is kinetically coupled to hydrogen atom abstraction. [65-67, 106, 107] While this is expected to be the case for the class III aminomutases, our results revealed no decrease in the rate constant for homolysis upon reaction of OAM with deuterium-labeled DABA. At first glance it would appear that homolysis is not in fact coupled to hydrogen atom abstraction in the aminomutases. However, given that homolysis is preceded by a transimination step, which exhibits a rate constant of the same order of magnitude, it is more likely that homolysis is gated by the formation of the external aldimine. Thus, the observed rate constant for homolysis in OAM likely reflects the rate of the preceding (and slower) transimination step, indicating that the rate constant for Co–C bond homolysis is likely faster than 500 s^{-1} and therefore not significantly slower than the rate constants observed in other AdoCbl-dependent isomerases.

2.9.2 Mechanism-based inactivation of OAM

Following homolysis in native OAM, the biradical state persists because abstraction of the C4 hydrogen from the 2,4-diaminobutyryl-PLP external aldimine by the 5'-deoxyadenosyl radical results in an unpaired electron on C4 that is proximal to the Schiff base (Figure 2.20).[64] Delocalization of the C4 radical through the conjugated π orbital system of the pyridine ring and imine linkage generates a highly stable 2,4-diaminobutyryl-PLP radical that is unable to re-abstract a hydrogen atom from 5'-deoxyadenosine. As a result, the 5'-deoxyadenosyl radical is unable to re-form to recombine with cob(II)alamin, leading to a build-up of the cob(II)alamin intermediate and mechanism-based inactivation of the enzyme. In contrast, abstraction of a hydrogen atom from C4 of the ornithinyl-PLP external aldimine results in a highly unstable radical intermediate that undergoes rapid intramolecular isomerization to form product. As a result, free radicals are not observed during steady-state turnover with the physiological substrate. The 4-fold increase in the aerobic inactivation rate of OAM upon addition of DABA compared to D-ornithine is attributed to the strong coupling between the 2,4-diaminobutyryl-PLP radical and the cob(II)alamin center, which causes a greater percentage of the enzyme to undergo homolysis and also allows the cob(II)alamin to persist for a greater period of time.[64, 108]

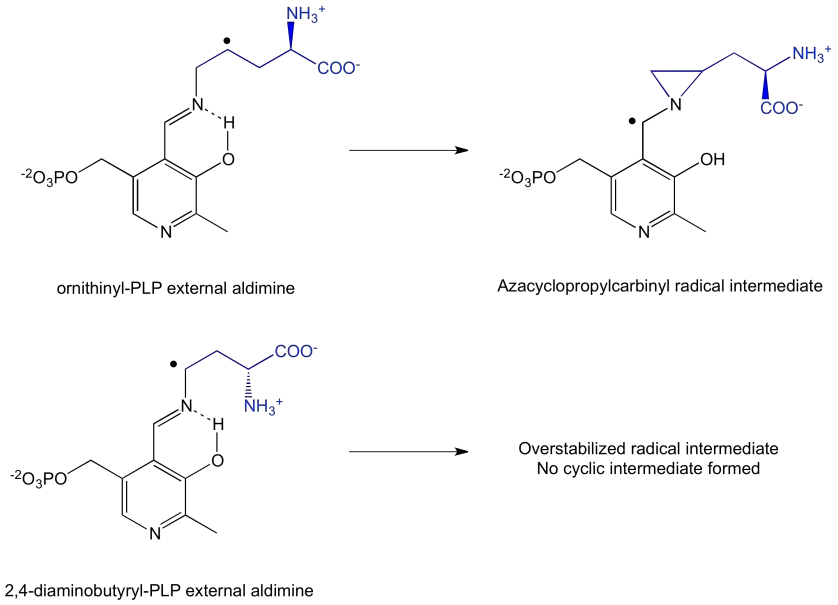

Figure 2.20 Mechanism-based inactivation of OAM. Reaction of OAM with the physiological substrate D-ornithine results in the formation of an unstable radical intermediate that rapidly proceeds through to product formation, and is therefore not detected spectrally. In contrast, the substrate analogue 2,4-diaminobutyrate is one carbon shorter than D-ornithine and abstraction of a hydrogen from C4 therefore results in the formation of a radical that becomes overstabilized through delocalization through the extended π system of the imine linkage and pyridine ring and cannot proceed through to product formation.

2.9.3 Kinetic and structural differences between OAM and 5,6-LAM

Despite being structural homologues, which perform analogous 1,2-amino shifts, OAM and 5,6-LAM exhibit several mechanistic differences. OAM displays high substrate specificity, acting only on the substrate D-ornithine. In contrast, 5,6-LAM is more promiscuous as it is able to accept D- and L-lysine, as well as L-β-lysine as substrates. In addition, even though their PLP binding sites overlay almost exactly, recombinant 5,6-LAM undergoes rapid suicide inactivation at a 10-fold higher rate than that observed in OAM under anaerobic conditions.[101, 108] The mechanism by which 5,6-LAM undergoes suicide inactivation involves direct electron transfer from cob(II)alamin to a substrate/product radical intermediate, thus resulting in a build-up of cob(III)alamin and 5'-deoxyadenosine which can no longer recombine to regenerate the Co–C bond.[101] Under aerobic conditions the

inactivation rate of OAM increases 5-fold, while 5,6-LAM appears to be insensitive to further inactivation by molecular oxygen. The differing abilities of these enzymes to stabilize and control their radical intermediates could be attributed to structural variations within their active sites.

5,6-LAM elicits a high $^{D}k_{cat}$ value of 10.4 ± 0.3 and a $^{D}k_{cat}/K_m$ value of 8.3 ± 1.9, suggesting that hydrogen atom abstraction is the rate-limiting step of the mechanism.[100] In comparison, OAM presents an unusual case in which the value of $^{D}k_{cat}/K_m$ (2.5 ± 0.5) is smaller than the corresponding kinetic isotope effect on k_{cat} (7.6 ± 0.5). The magnitude of $^{D}k_{cat}$ suggests that hydrogen atom abstraction is at least partially rate-determining in the enzyme-substrate complex, while the difference in the values of $^{D}k_{cat}$ and $^{D}k_{cat}/K_m$ may be the result of a large forward commitment to catalysis in OAM. The value of k_{cat}/K_m includes all the rate constants of the mechanism from the binding of substrate up to and including the first irreversible step. k_{cat} on the other hand is independent of substrate binding and includes only those rate constants following formation of the enzyme-substrate complex.. If an enzyme-substrate complex exhibits a greater tendency to dissociate back into free enzyme and substrate, rather than proceed forward through catalysis, then the values of $^{D}k_{cat}$ and $^{D}k_{cat}/K_m$ will be of a similar magnitude. However, if the rate of product formation is fast relative to the rate of dissociation of unreacted substrate from the enzyme then the observed $^{D}k_{cat}/K_m$ value will be suppressed relative to $^{D}k_{cat}$.[109, 110]

The suppression in the magnitude of the KIE on k_{cat}/K_m for OAM suggests that the substrate is ‘sticky’ or has a relatively tight binding affinity for the active site. The crystal structure of OAM shows numerous noncovalent interactions with the substrate, including a bidentate ionic interaction between the α-carboxylate of D-ornithine and the guanidinium side-chain of Arg297, a salt bridge between Glu81 and the α-amino group of the substrate, and a polar interaction between the imidazole side chain of His182 and the α-carboxylate of D-ornithine. Modeling of D-lysine and L-β-lysine into the active site of 5,6-LAM reveals fewer substrate-protein interactions. In 5,6-LAM, a single salt bridge to Lys370 replaces the Arg297 bidentate interaction with the α-carboxylate, the side chain Asp298 replaces Glu81 in securing the α-amino group, and there is no corresponding residue for His182 in OAM. More noncovalent interactions between the protein and ornithinyl-PLP complex may result in a slower rate of substrate release from the enzyme thereby accounting for the suppressed KIE

on $^{D}k_{cat}/K_m$. Fewer and weaker substrate interactions in 5,6-LAM likely increase the rate of substrate release relative to product formation (allowing for greater expression of the KIE on $^{D}k_{cat}/K_m$) and could account for the enzyme's ability to accommodate different isomers of lysine into the active site.

2.9.4 Weaker substrate binding interactions are deleterious in OAM

We have confirmed through mutagenesis studies that Arg297 and Glu81 are indeed important for substrate binding and formation of the external aldimine species in OAM. Mutation of Arg297 to a lysine residue effectively increases the size of the active site by ~2 Å. However, the strength of the interaction with the substrate is decreased due to replacement of the bidentate interaction with a single salt bridge. The R297K variant is unable to induce homolysis of the Co–C bond upon addition of D-lysine, indicating that although the active site is larger, OAM still cannot effectively accommodate the longer substrate. This could be explained by unfavorable positioning of the substrate within the active site, such that the α-amino group cannot interact with Glu81. Even though the polar interaction with the α-amino group of the substrate is retained (albeit weaker) in E81Q, the lack of a build-up of cob(III)alamin suggests that the variant is unable to accomplish the necessary structural rearrangements upon substrate binding to induce homolysis of the Co–C bond. In comparison, even though substrate binding is further hindered by complete removal of the α-amino group from the substrate, the wild-type enzyme displays evidence of the presence of radical intermediates (based on the accumulation of cob(III)alamin). The presence of Glu81 in the active site therefore appears to be more important than the presence of the α-amino group of the substrate with respect to radical generation and stabilization. The modeled closed structure of OAM shows that Glu81 is in close proximity to the adenosyl moiety of the AdoCbl cofactor (Figure 2.21), and therefore could also participate in Co–C bond labilization or stabilization of the Ado• transition state in addition to its role in securing the α-amino group of the substrate.

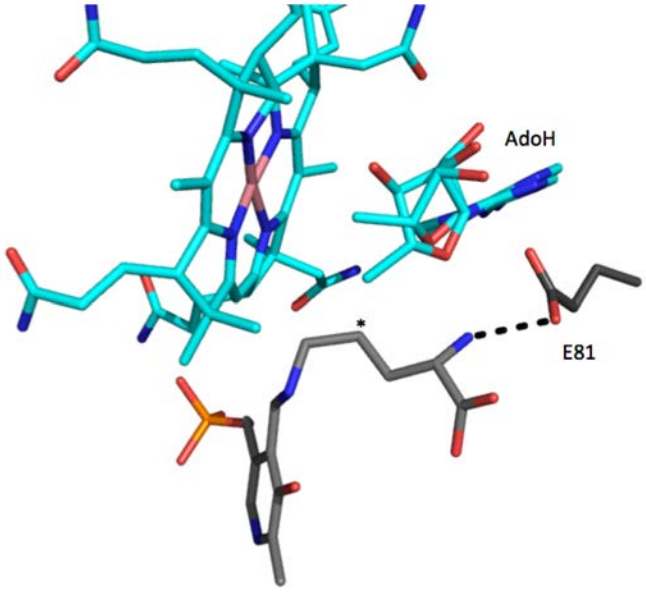

Figure 2.21 Modeled active site of OAM in the closed conformation. In addition to forming a salt bridge interaction with the α-amino group of the substrate (dashes), E81 is also in close proximity to the adenosyl moiety of the AdoCbl cofactor. An asterisk indicates the site of hydrogen atom abstraction from the substrate.

In summary, we have shown that the requirement of an additional cofactor to accomplish radical catalysis in the Class III aminomutases results in kinetic gating of Co–C bond homolysis by the preceding transimination step of the mechanism. We also propose that weaker substrate binding interactions contribute to increased substrate promiscuity in 5,6-LAM, but at the cost of the enzyme being more prone to spurious radical side reactions. In comparison, a tighter active site in OAM leads to increased substrate specificity, as well as more controlled radical chemistry. Attempts to increase the substrate promiscuity of OAM through weakening of substrate binding interactions were unsuccessful and deleterious to enzyme activity.

2.10 Experimental Procedures

2.10.1 Materials

AdoCbl, PLP, D-ornithine, L-ornithine, DL-2,4-diaminobutyric acid, D-lysine, and 5-aminovaleric acid were obtained from Sigma. L-ornithine-3,3,4,4,5,5-d_6 hydrochloride was obtained from C/D/N Isotopes Inc. The Ni^{2+}-nitrilotriacetic acid (Ni-NTA) column and Q-sepharose High Performance resins were from GE Biosciences. Restriction endonucleases were from New England Biolabs, *Pfu* Turbo DNA polymerase was from Agilent Technologies, and Rosetta(DE3)pLysS competent cells were purchased from EMD Biosciences. All other chemicals were purchased from Fisher Scientific and were of the highest grade available.

2.10.2 Cloning and expression of (2R,4S)-2,4-diaminopentanoate dehydrogenase (DAPDH)

The coding sequence for DAPDH was amplified from *C. difficile* genomic DNA (obtained as a gift from the Sanger Institute) with *Pfu* Turbo DNA polymerase using the primers 5'-CAT AAG TAG **CAT ATG** AGA AAA GTA AGA GTA GGA ATA TGG-3' (forward primer) and 5'-TGA TAC GAT **AAG CTT** ATT AGC CTT TGA TTC TTC TTC C-3' (reverse primer), which contain the NdeI and HindIII restriction sites (shown in boldface type), respectively. The PCR cycle parameters were as follows: 94 °C for 4 min followed by 30 cycles of 94 °C for 45 s, 53 °C for 1 min, and 72 °C for 6 min followed by a final 10 min extension at 72 °C. The PCR product was digested with NdeI and HindIII and inserted into the pET41a vector (EMD Biosciences), which had been digested with the same restriction enzymes. The ligation mixture was transformed into *Escherichia coli* strain XL1 Blue (Agilent). The cloning strategy inserted a hexahistidine tag onto the C-terminus of DAPDH and the resulting plasmid was designated pET-DAPDH. Sequencing of the plasmid by the DNA Sequencing Laboratory at University of British Columbia, Vancouver, Canada confirmed that no PCR-induced errors had occurred. pET-DAPDH was transformed into Escherichia coli strain Rosetta(DE3)pLysS, and a single transformed colony was used to

inoculate Luria-Bertani (LB) medium (5 ml) containing ampicillin (100 μg/mL) and chloramphenicol (35 μg/mL), and the culture was grown for 8 h at 37 °C. The 5 mL culture was used to inoculate LB medium (200 mL) with ampicillin (100 μg/mL) and chloramphenicol (35 μg/mL), which was subsequently grown at 37 °C for 16 h. Ten milliliters from the 200 mL starter culture was used to inoculate Terrific Broth (0.5 L) containing the same antibiotics. The culture was grown at 32 °C with shaking (220 rpm) until the culture reached an optical density at 600 nm of 1.0, at which time isopropyl β-D-1-thiogalactopyranoside (0.1 mM) was added. The temperature of the incubator was reduced to 25 °C, and the culture was allowed to grow for a further 16 h. Cells were harvested by centrifugation (4000 x g, 15 min, 4 °C), and the cell pellet was stored at –80 °C until purification.

2.10.3 Cloning and expression of ornithine racemase (OR)

The gene sequence encoding ornithine racemase (OR) was PCR-amplified from *Clostridium difficile* (Hall and O'Toole) Prevot (ATCC BAA-1382D-5) genomic DNA with *Pfu* DNA polymerase. The forward and reverse primers were 5'-CAT AAG TAG **CAT ATG** TAT CCT AGG TTA GAA ATA G-3' (NdeI restriction site in bold) and 5'-TGA TAC CAT **AAG CTT** CAC TAT AAT TTT TTT TGC AAC ATA TTT GC-3' (HindIII restriction site in bold), respectively. The PCR product was digested with NdeI and HindIII and then ligated into the pET-41a vector (EMD Biosciences) also cut with the same restriction enzymes. The resulting plasmid, designated pET-OR, was transformed into *E. coli* XL1-blue cells (Agilent Technologies). Sequencing by the NAPS DNA Sequencing Laboratory at University of British Columbia, Vancouver, Canada confirmed the absence of any PCR-induced errors. The pET-OR plasmid was then transformed into *E. coli* Rosetta(DE3)pLysS cells for overexpression of the protein. A single colony was used to inoculate 5 mL of LB broth containing 100 μg/mL of ampicillin and 34 μg/mL of chloramphenicol. The culture was grown for 8 hrs at 37 °C, transferred to 200 mL of LB broth containing the same antibiotics, and then grown at 37 °C for 16 hrs. Ten milliliters of the 200 mL starter culture was used to inoculate 0.5 L of Terrific Broth (TB) containing ampicillin (100 μg/mL) and

chloramphenicol (34 μg/mL), which was then grown at 30 °C until an $O.D._{600}$ of 1.0 at which point the cells were induced with 0.1 mM isopropyl-ß-D-1-thiogalactopyranoside, and then grown for an additional 16 hrs at 20 °C. The cells were pelleted and stored at –80 °C.

2.10.4 Construction of the OAM variants

The R297K and E81Q single-point mutations were introduced into the pETOAMH2 vector[64] using the QuikChange site-directed mutagenesis kit (Agilent Technologies, Mississauga, ON). The complementary primers for the R297K variant are 5'-GAA GGA TAT AGA ATG AAA GCA CAG ATG AAT ACA AAG-3' and 5'-CTT TGT ATT CAT CTG TGC TTT CAT TCT ATA TCC TTC-3'. The forward and reverse primers for the E81Q variant are 5'-CCA GTA ATC ACA ACA CAG ATT GCT TCA GGA AG-3' and 5'-CT TCC TGA AGC AAT CTG TGT TGT GAT TAC TGG-3', respectively. The NAPS DNA Sequencing Laboratory at University of British Columbia, Vancouver, Canada, confirmed the sequences of the R297K and E81Q mutations.

2.10.5 Enzyme Purification

OAM, DAPDH, and OR were all purified using the same general protocol. All purification steps were carried out at 4 °C. Cells overexpressing the respective protein (15 g to 50 g, wet weight) were resuspended in 250 mL of 50 mM Tris pH 7.5, containing the protease inhibitors benzamidine (2 mM) and PMSF (1 mM). The mixture was then sonicated (8 s pulses every minute for 45 min, power setting 21 %) using a Misonix sonicator, followed by centrifugation at 25,000 × g for 45 minutes to remove cellular debris. Upon addition of NaCl and imidazole to a final concentration of 0.5 M and 20 mM, respectively, the crude extract was run over a 5 mL HisTrap-FF column (GE Biosciences) equilibrated with 50 mM Tris pH 7.5, 0.5 M NaCl, and 20 mM imidazole. The protein was eluted with 300 mM imidazole. Fractions containing the enzyme were pooled and dialyzed against 50 mM Tris pH 7.5, 1 mM EDTA, and 2 mM β-mercaptoethanol. OAM and DAPDH were dialyzed for 16 h at 4 C, while OR was only dialyzed for 2 h. Dialysis longer than 2 h resulted in precipitation of OR. The protein was then loaded onto a 58-mL Q-sepharose HP column (2.6

x 11 cm) equilibrated with 50 mM Tris pH 7.5. After application of the protein, the column was washed with 120 mL of 50 mM Tris pH 7.5, and eluted with a linear gradient from 0 mM to 500 mM NaCl. Fractions containing the enzyme were pooled and concentrated. A Lowry Assay, using bovine serum albumin as a standard, was performed to determine the concentration of each enzyme. After making 20 % glycerol stocks, the enzyme was flash frozen in liquid nitrogen and stored at –80 °C.

2.10.6 Preparation of DL-ornithine and DL-ornithine-3,3,4,4,5,5-d_6

Ornithine racemase was used to synthesize a racemic mixture of DL-ornithine from L-ornithine using the following procedure: a 10 mL mixture containing 100 mM L-ornithine, 10 μM ornithine racemase and water at pH 8.0, was stirred gently for 18 hr at 20 °C (pH monitored periodically). Aluminum foil was wrapped around the reaction flask to minimize exposure of the pyridoxal 5'-phosphate cofactor to ambient light. The reaction mixture was passed through a 30 kDa MW cutoff filter, to remove the enzyme, and then dried under reduced pressure. The resulting solid was washed with ethanol and then dried under reduced pressure, leaving behind a fine white powder. ^{1}H-NMR was used to confirm the purity of the ornithine product. The same procedure was used to synthesize DL-ornithine-3,3,4,4,5,5-d_6 from L-ornithine-3,3,4,4,5,5-d_6.

2.10.7 Coupled enzyme assays

OAM activity was measured using a coupled spectrophotometric assay with DAPDH. Kinetic assays were performed in a 1.0 mL volume at 25 °C using a 1 cm path length cuvette. OAM activity was measured by recording the absorbance change at 340 nm associated with the reduction of NAD^+ ($\Delta\varepsilon$ = 6220 M^{-1} cm^{-1}). Purified recombinant OAM is devoid of cofactor; therefore, to make a functionally active holoenzyme, equimolar amounts of PLP and AdoCbl were added to the apo-form of the protein. The reaction mixtures contained 50 mM NH_4^+EPPS, pH 8.5, 100 nM holoOAM, 100 nM DAPDH, 0.5 mM NAD^+ and variable concentrations of substrate. Reactions were performed under low ambient light conditions and were initiated with the addition of substrate (D-ornithine, DL-ornithine, or DL-

ornithine-3,3,4,4,5,5-d_6). Data from the substrate concentration dependence experiments were fit to the Michaelis-Menten equation (Eq. 2.1) using the computer program Origin, version 8.5 (MicroCal Software Inc.).

$$\upsilon_i = \frac{VA}{K_m + A} \qquad \text{Eq. 2.1}$$

where υ_i is the initial velocity, V is the maximal velocity, A is the concentration of substrate, and K_m is the Michaelis constant for the substrate. The kinetic parameter k_{cat} was determined by dividing the maximal velocity by the enzyme concentration.

2.10.8 Equilibrium constant determination

The equilibrium constant for the reaction of wild-type OAM with D-ornithine was determined using ^{1}H-NMR spectroscopy. An equimolar mixture (2 μM) of apo-OAM, AdoCbl, and PLP in 20 mM Tris pH 8.5 was reacted with 5 mM D-ornithine under anaerobic and low ambient light conditions for 18 h at 25 °C. The sample was then lyophilized, reconstituted in D_2O, and run at 400 MHz on a Varian Mercury VX Spectrometer at 298 K. The relative integrals were compared for the protons on C5 of D-ornithine and the product DAP, corrected to their relative number of protons.

2.10.9 Anaerobic UV-visible spectroscopy

Anaerobic UV-visible spectroscopic assays were performed in a Belle Technology glove box (O_2 <5 ppm) using a Hitachi U-1800 spectrophotometer at 25 °C. Buffer (100 mM NH_4^+EPPS, pH 8.5) was purged for 2 hrs with nitrogen and then brought into the glove box and allowed to equilibrate for 18 hrs in an oxygen-free environment. Solid AdoCbl, PLP, D-ornithine, and DL-2,4-diaminobutyric acid were introduced to the glove box and dissolved in anaerobic buffer. A concentrated protein sample (2 mL of 12 mg/mL) was introduced into the glove box and gel-filtered using a 10 mL Econo-pack column (Bio-Rad) equilibrated with anaerobic buffer. A reference spectrum was recorded using buffer alone. For reactions involving the holoenzyme, a 1 mL reaction mixture contained 15 μM apoOAM, 15 μM PLP,

and 15 μM AdoCbl in 100 mM NH_4^+EPPS, pH 8.5. The reaction was initiated by the addition of 2.5 mM D-ornithine or 2.5 mM DABA, and spectra were recorded from 700 to 300 nm every 60 seconds for 20 minutes.

2.10.10 Aerobic UV-visible spectroscopy

Aerobic spectral assays were carried out on a Perkin Elmer Lambda 25 spectrophotometer at 25 ºC. Each 1 mL reaction contained 15 μM apoOAM, 15 μM PLP, and 15 μM AdoCbl in 100 mM NH_4^+EPPS buffer (pH 8.5). Each reaction was initiated with the addition of 2.5 mM DL-2,4-diaminobutyrate or D-ornithine and scans were collected from 700 to 300 nm every minute for 30 to 60 minutes.

2.10.11 Stopped-flow spectroscopy

Anaerobic stopped-flow studies were performed using as SF-61DX2 stopped-flow instrument (TgK Scientific). The sample-handling unit of the stopped-flow instrument was housed in a specialized glove box (Belle Technology) in which the O_2 concentration was <5 ppm. Anaerobic solutions of buffer, enzyme, cofactors, substrate, and substrate analogues were prepared as described in section 2.10.9. Transient kinetic experiments were performed in 100 mM NH_4^+EPPS (pH 8.5) at 25 °C. The cofactors PLP and AdoCbl were added to the apoenzyme in equimolar concentrations to form the holoenzyme. HoloOAM (50 μM) was rapidly mixed with 5 mM DL-2,4-diaminobutyrate.

2.10.12 EPR spectroscopy

Approximately 2 ml of a protein sample (20 mg/ml) was introduced into the anaerobic glove box and gel-filtered over a PD10 column equilibrated with 100 mM NH_4^+EPPS, pH 8.5. The filtered sample was then concentrated under anaerobic conditions to > 0.6 mM using a Vivaspin 500 centrifugal concentrator with a molecular weight cutoff of 30 kDa (GE Biosciences). Powdered forms of the cofactors, substrate, and inhibitor were introduced into the glove box and dissolved in anaerobic buffer prior to use. An equimolar

mixture (600 μM) of enzyme, PLP, and AdoCbl was prepared and allowed to incubate for 5 min. After the addition of either 5 mM D-ornithine or DL-2,4-diaminobutyrate, the samples were mixed thoroughly, loaded into EPR tubes and frozen in liquid nitrogen. All sample preparation steps were carried out anaerobically at 25 °C under low light conditions to minimize photolysis of the AdoCbl Co–C bond. EPR samples were run at 77 K. EPR spectra were recorded at a frequency of 9.379 GHz, microwave power of 2.0 mW, time constant of 40.96 ms, and modulation amplitude of 6 G. Five two minute scans were averaged for each sample.

2.10.13 Substrate Docking Simulations

Molecular docking simulations were carried out using AutoDock version 4.2.5.1 obtained from the Scripps Research Institute (La Jolla, CA). The starting coordinates for lysine 5,6-aminomutase (1XRS)[75] were obtained from the Protein Data Bank (PDB). Since substrate binding results in breakage of a covalent bond between the enzyme and the PLP cofactor, followed by formation of a new covalent bond between PLP and the substrate, the PLP cofactor coordinates were removed from the original PDB file. The PLP-substrate adduct was then modeled into the active site of the enzyme. Given that LAM accepts both D-lysine and L-β-lysine, input files for PLP- D-lysine and PLP- L-β-lysine were generated with hydrogen atoms using ChemBio3D Ultra 12.0 (CambridgeSoft Corp., Cambridge, MA). Both input files were energy minimized using MM2 prior to running AutoDock.

AutoDock Tools was used to prepare the ligand and rigid receptor coordinate files for the two docking simulations. Hydrogen atoms were added to the receptor and Gasteiger partial atomic charges were assigned to the ligand and the receptor. In both simulations, 10 of the possible 12 torsions in the respective ligand were active in order to preserve the intramolecular hydrogen bond, which exists between the imine nitrogen and the hydroxyl group of the pyridine ring. The search space was confined to a 22.5 Å x 22.5 Å x 22.5 Å box centered at 57.000, 42.000, and 80.101 so as to include the site of the original PLP cofactor. One hundred structures were generated using the Lamarkian genetic algorithm. Default parameters were used and the number of energy evaluations was set to 250000. Solution

structures were clustered according to their conformational similarities and then ranked from lowest to highest energy within each cluster.

Chapter 3 : Mutagenesis of a Conserved Glutamate Reveals the Contribution of Electrostatic Energy to Adenosylcobalamin Co–C Bond Homolysis in Ornithine 4,5-Aminomutase and Methylmalonyl-CoA Mutase

3.1 Chapter Summary

Binding of substrate to ornithine 4,5-aminomutase (OAM) and methylmalonyl-CoA mutase (MCM) leads to the formation of an electrostatic interaction between a conserved glutamate side chain and the adenosyl ribose of the adenosylcobalamin (AdoCbl) cofactor. The contribution of this residue (Glu338 in OAM from *Clostridium sticklandii* and Glu392 in human MCM) to AdoCbl Co–C bond labilization and catalysis was evaluated by substituting the residue with a glutamine, aspartate, or alanine. The OAM variants, E338Q, E338D, and E338A, showed 90-, 380-, and 670-fold reductions in catalytic turnover and 20-, 60-, and 220-fold reductions in k_{cat}/K_m, respectively. Likewise, the MCM variants, E392Q, E392D, and E392A, showed 16-, 330-, and 12-fold reductions in k_{cat}, respectively. Binding of substrate to OAM is unaffected by the single amino acid mutation as stopped-flow absorbance spectroscopy showed that the rates of external aldimine formation in the OAM variants were similar to that of the native enzyme. The decrease in the level of catalysis is instead linked to impaired Co–C bond rupture, as UV-visible spectroscopy did not show detectable AdoCbl homolysis upon binding of the physiological substrate, D-ornithine. AdoCbl homolysis was also not detected in the MCM variants, as it was for the native enzyme. We conclude from these results that a gradual weakening of the electrostatic energy between the protein and the ribose leads to a progressive increase in the activation energy barrier for Co–C bond homolysis, thereby pointing to a key role for the conserved polar glutamate residue in controlling the initial generation of radical species.

3.2 Identification of a conserved glutamate in the AdoCbl-dependent mutases

Although the aminomutases have not been structurally captured in the top-on arrangement, evidence that they populate this conformational state during catalysis is provided by EPR spectra of OAM[64] and 5,6-LAM[111] in the presence of substrate analogues. Modeling of OAM into the top-on state, via rigid-body alignment of the TIM barrels of OAM (PDB entry 3KOZ) and glutamate mutase (PDB entry 1I9C), generates a plausible catalytically ready conformation, as it places C5' of the adenosyl moiety in an optimal position for hydrogen atom abstraction from C4 of the ornithinyl-PLP complex.[76, 112] The top-on model also reveals a glutamate γ-carboxylate (Glu338) in position for polar contact with the 2'-OH and 3'-OH groups of the 5'-deoxyadenosyl ribose moiety (Figure 3.1A). Glu338 of OAM in the top-on model superimposes with Glu330 of glutamate mutase (GM),[83] highlighting the residue's potential catalytic role in both the class I mutases and class III aminomutases.

In the substrate-free structure of class I methylmalonyl-CoA mutase, the Rossmann-like domain is positioned directly above the pore of the TIM barrel, such that the 5'-deoxyadenosyl moiety is occluded from the bulk solvent and near the active site.[77] Despite the low level of sequence homology, this overall domain organization and top-on configuration is seemingly conserved within the class I mutases.[78] Methylmalonyl-CoA enters the MCM active site via the opposite end of the TIM barrel, inducing structural rearrangements that globally amount to a constriction and tightening of the TIM barrel channel.[113, 114] Several conserved residues lining the channel form new contacts with the substrate and/or cofactor. Of particular note is Glu392, which rotates upon substrate binding to form new polar interactions with the ribose 2'-OH and 3'-OH groups (Figure 3.1B), adopting a conformation similar to that of Glu330 in GM and Glu338 in OAM (Figure 3.1A). Formation of this new noncovalent contact between the protein and cofactor is hypothesized, from computational calculations, to lower the activation energy barrier to Co–C bond homolysis in MCM by contributing to electrostatic stabilization of the 5'-deoxyadenosyl radical.[60, 68]

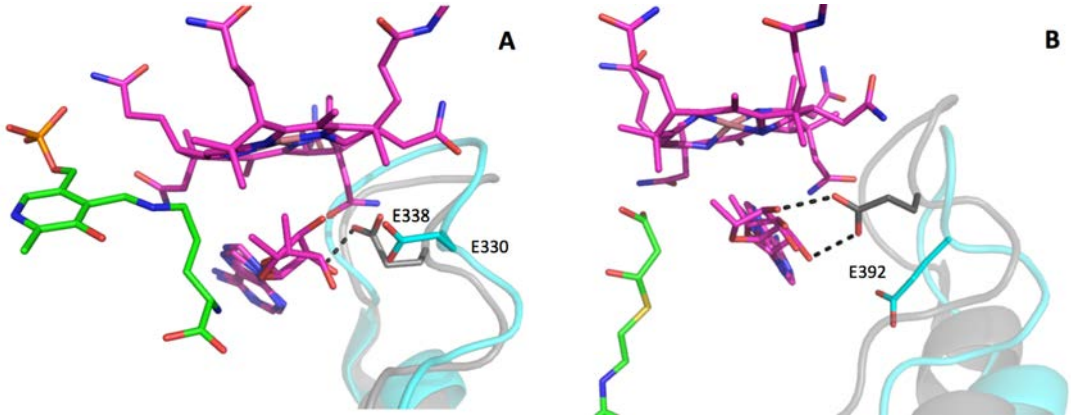

Figure 3.1 Positioning of a conserved glutamate within the active site of AdoCbl-dependent mutases upon substrate binding. (A) The modeled closed conformation of OAM (gray) with ornithinyl-PLP complex (green), showing relative orientation of Glu338 with respect to the 5'-deoxyadenosyl ribose moiety. Shown in cyan is the superimposed TIM barrel of glutamate mutase showing analogous glutamate residue, Glu330. (B) Superposition of substrate-free MCM (cyan) and substrate-bound MCM (gray) showing rotation of Glu392.

A sequence alignment of several different AdoCbl mutases reveals that this glutamate residue is conserved across the class I mutases, with sequences 4–39% similar to that of MCM (Figure 3.2). Given that the ribose-coordinated glutamate potentially plays a catalytic role we have mutated this residue to an alanine, glutamine, and aspartate in OAM and human MCM.

MCM	TQSLHTNSFD**E**ALGLPTV	399
HCM	AQSLHTNGYD**E**AFAIPTE	379
ICM	TNSLHTNALD**E**TLALPSE	369
ECM	ARAVQLPAWN**E**ALGLPRP	307
GM	ATKVIVKTPH**E**AIGIPTK	337
MAM	ADKIITKTKQ**E**ASGIPTK	323

Figure 3.2 Multiple-sequence alignment of different AdoCbl mutases showing the conserved glutamate residue. Human methylmalonyl-CoA mutase (AAA59569.1), HCM (hydroxisobutyryl-CoA mutase) from *Methylibium petroleiphilum* (YP_001023546.1), ICM (isobutyryl-CoA mutase) from *Streptomyces clavuligerus* (EFG09395.1), ECM (ethylmalonyl-CoA mutase) from Rhodobacter sphaeroides (YP_354045.1), GM (glutamate mutase) from *Clostridium tetanomorphum* (CAA49910.1), and MAM (methylaspartate mutase) from *Arcobacter nitrofigilis* (ADG93549.1). Relative to human MCM, the levels of sequence similarity are as follows: 39% for HCM, 38% for ICM, 33% for ECM, 4% for GM, and 4% for MAM.

3.3 Steady-state kinetic properties of the OAM E338 variants

Catalytic turnover for wild-type OAM and the E338 variants was monitored through a coupled spectrophotometric assay, as previously described in section 2.10.7. Wild-type OAM displayed a turnover number of 2.9 ± 0.1 s^{-1} and a K_m value of 190 ± 13 μM for D-ornithine. Substitution of Glu338 with a Gln, whereby the potential for electrostatic interactions with the 2'- and 3'-hydroxyl groups of the ribose moiety is retained, resulted in a 90-fold reduction in k_{cat} (Table 3.1). Displacement of the terminal carboxyl functional group by a distance of ~2 Å, through mutation of Glu338 to Asp, resulted in a more substantial 380-fold decrease in the rate of catalytic turnover. The most profound effect on k_{cat}, a 670-fold decrease, was observed when the polar side chain was removed altogether in the E338A variant. The K_m value for D-ornithine is 42.7 ± 3.3, 30.2 ± 2.1, and 60 ± 4.9 μM for the E338Q, E338D, and E338A variants, respectively. As a result of the altered k_{cat} and K_m values, the catalytic efficiency (k_{cat}/K_m) of each of the variants was decreased in comparison to that of wild-type OAM. Following the same trend observed for catalytic turnover, the E338Q, E338D, and E338A variants showed 20-, 60-, and 220-fold reductions in k_{cat}/K_m, respectively.

Table 3.1 Summary of steady-state kinetic parameters for wild-type OAM and the E338 variants upon reaction with D-ornithine.

Enzyme	k_{cat} (s^{-1})	K_m (μM)	k_{cat}/K_m ($\times 10^3$ $M^{-1}s^{-1}$)
Wild-type	2.9 ± 0.1	190 ± 13	15.2 ± 1.2
E338A	$4.3 \times 10^{-3} \pm 0.1 \times 10^{-3}$	60.6 ± 4.9	0.07 ± 0.01
E338Q	$3.2 \times 10^{-2} \pm 0.01 \times 10^{-2}$	42.7 ± 3.3	0.75 ± 0.08
E338D	$7.6 \times 10^{-3} \pm 0.1 \times 10^{-3}$	30.2 ± 2.1	0.25 ± 0.02

Deuterium kinetic isotope effects were also employed to further investigate the role of Glu338 in OAM catalysis. The kinetic parameters for wild-type OAM and the E338D variant upon reaction with DL-ornithine and DL-ornithine-3,3,4,4,5,5-d_6 are summarized in Table 3.2. Native OAM displays $^{D}k_{cat}$ and $^{D}k_{cat}/K_m$ values of 7.6 ± 0.5 and 2.5 ± 0.4, respectively, upon reaction with DL-ornithine-3,3,4,4,5,5-d_6. In comparison, the E338D variant showed a similar $^{D}k_{cat}$ value (7.2 ± 0.2) to wild-type OAM, while $^{D}k_{cat}/K_m$ was increased ~2.5-fold (6.5 ± 0.9), indicating that the KIE on k_{cat}/K_m is no longer suppressed relative to $^{D}k_{cat}$.

Table 3.2 Summary of steady-state kinetic parameters for wild-type OAM and the E338 variants upon reaction with DL-ornithine and DL-ornithine-3,3,4,4,5,5-d_6.

Enzyme	k_{cat} (s^{-1})	K_m (μM)	k_{cat}/K_m ($M^{-1}s^{-1}$)
Wild-type (DL-orn)	2.9 ± 0.1	570 ± 45	5100 ± 410
Wild-type (DL-orn-d_6)	0.38 ± 0.01	190 ± 11	2000 ± 170
E338D (DL-orn)	$5.7 \times 10^{-3} \pm 0.1 \times 10^{-3}$	59 ± 3	97 ± 7
E338D (DL-orn-d_6)	$7.9 \times 10^{-4} \pm 0.1 \times 10^{-4}$	51 ± 3	15 ± 1

3.4 Purification of methylmalonyl-CoA mutase (MCM)

The class I AdoCbl-dependent mutase, methylmalonyl-CoA mutase (MCM), was heterologously expressed in bacterial cells. The pNIC-CTHF plasmid construct attached a hexahistidine tag to the C-terminus of the enzyme, which was purified using Ni-NTA affinity and Q-sepharose anion exchange chromatography (Figure 3.3). The prominent protein band observed around 80 kDa is consistent with the expected molecular weight of human MCM (78 kDa).

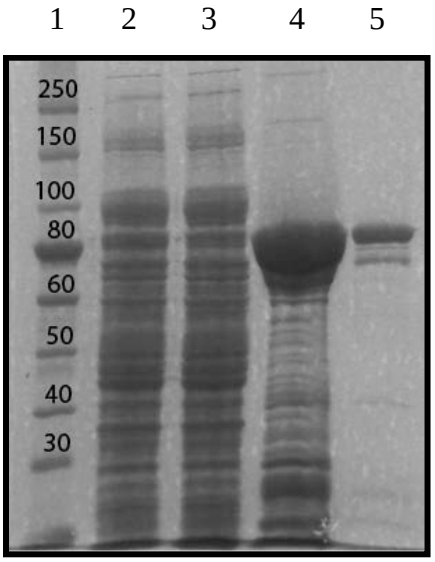

Figure 3.3 Purification of methylmalonyl-CoA mutase. SDS 10% polyacrylamide gel showing purification of human MCM by Ni-NTA affinity chromatography followed by Q-sepharose anion-exchange chromatography. Lane 1, protein molecular weight makers in kDa; Lane 2, crude extract from Rosetta(DE3)pLysS cells overexpressing MCM; Lane 3, flow-through from initial Ni-NTA column; Lane 4, Ni-NTA column eluate from first purification step; Lane 5, Q-sepharose eluate from final purification step.

3.5 Steady-state kinetic properties of the MCM E392 variants

MCM catalytic activity was measured by a continuous spectrophotometric assay using the coupling enzyme thiokinase (succinyl-CoA synthetase).[115] Thiokinase converts succinyl-CoA to succinate and CoA in a GDP-dependent fashion. Wild-type MCM displayed a turnover number of 3.9 ± 0.1 s^{-1} at 30 °C, similar to that reported for MCM from *Propionibacterium shermanii*.[116] The E392Q, E392D, and E392A variants showed 16-, 330-, and 12-fold reductions in the rate of catalytic turnover compared to that of the native enzyme, respectively (Table 3.3).

Table 3.3 Summary of catalytic turnover rates observed for wild-type MCM and the E392Q, E392D, and E392A variants.

Enzyme	k_{cat} (s^{-1})
Wild-type	3.95 ± 0.11
E392Q	0.25 ± 0.01
E392D	0.012 ± 0.001
E392A	0.32 ± 0.02

3.6 Absorption spectra of the OAM variants

To determine the effects of the mutations on transimination and Co–C bond homolysis, UV–visible spectra were obtained for the OAM variants (in holoenzyme form) when they were mixed with D-ornithine and DABA under anaerobic and aerobic conditions. The anaerobic conditions allow for detection of a stable biradical state with the inhibitor, while the aerobic conditions allow monitoring of cob(III)alamin formation. The interception of the cob(II)alamin intermediate by O_2 leads to the formation of cob(III)alamin, and this reaction, leading to enzyme inactivation, is noted by an increase in absorbance at 358 nm. As shown in section 2.5, cob(III)alamin formation occurs at a rate of 0.4 min^{-1} in the presence of substrate and 1.6 min^{-1} in the presence of DABA for native OAM.

Figure 3.4A shows the spectral shift in the holoenzyme form of E338Q upon addition of D-ornithine under aerobic conditions. The decrease in absorbance at 416 nm is consistent with transimination, but the lack of absorbance decrease at 528 nm indicates impaired Co–C bond homolysis. The absence of cob(III)alamin formation, even after 90 minutes, further suggests that generation of the cob(II)alamin intermediate by activation of AdoCbl is affected by the mutation. Similar spectral transitions were observed upon binding of D-ornithine to all three OAM variants under aerobic and anaerobic conditions.

Figure 3.4B shows a shift in the holoenzyme absorbance spectra for OAM E338Q with the addition of DABA under anaerobic conditions. Similar spectral transitions were

observed for all three variants, with or without O_2 in the reaction mixture. As with D-ornithine, the binding of DABA results in external aldimine formation (decrease at 416 nm), but unlike studies with the physiological substrate, there was a small decrease in absorbance at 528 nm suggesting limited Co–C bond homolysis. However, the usual buildup of the cob(II)alamin species (at 470 nm) observed in the wild-type OAM-DABA complex was absent in all three variants. Moreover, there was no accumulation of cob(III)alamin over 90 minutes, even in the presence of O_2. Taken together, these studies suggest that substitution of Glu338 does not affect the formation of the external aldimine but does impair subsequent radical initiation by the AdoCbl cofactor.

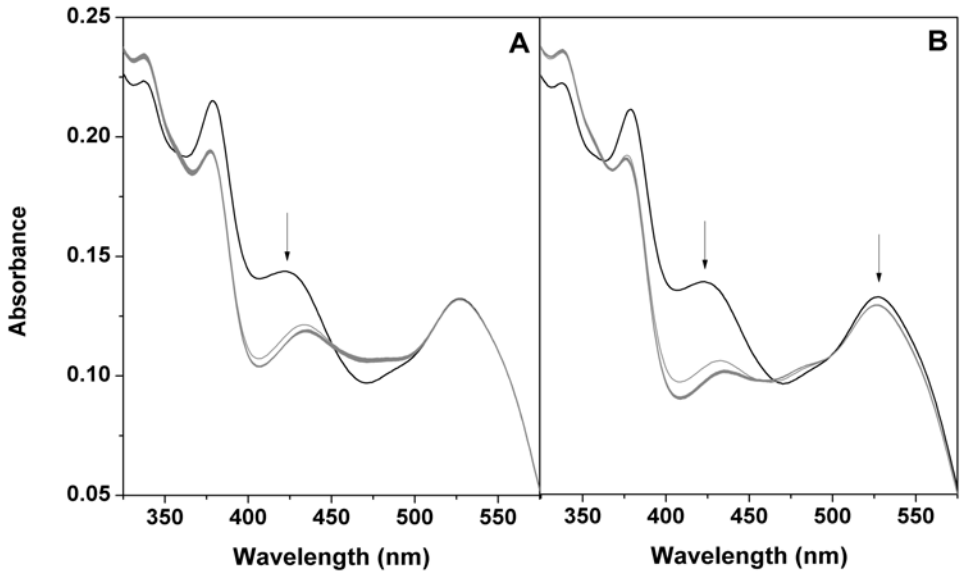

Figure 3.4 Changes in the UV-visible absorbance spectra of the OAM E338Q variant upon binding of D-ornithine and DL-2,4-diaminobutyrate. The holoenzyme reaction mixture contained 15 μM OAM, 15 μM PLP, and 15 μM AdoCbl in 100 mM NH_4^+EPPS. (A) Spectral changes for E338Q recorded before (black line) and after (gray lines) the addition of 5 mM D-ornithine under aerobic conditions. Similar spectral transitions were observed under aerobic conditions and with E338D and E338A. (B) Spectral changes for E338Q recorded before (black line) and after (gray lines) the addition of 5 mM 2,4-diaminobutyrate under anaerobic conditions. Similar spectral transitions were observed under aerobic conditions and with E338D and E338A. For both (A) and (B) optical changes were monitored every 2 min for 1 hour. Only representative spectra are shown.

3.7 Stopped-flow Analysis of OAM variants

Stopped-flow experiments have previously been used to measure rates of Co–C bond homolysis (absorbance decrease at 528 nm) and transimination (absorbance decrease at 416 nm) in holo-OAM upon addition of both D-ornithine and the substrate analogue, DL-2,4-diaminobutyric acid.[64] Observed rate constants for Co–C bond homolysis and transimination were found to be on the same order of magnitude (~ 500 s^{-1}) with both the substrate and inhibitor (section 2.4). Figure 3.5 shows that all three Glu338 variants elicited similar rates of transimination with DABA to that of wild-type OAM. A mono-exponential fit of the absorbance traces at 416 nm (1–20 ms) produced rate constants of 514 ± 26 s^{-1}, 577 ± 66 s^{-1}, and 454 ± 36 s^{-1} for E338Q, E338D, and E338A variants, respectively. In the absence of bound AdoCbl (i.e. with only PLP bound to the protein), the transimination rates are much slower (2500-fold) for the native enzyme.[64] Thus, the fact that these calculated rate constants are unchanged in the OAM variants suggests that AdoCbl binding is unaffected by the single point mutation, as impaired AdoCbl binding would likely result in slower rates of transimination.

The Co–C bond homolysis signal at 528 nm was detected upon rapid mixing of the native enzyme with DABA, giving an observed rate constant of 489 ± 40 s^{-1} (Figure 3.6). Consistent with the UV-visible spectral binding data, rapid mixing of the OAM variants with D-ornithine did not result in an absorbance decrease at 528 nm. Rapid-mixing with DABA also did not reproducibly show a homolysis signal at 528 nm. Given the small absorbance change in the AdoCbl cofactor that is generated by binding of the inhibitor to the holoenzyme variants under steady-state conditions, it is unlikely that we would be able to reliably detect this homolysis signal in the stopped-flow given the low signal to noise ratio of the instrument. These combined stopped-flow data indicate that the mutations do not compromise the rate of external aldimine formation or AdoCbl binding, but they do significantly impair radical generation, possibly by shifting the internal equilibrium of the Co–C bond homolysis step toward the intact cofactor.

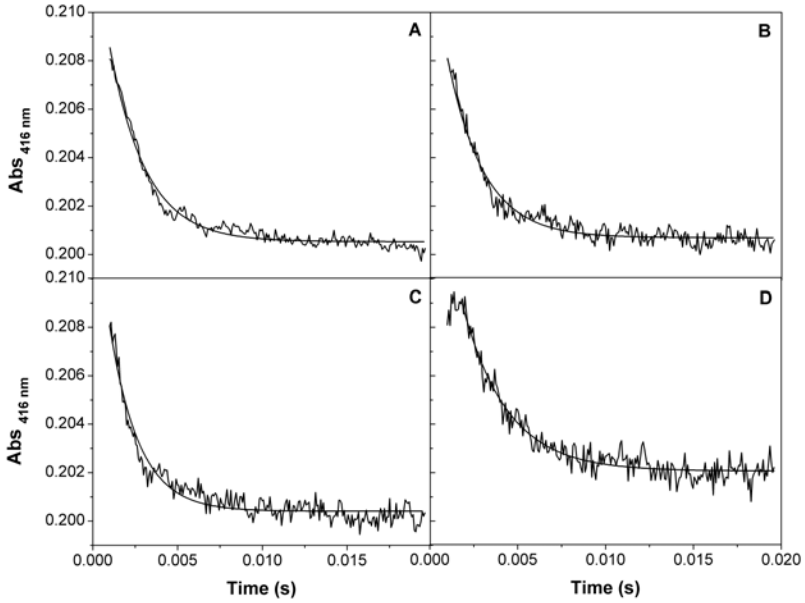

Figure 3.5 Stopped-flow absorbance changes following transimination in OAM. The transimination event was monitored at 416 nm over 20 ms following rapid-mixing of 50 μM wild-type (A), E338Q (B), E338D (C), and E338A (D) with 5 mM DABA, under anaerobic conditions. An average of 8−10 traces were fit to a single-exponential equation to generate the observed rate constants for transimination of 464 ± 36 s^{-1}, 514 ± 26 s^{-1}, 577 ± 66 s^{-1}, and 454 ± 36 s^{-1} for wild-type, E338Q, E338D, and E338A, respectively.

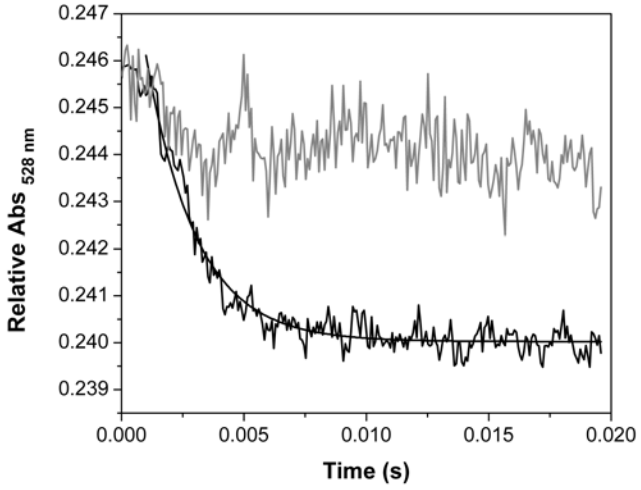

Figure 3.6 Stopped-flow absorbance changes following Co–C bond homolysis in OAM. The Co–C bond homolysis event was monitored at 528 nm over 20 ms following rapid-mixing of 50 μM wild-type (black line) with 5 mM DABA. An average of 8−10 traces were fit to a single-exponential equation to generate the observed rate constant of 489 ± 40 s^{-1} for homolysis. No detectable homolysis signal was detected for E338Q (gray trace) or the other two variants (data not shown).

3.8 Stopped-flow Analysis of MCM

Analogous stopped-flow experiments were conducted with MCM (wild-type and the variants) to determine if the corresponding residue (E392) activates radical chemistry. The observed rate constant for homolysis in wild-type MCM upon mixing with methylmalonyl-CoA at 10 °C was found to be 657 ± 29 s^{-1} (Figure 3.7A), similar to previously published results.[65] Recombination of the cofactor (absorbance increase at 525 nm) following depletion of the substrate in the reaction cell was observed after 8 seconds (Figure 3.7B). As with the OAM Glu338 variants, no homolysis signal was detected in any of the E392 variants upon mixing with methylmalonyl-CoA. These results point to a universal role of the highly conserved Glu in triggering AdoCbl homolysis in class I and class III isomerases.

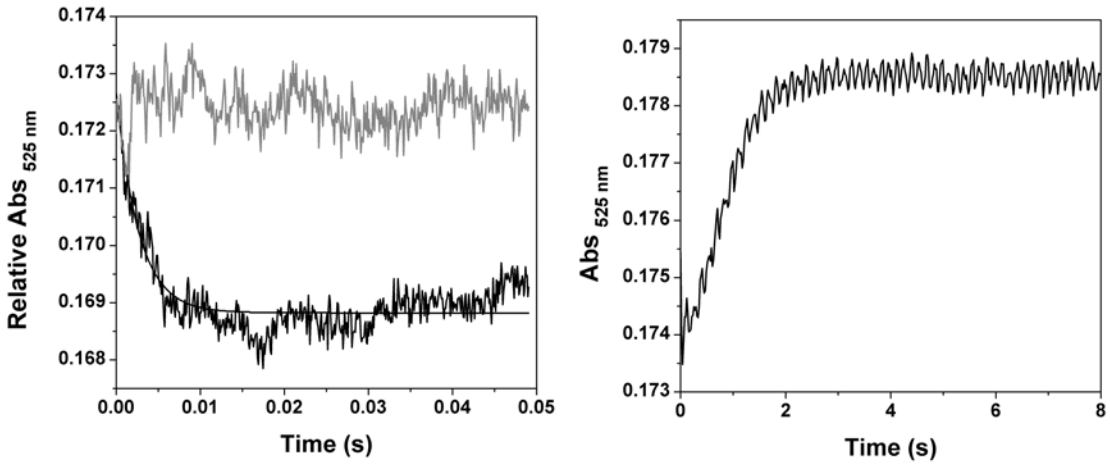

Figure 3.7 Stopped-flow absorbance changes following Co–C bond homolysis in holo-MCM upon mixing with methylmalonyl-CoA. (A) The Co–C bond homolysis step was monitored at 525 nm over 50 ms at 10 °C under anaerobic conditions. An average of 5−10 traces was fit to a single exponential equation, giving an observed rate constant of 657 ± 29 s^{-1} for wild-type methylmalonyl-CoA mutase. No homolysis signal was detected for E392D (gray line) or the other two variants (not shown). (B) Absorbance changes observed at 525 nm over 8 s following rapid-mixing of 50 μM wild-type MCM with 1 mM methylmalonyl CoA. The increase in absorbance at 525 nm reflects reformation of the Co–C bond following consumption of substrate. Analogous absorbance increases at 525 nm were not observed in any of the three MCM variants.

3.9 Adenosylcobalamin-binding Assays for MCM

The effect of mutating Glu392 in MCM on AdoCbl binding was assessed through a fluorescence-binding assay. Previously, it was shown that AdoCbl binding to MCM results in a quenching of the intrinsic tryptophan fluorescence. Figure 3.8 shows a decrease in the fluorescence emission at 340 nm as AdoCbl is gradually added to both the native enzyme and E392D. To extract equilibrium dissociation constants for both proteins, the data were fit to the quadratic binding isotherm (Eq. 3.1 in section 3.11.7), keeping the total concentration of each enzyme fixed. Native MCM generated an apparent K_d of 0.23 ± 0.01 μM for AdoCbl, which is similar to that of E392D (0.21 ± 0.02 μM) and previously published data.[117] The absence of a significant shift in the equilibrium dissociation constant suggests that mutation of the Glu392 side chain does not perturb cofactor binding.

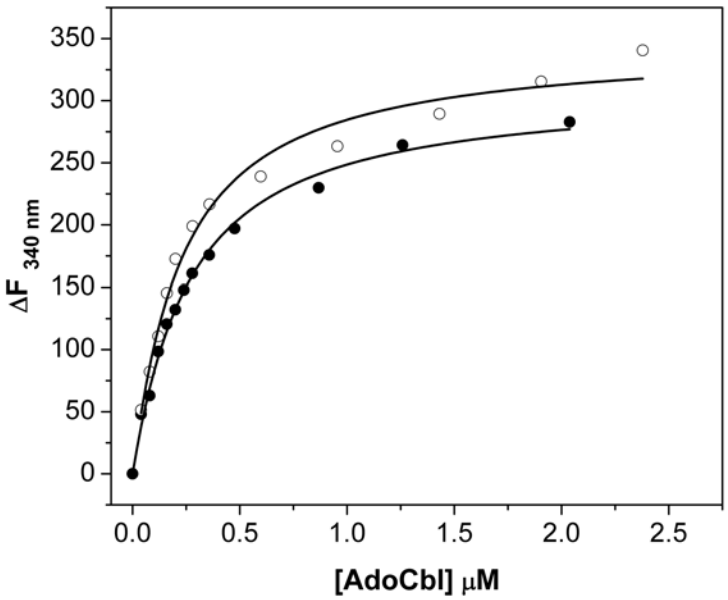

Figure 3.8 Determination of the equilibrium dissociation constant for AdoCbl for wild-type MCM and E392D. Native MCM (0.056 μM, solid circles) and E392D (0.040 μM, open circles) were titrated with AdoCbl (0.04-0.96 μM) at 3.2 °C in 50 mM potassium phosphate buffer at pH 7.5. The change in fluorescence at 340 nm is plotted against total concentration of AdoCbl and the data were fit to Eq 3.1 (solid line) keeping the total enzyme concentration fixed at 0.056 μM for MCM and 0.040 μM for E392D. The K_d was determined to be 0.21 ± 0.02 μM for native MCM and 0.23 ± 0.02 μM for E392D.

3.10 Discussion

3.10.1 Orientation of the Adenosyl Group and the Stability of the Co–C Bond

It is evident, especially in the case of OAM, that the adenosyl moiety undergoes a conformational switch upon substrate binding, and this process may place added strain on the Co–C bond. In the edge-on state, the Ado group is in the *syn* orientation with the adenine ring parallel to the B ring of the corrin macrocycle. The OAM Co–C bond is unusually stable in this conformation, as crystal structures show a 2.0 Å distance between the Co and the C5' atoms of the Ado group, revealing an unbroken Co–C bond in a protein structure.[76] Typically, the distance between the two atoms is ≥3 Å in crystal structures of B_{12} enzymes, as the relatively weak Co–C organometallic bond is partially or fully reduced by the X-ray beam.[75, 78, 114]

Insertion of the Ado moiety into the modeled closed active site of OAM requires rotation of the adenosyl group to the *anti* conformation about the glycosidic bond, and movement of the adenine ring, such that it is positioned perpendicular to the A pyrrole ring of the corrin macrocyle. This orientation of the Ado group is observed in the structures of MCM and GM.[78, 114] Quantum mechanical calculations of the AdoCbl cofactor (including the distally coordinated His) revealed a 21 kJ/mol difference in the bond dissociation energy between the two conformations, indicating that the relative orientation of the Ado moiety with respect to the corrin ring does not significantly influence the lability of the Co–C bond.[112] The orientation of the adenosyl group alone cannot account for the increased stability of the Co–C bond in the resting form of OAM or the activation of this bond during catalysis.

Interestingly, the Co–C bond is mostly cleaved in the crystal structure of lysine 5,6-aminomutase, also captured in the edge-on conformation. The lysine 5,6-aminomutase structure shows that the Ado moiety is also in the *syn* conformation about the glycosidic bond.[75] However, unlike in OAM, where the ribose moiety makes polar interactions with the solvent, the corresponding ribose 2'- and 3'-OH groups make electrostatic contacts with the main-chain carbonyls of Glu55 and Asp54 of lysine 5,6-aminomutase. These two residues stem from a six-residue distorted beta-hairpin structure that is absent in OAM. Outside of this

loop, the structures of OAM and lysine 5,6-aminomutase are structurally conserved. The absence of protein-based polar interactions with the ribose moiety may explain the anomalous stability of the Co–C bond in the OAM crystal structure.

3.10.2 Catalytic Role of Conserved Glutamate

In this work, we have shown that a highly conserved glutamate residue, shown to form polar contacts with the ribose moiety upon substrate binding, plays a major catalytic role in OAM and MCM. Pre-steady-state kinetic analysis of the OAM and MCM variants revealed no detectable Co–C bond homolysis signal with the natural substrate. For the OAM variants, the rate constants associated with external aldimine formation were similar to that of the native enzyme, suggesting that a reduced rate of catalytic turnover is not attributed to impaired substrate or cofactor binding. The residual activity observed in the OAM and MCM variants indicates that AdoCbl activation is still occurring, but the inability to spectrally observe Co–C bond homolysis suggests that the internal equilibrium constant for the chemical step is shifted in favor of the intact cofactor. Indeed, significantly reduced levels of AdoCbl homolysis observed with DABA further point to an inflated $\Delta G^{\ddagger}$ for radical initiation. Typically, binding of DABA to native OAM converts 40% of the enzyme population to the biradical state.[64]

Of the OAM variants, the E338Q substitution elicited the highest rate of turnover and catalytic efficiency. The observed ~90-fold reduction in activity potentially reflects the weaker nature of dipole–dipole interactions between the Gln side chain and the 2'- and 3'-OH groups of the ribose compared to the dipole–charge interactions present in the native enzyme. Swapping Glu338 for an Asp effectively separates the dipole–charge interaction between the functional groups by an additional ~2 Å. The substantial decrease in catalytic activity (~380-fold) associated with this variant is attributed to the fact that the strength of the charge–dipole interaction is inversely proportional to r^2, where r is the distance between the two atoms. The low dielectric of the pre-organized active site likely further magnifies the energy of interaction between functional groups, accounting for the large differences in activities between wild-type OAM and the E338D and E338Q variants. It also further suggests that the pre-organized active site is relatively rigid and that localized dynamic motion cannot

sufficiently compensate for the small increase in charge separation between the protein and the cofactor. Indeed, molecular dynamics simulations of OAM in the edge-on and top-on conformations reveal that the latter catalytically engaged state is significantly less flexible.[112]

The most pronounced decrease in OAM turnover rate occurred with complete removal of the polar side chain in E338A. The fact that catalytic activity is not completely abolished in E338A (turnover and catalytic specificity decreased 670- and 220-fold, respectively) suggests that Glu338 does not solely contribute to Co–C bond homolysis. Assuming that Co–C bond homolysis is the rate-limiting step in both wild-type OAM and the E338A variant, the catalytic contribution of Glu338 is ~16 kJ/mol (assuming $\Delta\Delta G^{\ddagger}$ is 73 kJ/mol with respect to the homolysis reaction in aqueous solution). Stopped-flow studies of wild-type OAM reveal that the rate of Co–C bond homolysis is >500 s^{-1}, significantly faster than the turnover rate of 3 s^{-1}.[64] Thus, if we assume that Co–C bond homolysis occurs at a rate of 500 s^{-1} in native OAM but becomes rate-limiting in E338A, with an estimated rate of 4.3 x 10^{-3} s^{-1}, then it follows (using the Eyring Equation) that the glutamate side chain is responsible for lowering the $\Delta G^{\ddagger}$ of the Co–C bond homolysis step by ~30 kJ/mol (upper limit). Strikingly, this value is 40 and 75% of the $\Delta\Delta G^{\ddagger}$ estimated for the stepwise and concerted pathways, respectively. The remaining catalytic effect (for surmounting the remaining 10–40 kJ/mol of the 73 kJ/mol barrier) is possibly distributed among other residues that coordinate the adenosyl group.

Kinetic isotope effect studies with E338D provide additional support for the involvement of Glu338 in lowering the barrier to Co–C bond homolysis in OAM. In the native enzyme, the value of $^{D}k_{cat}/K_{m}$ (2.5 ± 0.4) is suppressed relative to the value of $^{D}k_{cat}$ (7.6 ± 0.5) indicating that the enzyme has a large forward commitment to catalysis and that the formation of product is fast relative to substrate release. If through mutation of Glu338 to an Asp the barrier to homolysis were increased, then it would follow that the rate of formation of product is slowed relative to substrate release in the variant. This results in an unmasking of the intrinsic isotope effect on k_{cat}/K_{m} (6.5 ± 0.9), such that it is now similar in value to $^{D}k_{cat}$ (7.2 ± 0.2). Moreover, the value of $^{D}k_{cat}$ for E338D is unchanged compared to native OAM indicating that hydrogen atom abstraction is still rate-limiting in the mechanism but that the mutation has not made it more so. Given that mutation of Glu338 to an Asp is thought to

affect only homolysis rather than hydrogen atom abstraction, no increase in the value of $^{D}k_{cat}$ is expected.

The rate of catalytic turnover for the MCM E392Q and E392D variants was reduced by 16- and 330-fold, respectively, consistent with the results observed for the corresponding OAM variants. Interestingly, where the glutamate to alanine mutation was the slowest of the OAM variants, MCM E392A retained the highest catalytic activity of the MCM variants. A possible explanation for this unexpected result is that the short methyl side chain of alanine allows sufficient space for one or more water molecules to enter the active site of MCM and substitute as a polar contact with the hydroxyl groups of the ribose moiety. The importance of the electrostatic interaction with the ribose 2'- and 3'-OH groups is supported by an earlier study that showed that substitution of AdoCbl with 2',5'-dideoxyadenosylcobalamin resulted in a holo-MCM with only 1–2% activity.[118]

It appears from these data that the conserved Glu significantly reduces the $\Delta G^{\ddagger}$ for Co–C bond homolysis, but the question of whether the side chain weakens the Co–C bond through enforced strain on the ribose (leading to ground-state destabilization) or whether the residue stabilizes the transition state via electrostatic interactions with the ribose remains. Our combined results suggest that the activation barrier to homolysis appears to be dependent on the strength of the electrostatic interaction, given that the strength of the interaction with the 2'- and 3'-OH groups is expected to decrease in a low dielectric environment with formal charge reduction (E338Q), followed by a 2 Å increase in the length of the charge–dipole interaction (E338D) and then with complete removal of the polar side chain (E338A).

A combined experimental and computational investigation of the analogous glutamate residue (Glu330) in glutamate mutase (GM) has subsequently been published,[119] with results similar to those obtained here for OAM and MCM. Replacement of Glu330 with an aspartate, alanine, and a glutamine greatly reduced GM activity to less than 1% of the wild-type enzyme. In addition, no cob(II)alamin intermediate was spectrally detected in any of the variant enzymes. Given that homolysis of the Co–C bond is coupled to hydrogen atom abstraction, the rate of tritium exchange between AdoCbl and the substrate was used to examine the rate of the homolysis step. Consistent with our findings, the rate of tritium exchange was found to decrease as the strength of the electrostatic interaction decreased (E330A < E330D < E330Q < wild-type). Furthermore, complementary molecular dynamics

simulations were used to show that the increased number of hydrogen bonds to the 2'- and 3'-OH groups of the ribose moiety plays a pivotal role in not only stabilizing the dissociated state of the cofactor, but also in correctly positioning the adenosyl radical for hydrogen atom abstraction.

3.10.3 Activation of the Co–C Bond in the Eliminases

Interestingly, class II eliminases do not appear to have a corresponding Glu coordinated to the adenosyl ribose, suggesting that coordination of protein to the ribose 2'- and 3'-OH groups is not as critical for Co–C bond labilization. This is supported by studies that showed that diol dehydratase retained 31 and 19% activity complexed with 2'-deoxyAdoCbl and 3'-deoxyAdoCbl analogues, respectively.[120] Simulations of EPR spectra of the biradical enzyme reveal that the distance between the cob(II)alamin and the substrate radical is ~11 Å in ethanolamine ammonia lyase[121] and diol dehydratase,[122] whereas the distance between the paramagnetic centers in OAM,[64] MCM,[123] and GM[104] is ~6–6.6 Å. The increased distance indicates that Ado• traverses (and likely rotates within) the active site in eliminases. Indeed, high-resolution EPR studies with ethanolamine ammonia lyase show that the C5' radical center migrates 5–7 Å to form the substrate-derived radical.[124] Perhaps coordination of the adenosyl moiety to a polar side chain potentially disrupts movement of the radical intermediate along the reaction coordinate.

Studies conducted by Schwartz and Frey with class II diol dehydratase (DD) show that binding of potassium (a necessary cofactor for catalysis) to the enzyme activates the Co–C bond (2500-fold).[53] The crystal structure of DD in complex with the cofactor analogue adeninylpentylcobalamin (PDB entry 1EEX) reveals that the K^+ ion binds in close proximity to the adenine ring (Figure 3.9). Electrostatic interactions between the K^+ ion and nitrogen atoms within the adenine ring could account for this activation. Substrate binding completes activation of the Co–C bond. The substrates acted upon by the eliminases are much smaller than substrates of the class I and class III enzymes. It is likely the case that binding of both the K^+ ion and the substrate is required to induce the necessary structural rearrangements that result in Co–C bond homolysis.

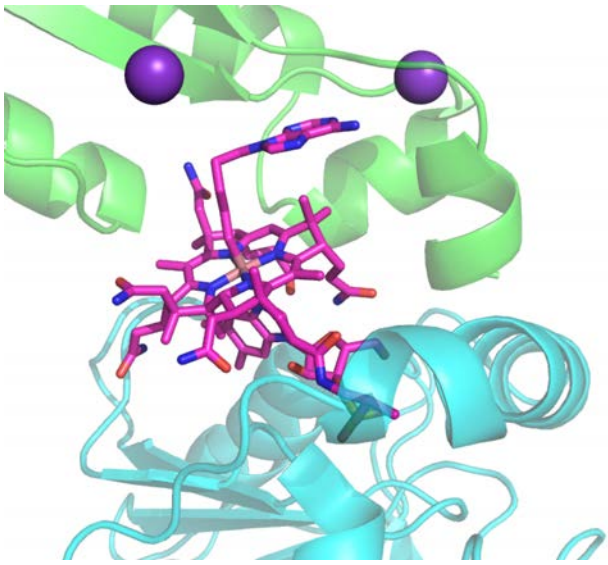

Figure 3.9 Crystal structure of diol dehydratase in complex with cofactor analogue adeninylpentylcobalamin showing the adenine binding pocket (PDB entry 1EEX). The additional potassium ions (purple), shown to be important to Co–C bond labilization, are located in close proximity to the adenine ring of adeninylpentylcobalamin (pink).

3.10.4 Concluding remarks

The work herein highlights the importance of electrostatic interactions between specific active site residues and the adenosyl group to the Co–C bond homolysis event in the class I mutases and the class III aminomutases. In particular, a highly conserved glutamate residue potentially accounts for approximately half of the observed decrease in the free energy of activation achieved through binding of the cofactor to these enzymes. Conformational changes upon substrate binding, bringing the glutamate into close contact with the Ado group, afford AdoCbl-dependent enzymes additional control over the generation of reactive radical species during catalysis. Displacement of the glutamate residue from the ribose in the resting state of MCM potentially safeguards against spurious radical generation and enzyme inactivation. This strategy also applies for OAM: rotation of the Rossmann domain away from the active site to form the edge-on conformation likely protects against aberrant Co–C bond homolysis in the absence of substrate. While this mechanism appears to be conserved among the class I and class III enzymes, the class II eliminases, which lack a homologous glutamate residue, likely achieve Co–C bond homolysis through a distinct mechanism.

3.11 Experimental Procedures

3.11.1 Materials

AdoCbl, PLP, D-ornithine, DL-2,4-diaminobutyric acid, GDP, DTNB, and methylmalonyl-CoA were obtained from Sigma. The Ni^{2+}-nitrilotriacetic acid (Ni-NTA) column and Q-sepharose High Performance resins were from GE Biosciences. Restriction endonucleases were from New England Biolabs, *Pfu* Turbo DNA polymerase was from Agilent Technologies and Rosetta(DE3)pLysS competent cells were purchased from EMD Biosciences. Thiokinase (succinyl-CoA synthetase) was purchased from Cedarlane Labs. All other chemicals were purchased from Fisher Scientific and were of the highest grade available.

3.11.2 Construction of MCM and OAM variants

The OAM and MCM single point mutations described in the paper were introduced into the pOAMH2[64] and pNIC-CTHF vectors,[114] respectively, using the QuikChange site directed mutagenesis method (Agilent Technologies, Mississauga, ON). The DNA Sequencing Laboratory at University of British Columbia (Vancouver, Canada) sequenced each variant to verify that the mutation was successfully engineered into the construct and to confirm that no other PCR-induced errors had occurred. Following is a list of the complementary primers used to generate each variant:

OAM E338D:

```
5′- CAA TTA CTC CTG ACG ACG GAA GAA ACG TTC CTT GG -3′
5′- CCA AGG AAC GTT TCT TCC GTC GTC AGG AGT AAT TG -3′
```

OAM E338A:

```
5′- CAA TTA CTC CTG ACG CCG GAA GAA ACG TTC CTT GG -3′
5′- CCA AGG AAC GTT TCT TCC GGC GTC AGG AGT AAT TG -3′
```

OAM E338Q:

5′- CAA TTA CTC CTG ACC AGG GAA GAA ACG TTC CTT GG -3′
5′- CCA AGG AAC GTT TCT TCC CTG GTC AGG AGT AAT TG -3′

MCM E392D:

5′-C ACA AAT TCT TTT GAT GAC GCT TTG GGT TTG CCA AC-3′
5′-GT TGG CAA ACC CAA AGC GTC ATC AAA AGA ATT TGT G-3′

MCM E392A:

5′-C ACA AAT TCT TTT GAT GCA GCT TTG GGT TTG CCA AC-3′
5′-GT TGG CAA ACC CAA AGC TGC ATC AAA AGA ATT TGT G-3′

MCM E392Q:

5′-C ACA AAT TCT TTT GAT CAA GCT TTG GGT TTG CCA AC-3′
5′-GT TGG CAA ACC CAA AGC TTG ATC AAA AGA ATT TGT G-3′

3.11.3 Enzyme purification

The OAM variants and wild-type DAPDH were purified as previously described in section 2.10.5.[64, 125] The plasmid construct containing the coding sequence for human MCM, pNIC-CTHF, was obtained from the Structural Genomics Consortium, Oxford. A hexahistidine tag was engineered onto the C-terminus of the MCM cDNA in the pNIC-CTHF construct allowing for purification of the recombinant protein by Ni^{2+}-NTA affinity chromatography. Wild-type MCM and the engineered point variants were transformed into *Escherichia coli* Rosetta(DE3)pLysS and the proteins were expressed as described.[114]

MCM was purified as described with minor modifications.[114] Rosetta(DE3)pLysS cells (24 g, wet weight) overexpressing MCM were resuspended in 200 mL of 50 mM HEPES-KOH, pH 7.5, 5% glycerol, 10 mM imidazole, 0.5 mM TCEP and 0.1 mM PMSF. Cells were disrupted by sonication (5 second pulses separated by a 50 second interval for 30 min, power setting 22%) using a Misonix sonicator. The cell suspension was clarified by centrifugation at 39,000 g for 45 min. The supernatant, following the addition of sodium chloride (0.5 M), was applied to a 5 mL Ni^{2+}-nitrilotriacetic acid (Ni^{2+}-NTA) column equilibrated with 50 mM HEPES-KOH, pH 7.5, 0.5 M NaCl, 0.5 mM TCEP, and 10 mM imidazole. The column was washed with 30 mL of 50 mM HEPES-KOH, 0.5 M NaCl, pH 7.5 and 10 mM imidazole, and

then 25 mL of 50 mM HEPES-KOH, 0.5 M NaCl, pH 7.5 with 40 mM imidazole. The protein was eluted with application of 25 mL of 50 mM HEPES-KOH, 0.5 M NaCl, pH 7.5 and 350 mM imidazole to the Ni^{2+}-NTA column. Fractions containing MCM were pooled and diluted 5-fold with 50 mM HEPES-KOH, pH 7.5, and directly applied to a 60 mL Q-sepharose HP column (2.6 × 11 cm) equilibrated with 50 mM HEPES-KOH, pH 7.5. The column was washed with 120 mL of 50 mM HEPES-KOH, pH 7.5 and the protein was eluted with a 1.2 L linear gradient to 0.5 M NaCl at a flow rate of 2 mL/min. Fractions containing purified MCM, as judged by an absorbance reading at 280 nm and SDS-PAGE analysis, were pooled and concentrated using Centricons with a 30 kDa MW cutoff filter. Concentrated protein samples containing 20 % glycerol were then flash-frozen in liquid nitrogen and stored at –80 °C. Protein concentrations were determined by the Lowry method using bovine serum albumin as a standard.

3.11.4 Coupled enzyme assays

OAM activity was measured using a coupled spectrophotometric assay with DAPDH as previously described.[125] Data from the substrate concentration dependence experiments were fit to the Michaelis−Menten equation (Eq. 2.1) as described in section 2.10.7. MCM activity was measured using a coupled spectrophotometric assay with thiokinase (succinyl-CoA synthetase), as previously described[126] with the exception that 50 mM Tris buffer, pH 7.5 was used in place of a Tris phosphate buffer, pH 7.5 (50 mM in phosphate). The total volume of the reaction mixture was 300 µL. Saturating concentrations of (R,S) methylmalonyl-CoA were used to obtain average k_{cat} values for wild-type MCM as well as the E392Q, E392D, and E392A variants. The background activity at 412 nm prior to addition of MCM was recorded for 5 min and subtracted from the activity recorded over 5 min following the addition of MCM. Assays were performed in triplicate at 30 °C to obtain the reported turnover rate.

3.11.5 Aerobic and anaerobic UV-visible spectroscopy

Aerobic and anaerobic UV-visible spectral data for the OAM E338 variants were collected as described in sections 2.10.9 and 2.10.10.

3.11.6 Stopped-flow spectroscopy

Anaerobic stopped-flow studies were performed using an SF-61DX2 stopped-flow instrument (TgK Scientific). The sample-handling unit of the stopped-flow instrument was housed in a specialized glove box (Belle Technology) in which the O_2 concentration was < 5 ppm. Anaerobic solutions of buffer, enzyme, cofactors, substrate, and substrate analogues were prepared as previously described.[64] For the OAM variants, transient kinetic experiments were performed in 100 mM NH_4^+ EPPS, pH 8.5 at 25 °C. The cofactors, PLP and AdoCbl, were added to the apoenzyme in equimolar concentrations to form the holoenzyme. Holo-OAM (50 μM) was rapidly mixed with 5 mM D-ornithine or DL-2,4-diaminobutyrate and transimination and Co-C bond homolysis were followed at 416 and 528 nm, respectively.

MCM pre-steady state analysis was performed in 50 mM potassium phosphate buffer, pH 7.5 at 10 °C. Holo-MCM was generated by adding an equimolar amount of AdoCbl to the apoenzyme, and then a 50 μM solution of holoenzyme was rapidly mixed with 1 mM methylmalonyl-CoA. AdoCbl homolysis was monitored following a change in absorbance at 525 nm. Concentrations of holoenzyme, substrate and substrate analogue in the text and figure legends refer to syringe concentrations (i.e. before the mixing event). Substrate, substrate analogue, and holoenzymes were diluted 2-fold after the mixing event. Eight to ten absorbance traces were averaged and then fit to a single exponential equation to extract observed rate constants.

3.11.7 Adenosylcobalamin equilibrium binding assay

Fluorescence spectroscopy was used to determine the equilibrium dissociation constant of AdoCbl following a previously published protocol.[9] The assays were performed on a Perkin Elmer LS45 fluorescence spectrometer with excitation and emission slit widths

of 10.0 nm. The assay relies on quenching of the intrinsic tryptophan residues that occurs with binding of AdoCbl to the protein. Sequential additions of 2-4 µL of a concentrated AdoCbl stock were made to a 3 mL quartz fluorescence cuvette with 2980 µL of either 0.04 or 0.056 µM apo-MCM, achieving AdoCbl concentrations that ranged from 0.04-0.96 µM. The titration was performed in 50 mM potassium phosphate buffer, pH 7.5. After each AdoCbl addition, the cuvette was inverted several times and incubated for 20 minutes at 3.2 °C. Tryptophan residues were then excited at 282 nm and fluorescence emission was detected between 300–380 nm. Five scans (240 nm/min) at each AdoCbl concentration were averaged. The change in the fluorescence emission at 340 nm was fitted to the quadratic binding isotherm (Eq 3.1).

$$\Delta F = \left(\frac{\Delta F_{\max}}{2E_o}\right)\left\{E_o + L_o + K_d - \left[\left(E_o + L_o + K_d\right)^2 - 4E_oL_o\right]^{1/2}\right\} \qquad \text{Eq. 3.1}$$

where L_o is total AdoCbl concentration; E_o is total enzyme concentration; ΔF is the change in fluorescence, $\Delta F_{\max}$ is the maximum change in fluorescence emission; and K_d is the dissociation constant for the AdoCbl-MCM complex.

Chapter 4 : Isotope Effects for Deuterium Transfer in Adenosyl-cobalamin-dependent Ornithine 4,5-aminomutase Provide Mechanistic Insight into the Catalytic Roles of Tyr187 and Tyr160

4.1 Chapter summary

Several residues are positioned proximal to the pyridoxal 5'-phosphate cofactor in ornithine 4,5-aminomutase, which have the potential to further modulate radical stability and catalysis. Here we have investigated the role of tyrosine 187, which forms a π-stacking interaction with the pyridine ring of PLP in OAM, through site-directed mutagenesis. Tyrosine 187 was substituted with a phenylalanine and an alanine. The Y187F and Y187A variants showed a 25- and 1260-fold decrease in k_{cat}, respectively. Pre-steady-state kinetic analysis revealed that the rate constants for transimination and Co–C bond homolysis were both reduced 2- and 6-fold for Y187F and Y187A, respectively. Isotope effect studies indicate that hydrogen atom abstraction is more rate limiting in Y187F and less rate determining in Y187A. The reduction in turnover rate of the Y187 variants is attributed to a slower rate of external aldimine formation and an increase in the barrier to homolysis and hydrogen transfer. EPR studies of Y187F suggest that the integrity of the active site is maintained, as the cob(II)alamin and PLP-organic radical species remain tightly coupled. Radical intermediates were not detected for the Y187A variant. From these results, we propose that Y187 optimally positions the PLP cofactor for external aldimine formation and positions the substrate relative to the adenosyl radical for hydrogen atom abstraction. Computational researchers have proposed that a second active site tyrosine residue, tyrosine 160, mediates labilization of the Co–C bond in OAM through a proton-coupled electron transfer mechanism. Here we have evaluated this hypothesis through mutation of Y160 to a phenylalanine. The Y160F variant showed a 130-fold decrease in k_{cat} and elevated deuterium kinetic isotope effects on k_{cat} and k_{cat}/K_m. The rate constant for transimination was reduced 3-fold indicating that, like Y187, Y160 is involved in positioning the substrate relative to the PLP cofactor for external aldimine formation. UV-visible spectroscopy revealed limited Co–C bond homolysis and a reduced sensitivity of the variant to inactivation by molecular oxygen, however pre-steady-state kinetic analysis showed only a 2-fold decrease in the rate

constant for homolysis. These results suggest that Y160 does not play a major role in labilizing the Co–C bond. The potential contribution of proton-coupled electron transfer (PCET) to activation of the Co–C bond in OAM and the AdoCbl-dependent mutases is discussed.

4.2 Positioning of Tyr187 in the OAM active site

The active site of OAM reveals a tyrosine residue (Y187), which forms a π-stacking interaction with the PLP cofactor (Figure 4.1). Y187 additionally secures PLP within the active site through hydrogen bond contact with the phosphate moiety. Residues proximal to the PLP cofactor are likely to further modulate radical stability and catalysis. For example, the analogous tyrosine residue (Y263α) in 5,6-LAM was recently implicated in stabilizing the azacyclopropylcarbinyl radical intermediate, as well as protecting the enzyme from inactivation by molecular oxygen. To investigate the role of Y187 in OAM catalysis we have created two variant forms of the enzyme. In the first variant (Y187F), the hydrogen bond contact with the phosphate moiety is severed through replacement of Y187 with a phenylalanine. In the second (Y187A), the phenoxy side-chain is removed altogether and replaced with a methyl group.

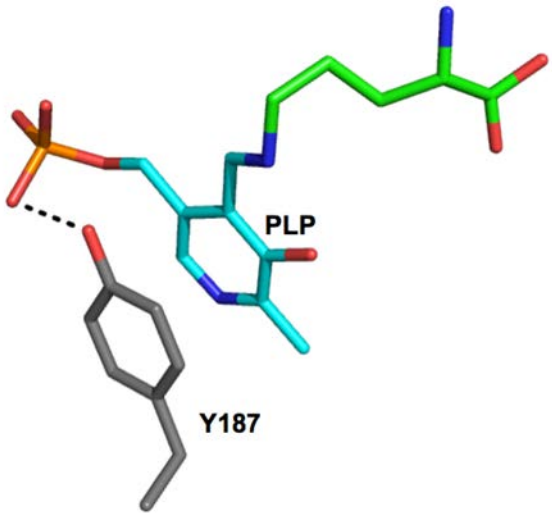

Figure 4.1 Substrate-bound active site of OAM showing the relative position of Y187 with respect to the PLP cofactor (PDB entry 3KOZ). Y187 (gray) interacts with the PLP cofactor (cyan) through a hydrogen bond with the phosphate moiety, and also forms a π-stacking interaction with the pyridine ring.

4.3 Steady-state kinetic properties of the Y187 variants

The steady-state kinetic parameters for the Y187 variants are summarized in Table 4.1. Mutation of Tyr187 to a Phe resulted in a 25-fold decrease in catalytic turnover and a 7-fold decrease in overall catalytic efficiency. Complete removal of the phenoxy side-chain in Y187A resulted in a considerably larger 1260-fold decrease in k_{cat} and a 150-fold decrease in k_{cat}/K_m. The Y187F variant showed a 2-fold increase in both $^{D}k_{cat}$ and $^{D}k_{cat}/K_m$, suggesting that hydrogen atom abstraction is more rate-limiting in the variant. In contrast, the 3-fold decrease in $^{D}k_{cat}$ for the Y187A variant compared to the wild-type enzyme suggests that a step in the mechanism other than hydrogen atom abstraction has now become rate limiting.

Table 4.1 Summary of steady-state kinetic parameters for k_{cat} and k_{cat}/K_m for wild type OAM and the Y187 variants with substrate DL-ornithine and the observed kinetic isotope effects upon reaction with deuterium-labeled substrate DL-ornithine-3,3,4,4,5,5-d_6.

Enzyme	k_{cat} (s^{-1})	K_m (μM)	k_{cat}/K_m ($M^{-1}s^{-1}$)	$^{D}k_{cat}$	$^{D}k_{cat}/K_m$
Wild type	2.9 ± 0.1	567 ± 45	5120 ± 410	7.6 ± 0.5	2.5 ± 0.4
Y187F	$1.15 \times 10^{-1} \pm 0.01 \times 10^{-1}$	162 ± 5	710 ± 28	16.7 ± 0.4	5.3 ± 0.6
Y187A	$2.3 \times 10^{-3} \pm 0.1 \times 10^{-3}$	68 ± 6	34 ± 5	2.7 ± 0.2	ND[a]

[a] Due to the slow rate of turnover we were unable to determine a value of $^{D}k_{cat}/K_m$ for the Y187A variant.

4.4 Anaerobic absorption spectra of the Y187 variants

To examine the effects of the Y187 substitutions on substrate binding, Co–C bond homolysis, and cob(II)alamin build-up, anaerobic UV-visible binding spectra were obtained for each of the variants upon mixing with DL-2,4-diaminobutyrate and D-ornithine (Figure 4.2). The binding spectra obtained for the Y187F variant were similar to those previously

published for wild-type OAM.[64] Binding of both the substrate D-ornithine (Figure 4.2A) and DL-2,4-diaminobutyrate (Figure 4.2B) resulted in a decrease in absorbance at 416 nm, indicating transimination. Examination of the absorbance decrease at 528 nm revealed that DL-2,4-diaminobutyrate induces a greater percentage of Y187F to undergo homolysis than does D-ornithine, consistent with the native enzyme.[64] In both the DABA and D-ornithine cases, the degree of homolysis is reduced in Y187F compared to wild-type OAM. Figure 4.2B shows a small absorbance increase at 470 nm indicating that the persistent PLP-DABA radical still forms in Y187F and is coupled to the cob(II)alamin species.

The binding spectra for the Y187A variant exhibited marked differences from those of both wild-type OAM and the Y187F variant. While transimination is evident upon binding of DL-2,4-diaminobutyrate (Figure 4.2D) to Y187A, the small decrease in absorbance at 416 nm in Figure 4.2C indicates that transimination upon binding of D-ornithine is impaired in the Y187A variant. Moreover, no cob(II)alamin species was detected upon mixing of Y187A with DABA, which could be attributed to decreased stability of the PLP-DABA derived radical species.

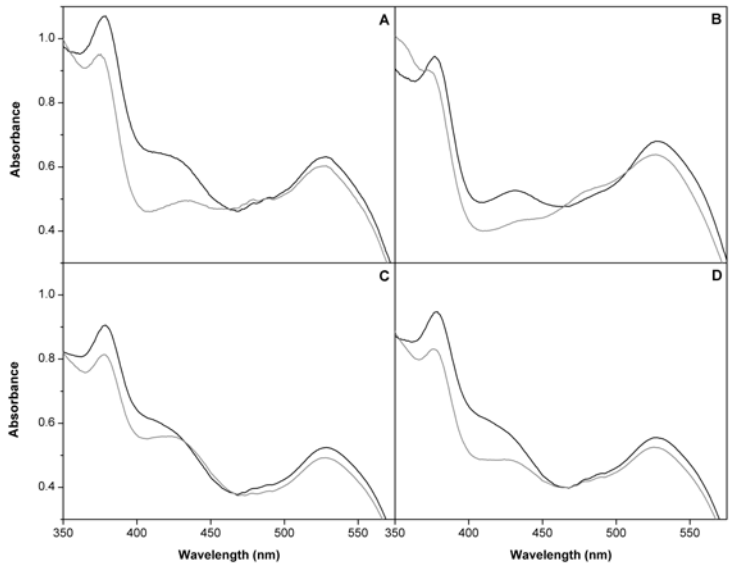

Figure 4.2 Anaerobic binding spectra for the Y187 variants. The holoenzyme solution contained 40 μM OAM, 40 μM PLP, and 40 μM AdoCbl in 100 mM NH_4^+EPPS pH 8.5. Spectral changes for Y187F (A and B) and Y187A (C and D) were recorded before (black line) and 10 minutes after (gray line) the addition of 2.5 mM D-ornithine (A and C) and the inhibitor DL-2,4-diaminobutyric acid (B and D).

4.5 Aerobic absorption spectra of the Y187 variants

Wild-type OAM shows an aerobic inactivation rate of 0.4 min^{-1} and 1.6 min^{-1} (absorbance increase at 358 nm) in the presence of D-ornithine and DL-2,4-diaminobutyrate, respectively, as shown in section 2.6.[108] The 4-fold difference in these rate constants is attributed to the inhibitor's ability to form an overstabilized organic radical that persists alongside the oxygen-sensitive cob(II)alamin species.[64, 108] A rapid increase in absorbance at 358 nm, representing interception of the cob(II)alamin species by O_2 to form cob(III)alamin, was observed in the aerobic binding spectra of both Tyr187 variants (Figure 4.3). In comparison to wild-type, the rate of inactivation is decreased 4- and 7-fold in the Y187F variant with DL-2,4-diaminobutyrate (0.38 min^{-1}) and D-ornithine (0.06 min^{-1}), respectively (Figure 4.4). In contrast, the Y187A variant shows a higher O_2 inactivation rate with D-ornithine (0.19 min^{-1}), such that it approximates the rate of inactivation in the presence of DL-2,4-diaminobutyrate (0.21 min^{-1}). The increased rate of cob(III)alamin formation with the physiological substrate points to an increased sensitivity of the Y187A variant to molecular oxygen.

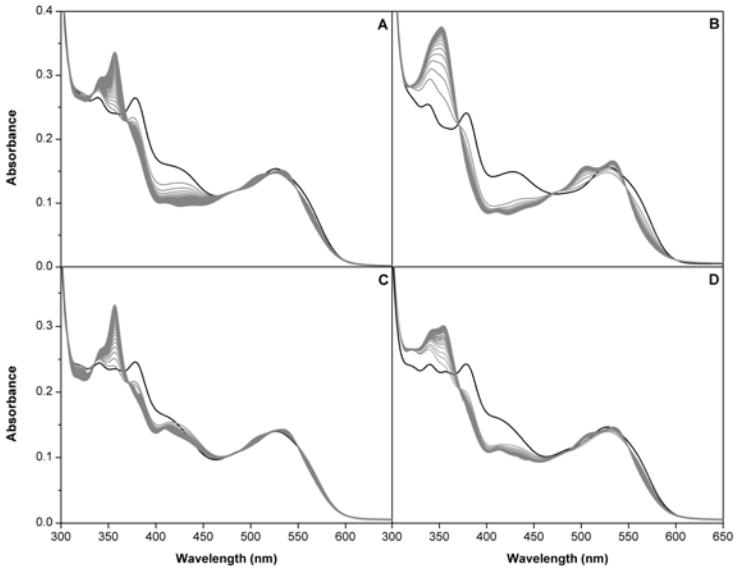

Figure 4.3 Aerobic binding spectra for the Y187 variants. The holoenzyme solution contained 15 μM OAM, 15 μM PLP, and 15 μM AdoCbl in 100 mM NH_4^+EPPS pH 8.5. Spectral changes for Y187F (A and B) and Y187A (C and D) were recorded prior to the addition of substrate (black lines) and then every minute for 30 minutes following the addition of 2.5 mM D-ornithine (A and C) and 2.5 mM DL-2,4-diaminobutyric acid (B and D).

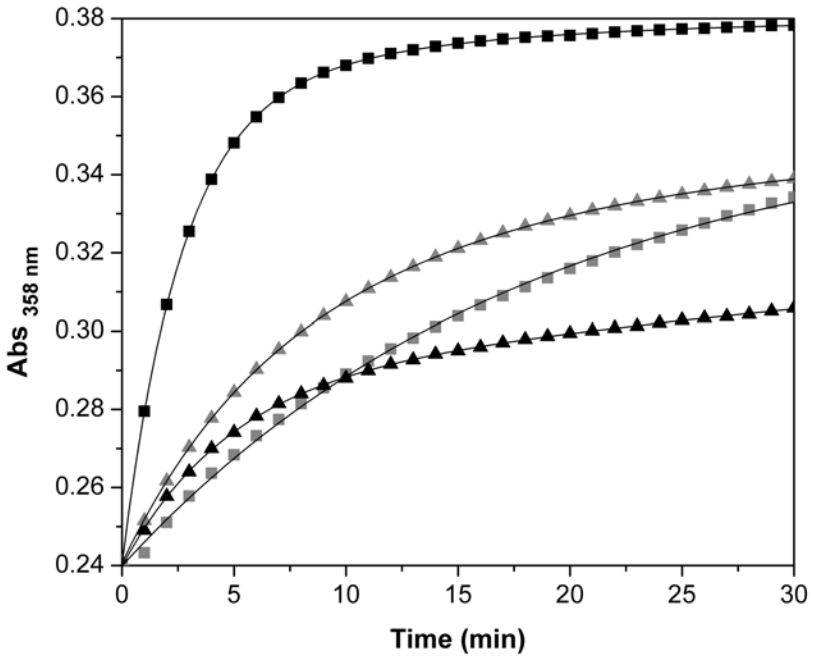

Figure 4.4 Rates of hydroxycobalamin formation in the Y187 variants. The rate of hydroxycobalamin formation was followed at 358 nm for Y187F (squares) and Y187A (triangles) upon reaction with DABA (black fill) and D-ornithine (gray fill). Data were fit to either a double or a single exponential equation to determine the observed rate constant for hydroxycobalamin formation. The Y187F variant showed inactivation rates of 0.38 ± 0.01 and 0.06 ± 0.01 min^{-1} for DABA and D-ornithine, respectively. The Y187A variant showed inactivation rates of 0.21 ± 0.01 and 0.19 ± 0.01 min^{-1} for DABA and D-ornithine, respectively.

4.6 Stopped-flow analysis of OAM and Y187 variants

Stopped-flow experiments were performed with the Y187F and Y187A variants upon reaction with DL-2,4-diaminobutyrate to determine the effect of the mutations on the observed rate constants for Co–C bond homolysis and transimination. The rate constant for transimination was reduced 2- and 6-fold for Y187F (266 ± 4 s^{-1}) and Y187A (75 ± 1 s^{-1}), respectively (Figure 4.5), compared to the native enzyme.[64] These results are consistent with the UV-visible spectral binding data (Figure 4.2), which showed smaller amplitude changes associated with external aldimine formation for D-ornithine and DL-2,4-diaminobutyate.

Similarly, the observed rate constant for Co–C bond homolysis was also reduced 2- and 6-fold for Y187F (531 ± 19 s^{-1}) and Y187A (165 ± 12 s^{-1}), respectively.

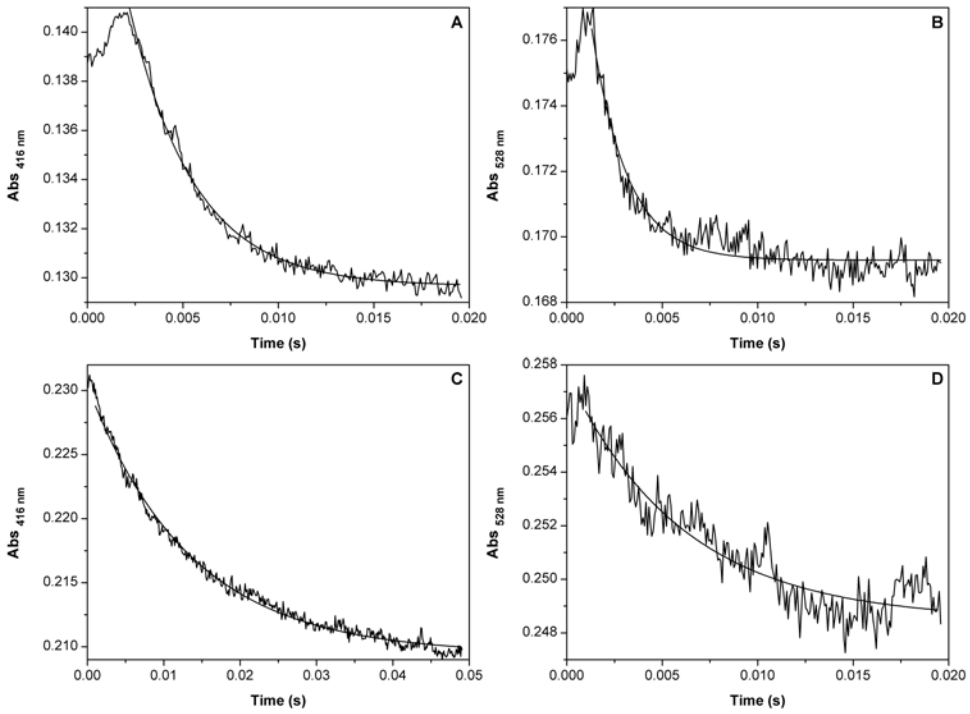

Figure 4.5 Stopped-flow absorbance changes following transimination and homolysis in the Y187 variants. Transimination and homolysis were monitored at 416 nm and 528 nm, respectively, following rapid mixing of 50 μM Y187F (A and B) and Y187A (C and D) with 5 mM DABA under anaerobic conditions. The rate constants for transimination were 266 ± 4 s^{-1} and 75 ± 1 s^{-1} for Y187F and Y187A, respectively. The rate constants for homolysis were 531 ± 19 s^{-1} and 165 ± 12 s^{-1} for Y187F and Y187A, respectively.

4.7 EPR Spectroscopy

Like OAM, native 5,6-LAM radical intermediates are also not detected by EPR during turnover with D- or L-lysine.[91] Instead, the radical intermediates of 5,6-LAM are typically studied using the substrate analogue 4-thia-L-lysine. Mutation of Y263α of 5,6-LAM, which is the analogous residue to Y187 in OAM, results in significant changes to the EPR spectrum obtained with 4-thia-L-lysine.[127] Most notable is the fact that the cob(II)alamin

and the organic radical become uncoupled in the variant enzyme, indicating that the distance between the paramagnetic centers increases to > 7 Å.

EPR spectra were obtained for Y187F and Y187A to determine whether an uncoupling of the two paramagnetic centers was also occurring in the OAM variants. The EPR spectrum of WT-OAM with DABA shows a major peak with a $g_{\perp}$ value of 2.11, along with a hyperfine splitting pattern further up field (Figure 4.6). The EPR spectrum of the Y187F variant shows a major peak also centered at g = 2.11 (Figure 4.6 inset); however, the signal intensity is weakened 9-fold compared to that of WT-OAM, indicating a lower level of radical formation, which is consistent with both the aerobic and anaerobic spectral studies. The shape of the EPR spectrum is otherwise identical to that of WT-OAM. Unlike the analogous mutation in 5,6-LAM, mutation of Tyr187 to a Phe does not result in decoupling of the cob(II)alamin and organic radical species. No EPR signal was detected for the Y187A variant upon reaction with DABA, indicating that even though the variant is still active, the radical does not accumulate to detectable levels.

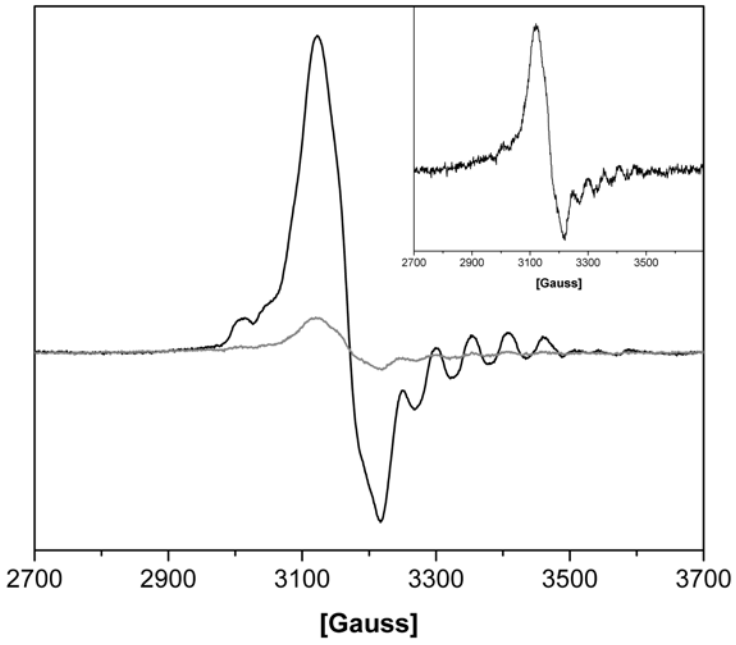

Figure 4.6 EPR spectra of holo-OAM and the Y187F variant mixed with DL-2,4-diaminobutyric acid. The EPR spectrum of wild-type OAM is shown in black. On the same vertical scale is the spectrum for Y187F (gray line) showing decreased signal intensity. The shape of the Y187F spectrum (inset) is identical to that of wild-type OAM.

4.8 Probing the possible role of PCET in OAM

We have shown in Chapter 3 that a highly conserved glutamate residue is involved in lowering the energy barrier to Co–C bond homolysis in the Class I mutases and Class III aminomutases. An alternative theory put forward by the Kozlowski computational research group suggests that proton-coupled electron transfer (PCET), mediated by an active site tyrosine residue, may also be involved in activation of the Co–C bond upon substrate binding.[128-131] The crystal structures of MCM from *Propionibacterium shermanii* (PDB entry 4REQ) and GM from *Clostridium cochlearium* (PDB entry 1I9C) show a tyrosine residue that coordinates to the carboxylate group of the substrate and is within 10 Å of the cobalt ion of AdoCbl (Figure 4.7). The Kozlowki group hypothesizes that the carboxylate group of the substrate deprotonates the neutral tyrosine residue (YOH) to produce a phenolate anion (YO^-) (Figure 4.8). The phenolate anion then transfers an electron to AdoCbl resulting in a $YO^{\bullet}$/$[AdoCbl]^{\bullet -}$ diradical system. The addition of an electron to AdoCbl thus lowers the Co–C bond dissociation energy.[128, 129]

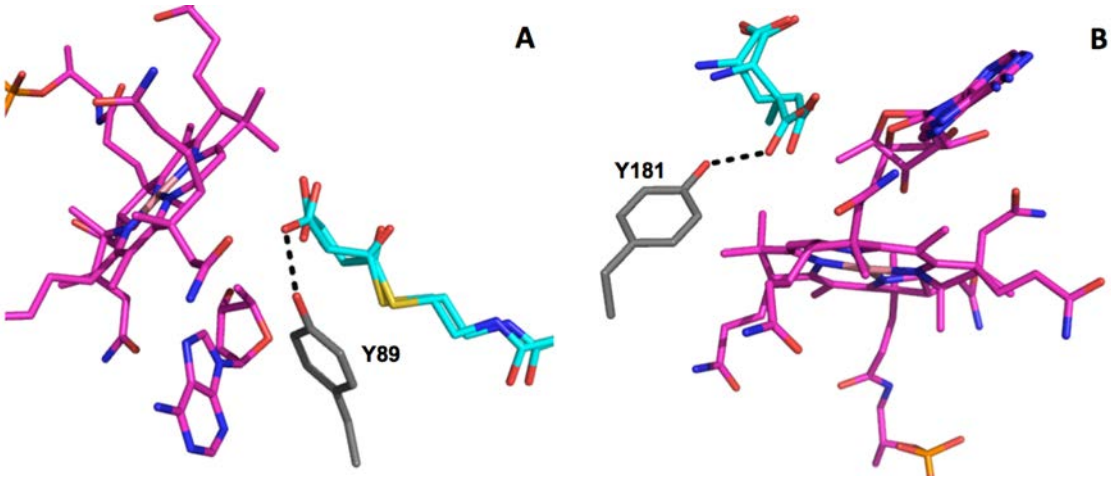

Figure 4.7 Substrate-bound active sites of methylmalonyl-CoA mutase and glutamate mutase showing location of possible PCET-linked tyrosine residue. (A) The active site of MCM from *Propionibacterium shermanii* (PDB entry 4REQ) showing the position of Y89 (gray) with respect to AdoCbl (pink) and substrate methylmalonyl-CoA (cyan). (B) The active site of GM from *Clostridium cochlearium* (PDB entry 1I9C) showing a similar interaction, between Y181 (gray) and the substrate glutamate (cyan), to that observed in MCM. Like Y89, Y181 is in close proximity to AdoCbl (pink).

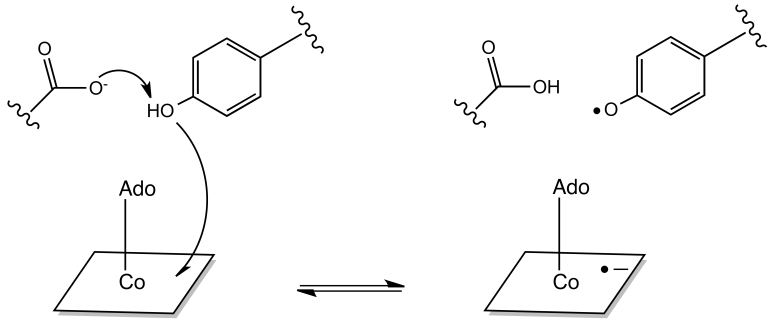

Figure 4.8 Proposed activation of the Co–C bond of AdoCbl-dependent isomerases through proton-coupled electron transfer. Substrate binding results in deprotonation of an active site tyrosine residue to produce a phenolate anion. The phenolate anion then transfers an electron to the AdoCbl cofactor, thus generating a diradical system.[128, 129]

Given that a similarly positioned tyrosine residue exists in both MCM and GM, a sequence alignment of several AdoCbl-dependent mutases was performed to investigate whether the tyrosine residue is structurally conserved. The alignment results shown in Figure 4.9 indicate that Y89 of MCM is not conserved amongst the other mutases. Moreover, the corresponding residue in GM is in fact an alanine rather than a tyrosine. A sequence alignment with respect to Y181 of GM was subsequently performed with similar results. As such, unlike the previously investigated glutamate, the tyrosine residue in question does not appear to be conserved amongst the class I mutases.

```
MCM    RPWTIRQYAGFSTAKE 97
HCM    RTWTMRQIAGFGTGED 98
ICM    RTWTIRQFAGFGNAEQ 88
ECM    SPWLFRTYAGHSTAKA 21
GM     ITLAQPRAGVALLDEH 75
MAM    LPCTIDSNTRLNDYAT 92
```

Figure 4.9 Multiple-sequence alignment of several AdoCbl-dependent mutases showing that Y89 of MCM is not a conserved residue: MCM (methylmalonyl-CoA mutase) from *Propionibacterium shermanii* (NC_014215.1), HCM (hydroxisobutyryl-CoA mutase) from *Methylibium petroleiphilum* (YP_001023546.1), ICM (isobutyryl-CoA mutase) from *Streptomyces clavuligerus* (EFG09395.1), ECM (ethylmalonyl-CoA mutase) from Rhodobacter sphaeroides (YP_354045.1), GM (glutamate mutase) from *Clostridium tetanomorphum* (CAA49910.1), and MAM (methylaspartate mutase) from *Arcobacter nitrofigilis* (ADG93549.1).

The crystal structure of substrate-bound OAM (PDB entry 3KOZ) reveals a tyrosine residue (Y160) that interacts with the α-carboxylate of the substrate and is in close proximity to the AdoCbl cofactor (Figure 4.10). Here we have mutated the residue to a phenylalanine to examine whether or not Y160 contributes to activation of the Co–C bond in OAM.

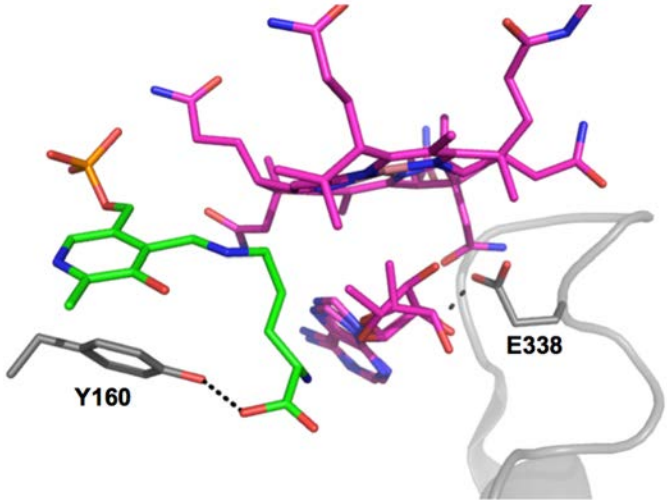

Figure 4.10 Substrate-bound active site of ornithine 4,5-aminomutase showing relative positions of Y160 and E338 with respect to the substrate and AdoCbl cofactor. Modeled closed active site of OAM showing the interaction that forms between E338 (gray) and the 5'-deoxyadenosyl moiety (pink) upon substrate binding. Y160 (gray) interacts with the α-carboxylate of the substrate (green) and is thought to participate in proton-coupled electron transfer.

4.9 Steady-state kinetic properties of the Y160F variant

As shown in Table 4.2, replacement of Y160 with a phenylalanine resulted in a 130-fold decrease in k_{cat} and a 30-fold decrease in k_{cat}/K_m. In addition, deuterium kinetic isotope effect studies with Y160F revealed a 2-fold increase in $^{D}k_{cat}$ and a 3.4-fold increase in $^{D}k_{cat}/K_m$ compared to the native enzyme (Table 4.3), suggesting that hydrogen atom abstraction is more rate-limiting in the variant. In comparison, E338D (investigated in Chapter 3) showed a 380-fold reduction in catalytic turnover and a 60-fold reduction in catalytic efficiency. In contrast to Y160F, E338D showed an ~2.5-fold increase in $^{D}k_{cat}/K_m$ while $^{D}k_{cat}$ remained unchanged relative to wild-type OAM. The significance of these differences is discussed later.

Table 4.2 Summary of steady-state kinetic parameters for the Y160F and E338D variants upon reaction with DL-ornithine and DL-ornithine-3,3,4,4,5,5-d_6.

Enzyme	k_{cat} (s^{-1})	K_m (DL-orn) μM	k_{cat}/K_m (DL-orn) $M^{-1}s^{-1}$
Y160F (DL-orn)	$2.3 \times 10^{-2} \pm 0.05 \times 10^{-2}$	131 ± 9	176 ± 16
Y160F (DL-orn-d_6)	$15.0 \times 10^{-4} \pm 0.4 \times 10^{-4}$	70 ± 5	21 ± 2
E338D (DL-orn)	$5.7 \times 10^{-3} \pm 0.1 \times 10^{-3}$	59 ± 3	97 ± 7
E338D (DL-orn-d_6)	$7.9 \times 10^{-4} \pm 0.1 \times 10^{-4}$	51 ± 3	15 ± 1

Table 4.3 Summary of observed kinetic isotope effects on k_{cat} and k_{cat}/K_m for wild type OAM and the Y160F and E338D variants.

Enzyme	$^{D}k_{cat}$	$^{D}k_{cat}/K_m$
Wild type	7.6 ± 0.5	2.5 ± 0.4
Y160F	15.3 ± 0.7	8.4 ± 1.5
E338D	7.2 ± 0.2	6.5 ± 0.9

4.10 Anaerobic and aerobic UV-visible spectroscopic characterization of Y160F

Anaerobic and aerobic UV-visible studies were conducted with Y160F to determine the effect of the mutation on formation of the external aldimine, homolysis of the Co–C bond, as well as the susceptibility of the variant to inactivation by molecular oxygen. Figure 4.11A shows the spectral changes observed upon addition of the natural substrate D-ornithine to the holoenzyme under anaerobic conditions. The decrease in absorbance at 416 nm, reflecting transimination, is similar to that of wild-type OAM. The decrease in absorbance at 528 nm (signifying homolysis), however, is much smaller compared to native OAM (Figure

2.7A). Figure 4.11B shows the spectral changes observed upon addition of the substrate analogue DL-2,4-diaminobutyrate. DABA induces a similar decrease in absorbance at 416 nm to that seen in wild-type OAM (Figure 2.7B), but as seen upon addition of D-ornithine homolysis is greatly impaired in Y160F. Additionally, no build-up of the cob(II)alamin species is observed at 470 nm.

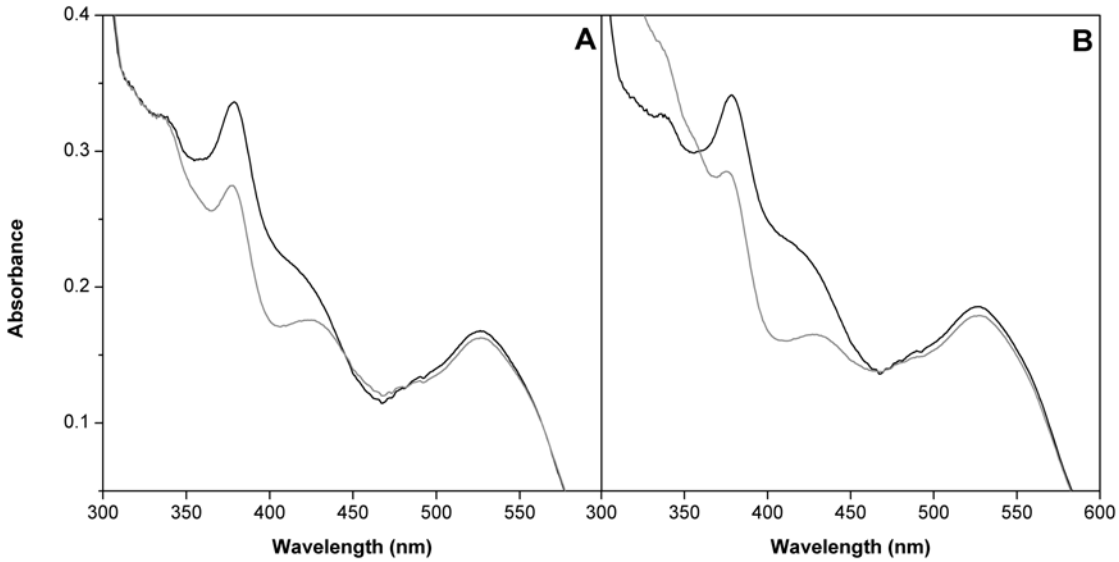

Figure 4.11 Changes in the anaerobic UV-visible absorbance spectra of OAM Y160F upon substrate binding. The holoenzyme reaction mixture contained 15 μM apoOAM, 15 μM PLP, and 15 μM AdoCbl in 100 mM NH_4^+EPPS buffer, pH 8.5. Spectral changes were recorded before (black line) and 10 minutes after (gray line) the addition of (A) 2.5 mM D-ornithine and (B) 2.5 mM DL-2,4-diaminobutyrate.

The aerobic UV-visible spectroscopic studies (Figure 4.12), followed over the time course of 45 minutes, suggest that the rate of formation of the external aldimine species in Y160F is slower than that of wild-type OAM. Notably, the addition of both D-ornithine (Figure 4.12A) and DL-2,4-diaminobutyrate (Figure 4.12B), results in a more gradual decrease in absorbance at 416 nm than that observed for the native enzyme (Figure 2.11). In addition, the variant appears to be less sensitive to inactivation by molecular oxygen. No build-up of cob(III)alamin (absorbance increase at 358 nm) is observed for Y160F in the presence of D-ornithine, while the rate constant for cob(III)alamin formation is 0.03 min^{-1} with DL-2,4-diaminobutyrate (Figure 4.12B). This represents a 50-fold decrease in the rate of

inactivation relative to the wild-type enzyme. Together these results suggest that mutation of Y160 to a phenylalanine affects the rate of external aldimine formation and Co–C bond homolysis.

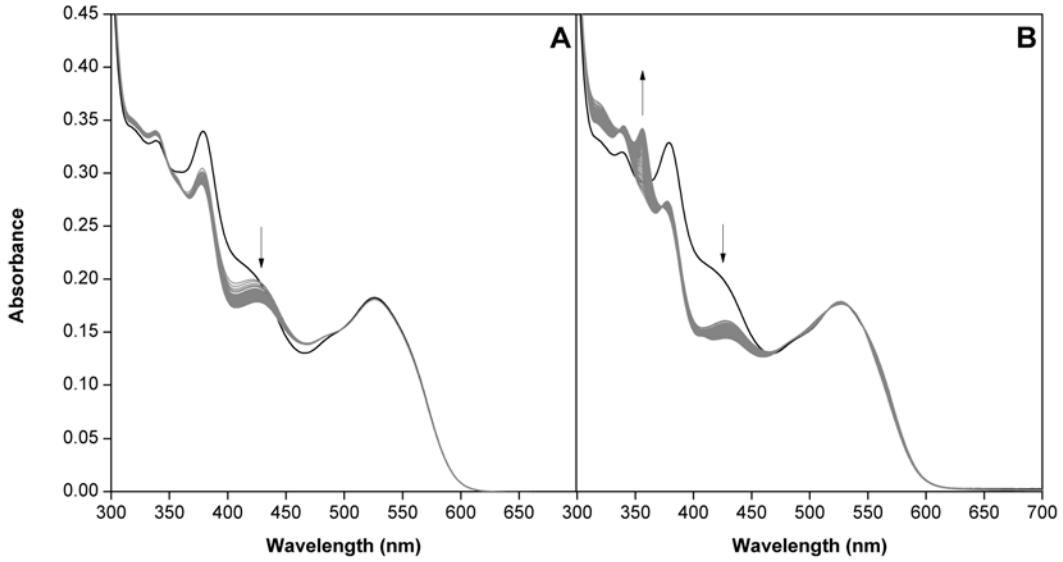

Figure 4.12 Aerobic UV-visible spectra of the OAM Y160F variant. The holoenzyme solution contained 15 μM apoOAM, 15 μM PLP, and 15 μM AdoCbl in 100 mM NH_4^+EPPS, pH 8.5. Spectral changes were recorded prior to the addition of substrate (black line) and then every minute for 45 minutes (gray lines) following the addition of (A) 2.5 mM D-ornithine and (B) 2.5 mM DL-2,4-diaminobutyrate. A slow absorbance decrease is observed at 416 nm over the time course of the reaction, upon addition of (A) D-ornithine and (B) DABA. The increase in absorbance at 358 nm in the presence of DABA signifies a build-up of cob(III)alamin. The rate constant for cob(III)alamin formation for DABA is 0.03 min^{-1}.

4.11 Pre-steady-state kinetic analysis of the Y160F variant

Based on the results of the UV-visible spectroscopic studies conducted under steady-state conditions, which point to impaired Co–C bond homolysis and slower substrate binding, pre-steady-state kinetic experiments were also performed with Y160F. As shown in Figure 4.13, the rate of external aldimine formation (138 ± 5 s^{-1}) was found to be 3-fold slower than that of wild-type OAM (464 ± 36 s^{-1}), while the observed rate of homolysis (553 ± 39 s^{-1}) showed a 2-fold decrease compared to wild-type (980 ± 88 s^{-1}).

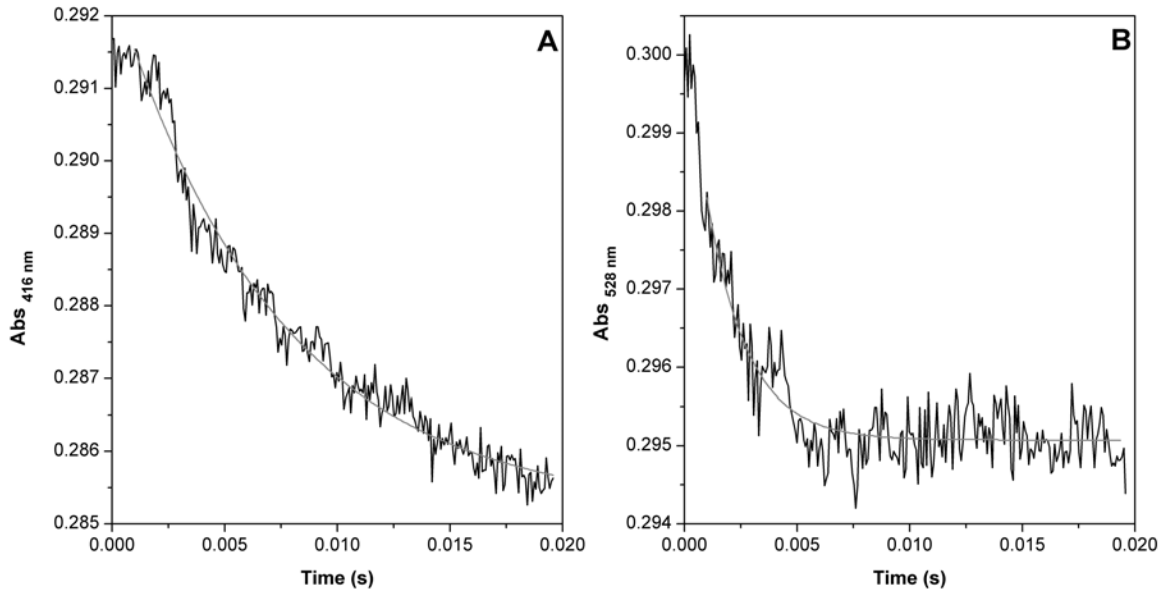

Figure 4.13 Stopped-flow absorbance changes following transimination and Co–C bond homolysis in Y160F. Formation of (A) the external aldimine and (B) homolysis of the Co–C bond of AdoCbl were followed at 416 nm and 528 nm, respectively. The absorbance changes were monitored over 20 ms following rapid mixing of 50 μM holoenzyme with 5 mM DL-2,4-diaminobutyrate. An average of 8–10 traces were fit to a monoexponential equation to obtain the observed rate constants for transimination (138 ± 5 s^{-1}) and homolysis (553 ± 39 s^{-1}).

4.12 Discussion

While the protein scaffold is sufficient for stabilizing the radical rearrangements performed by the Class I mutases, the Class III aminomutases also require the cofactor pyridoxal 5'-phosphate. PLP is traditionally known for stabilizing an α-carbanion intermediate, central to the reaction mechanism of most PLP-dependent enzymes, by electronic delocalization through the conjugated π-system. In the PLP-dependent aminomutases, computational studies suggest that PLP lowers the barrier to intramolecular isomerization and stabilizes the proposed cyclic azacyclopropylcarbinyl radical intermediate through captodative effects.[96] Recent studies of PLP-dependent enzymes have shown that external hydrogen-bond donors and acceptors to the pyridine nitrogen, imine nitrogen, and the phenolic oxygen influence the catalytic role of PLP and thereby control reaction specificity.[98, 132] Similarly, there is now growing evidence to suggest that residues positioned around PLP modulate the cofactor's role in radical catalysis within the PLP-dependent

aminomutases.[108, 127] Herein we have examined the role of Y187, which forms a π-stacking interaction with the pyridine ring of PLP in OAM, and therefore has the potential to influence catalysis. We also provide additional evidence to suggest that Co–C bond homolysis is kinetically gated by transimination. Finally, we have investigated the potential contribution of proton-coupled electron transfer to Co–C bond activation, which is thought to be mediated by Y160 in OAM.

4.12.1 Catalytic Role of Conserved π-stacking Tyrosine Residue

We have shown that Tyr187 is an important residue in OAM catalysis through its interaction with the PLP cofactor. In addition to the π-stacking interaction with the pyridine ring of PLP, Tyr187 also forms a hydrogen bond to the phosphate moiety of PLP via its hydroxyl group. Tyr263α makes identical contact to the PLP cofactor in the active site of 5,6-LAM. Removal of the hydroxyl group in Y263F, which disrupts the hydrogen bond to the phosphate moiety and thus allows the aromatic side-chain more rotational freedom, abolishes catalytic activity in 5,6-LAM.[127] In contrast, the corresponding mutation in OAM (Y187F) resulted in a 25-fold reduction in OAM turnover, while complete removal of the phenoxy side-chain in Y187A had a more pronounced affect, reducing activity 1260-fold. Pre-steady-state kinetic analysis revealed that mutation of Y187 leads to a slight decrease in the rate constant for transimination, thereby suggesting that the residue is involved in optimally positioning the PLP cofactor for external aldimine formation. UV-visible and EPR spectroscopy also revealed that the equilibrium between the intact AdoCbl cofactor and the organic radical and cob(II)alamin species is pushed towards the reactants, indicating that Y187F and Y187A are less susceptible to Co–C bond homolysis. A high activation energy barrier for Co–C bond homolysis is also consistent with the elevated deuterium kinetic isotope effects on k_{cat} and k_{cat}/K_m observed for Y187F because it indicates that hydrogen atom abstraction is more – if not fully – rate-determining. The fact that $^{D}k_{cat}$ (16.7 ± 0.4) greatly exceeds the expected semi-classical limit of 7 indicates a dramatic increase in the probability of hydrogen tunneling in this OAM variant, and/or that the substitution unmasks the underlying contribution of tunneling to the observed KIE. A precedent for hydrogen tunneling in adenosylcobalamin-dependent enzymes has been set by temperature-dependence

studies of the kinetic isotope effects in both glutamate mutase[133] and methylmalonyl-CoA mutase.[134] In summary, the combined reductions in the rate constants for transimination, Co–C bond homolysis, and hydrogen atom transfer likely account for the pronounced decreases in catalytic turnover for the Tyr187 variants.

In 5,6-LAM, the analogous tyrosine mutation (Y263F) not only abolishes enzyme activity, but also affects the integrity of the active site. The PLP-substrate radical is no longer able to maintain its distance from the Co(II) center, resulting in an uncoupling of the radical signals in the EPR spectrum.[127] The enzyme is in turn more susceptible to O_2 inactivation. In contrast, the EPR spectrum of Y187F is identical in line shape to that of wild-type OAM and the variant is less susceptible to inactivation by molecular oxygen. The intensity of the Y187F EPR signal is greatly reduced (9-fold) compared to wild-type OAM, but this is consistent with the UV-visible spectroscopic data that show a reduced level of cob(II)alamin formation. Thus, disruption of hydrogen bond contact with the PLP phosphate is less deleterious in OAM compared to 5,6-LAM. While removal of the stabilizing hydroxyl group in Y187F affects both transimination and radical initiation in OAM, it does not lead to uncoupling of the cob(II)alamin and organic radical species, indicating that the integrity of the OAM active site is retained. This perhaps explains why Y187F is not more susceptible to O_2 inactivation.

In OAM, only once the tyrosine residue was replaced with a less conservative amino acid, alanine, did the enzyme become more susceptible to oxygen inactivation. It is unclear why the mutation of the PLP-stacking tyrosine leads to differential effects on OAM and 5,6-LAM catalysis. It may be linked to active site architecture and the fact that OAM enlists more residues in securing the substrate within the active site. This extensive network of other noncovalent interactions may compensate for the effects of minor mutations, like Y187F. More tenuous substrate-protein interactions in 5,6-LAM likely ensure a broader substrate range, but they also offer a potential explanation as to why this enzyme is more prone to suicide inactivation with the physiological substrate.

Further evidence to suggest kinetic gating of homolysis by transimination is provided by the stopped-flow experiments performed with the Y187F and Y187A variants. Mutation of this residue to a Phe and Ala leads to a 2- and 6-fold reduction, respectively, in the rate constants for both homolysis and transimination. The modeled closed structure of OAM

shows that tyrosine 187 does not interact with the adenosylcobalamin cofactor. As such, its mutation is not expected to directly affect Co–C bond homolysis. Thus, the reduction in the rate constant for homolysis is likely a reflection of the reduced rate of external aldimine formation, rather than an increase in the energy barrier for homolysis. These results, combined with the lack of an observable kinetic isotope effect on the rate constant for Co–C bond homolysis, as shown in Chapter 2, suggest that homolysis is kinetically gated by the preceding (and slower) transimination step.

4.12.2 Does PCET contribute to Co–C bond activation in AdoCbl-dependent enzymes?

Computational studies of methylmalonyl-CoA mutase from *Propionibacterium shermanii* provide much of the support for the participation of PCET in the activation of the Co–C bond in AdoCbl-dependent enzymes.[128-131] An active site tyrosine residue (Y89 in MCM), which forms a hydrogen bond with the carboxylate group of the substrate (Figure 4.6A), is thought to act as an internal redox center by donating an electron to the corrin ring of AdoCbl (Figure 4.7).[128-131] DFT calculations allowing for spin polarization indicate that when the phenolate anion (YO^-) is positioned in close proximity to AdoCbl (mimicking crystal structure coordinates) the system was better described as the diradical species $YO^{\bullet}/[AdoCbl]^{\bullet -}$. In other words, the phenolate anion becomes oxidized following electron transfer to AdoCbl. The spin density was found to be equally distributed between the aromatic ring of tyrosine and the corrin ring of AdoCbl, and the diradical state was estimated to be ~7 kcal/mol lower in energy than the anionic state (gas phase calculations).[128] A follow-up study showed that when the enzymatic environment was taken into account the energy difference between the two states was only ~0.53 kcal/mol, but the diradical state was still favoured.[129] Additionally, it was shown that rotation of Y89 away from its crystal structure coordinates resulted in loss of formation of the diradical state, indicating that a specific orientation of the residue is required for electron transfer to occur.[129]

Two main experimental studies are taken as additional support for the proposed PCET mechanism in MCM. Firstly, mutation of Y89 to a phenylalanine residue resulted in a 580-fold reduction in the catalytic activity of MCM. In addition, the crystal structure of the Y89F variant (PDB entry 5REQ) revealed no significant structural differences from the wild-

type enzyme, indicating that the loss of enzyme function could be solely attributed to the removal of the phenolic hydroxyl group.[135] It was later proposed that Y89 alone accounted for ~10^3–10^4 of the observed $10^{12\pm1}$-fold rate enhancement for Co–C bond homolysis achieved by MCM.[136] Secondly, it has been shown that electrochemical reduction of AdoCbl to form the AdoCbl radical anion ($AdoCbl^{\bullet-}$) results in a $\geq 10^{12\pm2}$-fold rate enhancement for the homolysis step.[70, 137, 138] As such, a chemical precedent has been established for the proposed PCET mechanism whereby the additional electron enters the antibonding σ* LUMO of the Co–C bond to form a weakened $(\sigma)^2(\sigma^*)^1$ "three-electron bond", which is then cleaved to produce cob(I)alamin and the adenosyl radical.[70, 129] Thus, computational and experimental studies appear to support a role for PCET in Co–C bond activation.

There are, however, several issues that call into question the biological relevance of the one electron reduced cofactor, as well as the ability of a tyrosine residue to facilitate electron transfer to AdoCbl. First and foremost is the highly negative reduction potential of adenosylcobalamin (-1.2 to -1.6 V vs SCE) compared to the positive reduction potential of a tyrosine residue (+0.51 to +0.76 V), which makes electron transfer from YO^- to AdoCbl a highly thermodynamically unfavorable process.[70, 129, 130, 137, 139] Those in favor of the PCET theory argue that enzymes can appreciably tune the redox potentials of the donor and acceptor species to make electron transfer more favorable.[129] Even so, it seems unlikely that AdoCbl-dependent enzymes would be able to compensate for such a large energy gap.

A second issue stems from the proposed mechanism of formation of the phenolate anion, in which a carboxylate group with a pK_a ~4 deprotonates a tyrosine residue with a pK_a ~10. Given the acidity of the carboxylate group, proton transfer in this manner presents another thermodynamic barrier to PCET.

Thirdly, cob(II)alamin, rather than the expected cob(I)alamin intermediate, is observed during catalysis in AdoCbl-dependent enzymes, and no tyrosyl radicals have thus far been detected.[64, 140, 141] It is, however, suggested that the lack of experimental detection of cob(I)alamin and the tyrosyl radical could be attributed to rapid back transfer of an electron from cob(I)alamin to the tyrosyl radical, such that cob(II)alamin becomes the observed intermediate.[128]

Finally, the same findings that established a chemical precedent for Co–C bond activation, through one electron reduction of the cofactor, can also be taken as evidence

against the theory.[70] Given that electrochemical reduction of AdoCbl results in a $10^{12\pm2}$-fold rate enhancement for homolysis, mutation of Y89 in MCM would be expected to have a more profound effect on the rate of homolysis if it were participating in activation of the Co–C bond through PCET. Overall, even though PCET has been shown to participate in a number of radical enzymes, it remains unclear whether PCET is occurring in AdoCbl-dependent enzymes. Given that the residue is not well conserved across all AdoCbl-dependent mutases (Figure 4.9), even if PCET contributes to Co–C bond homolysis in MCM, it is an unlikely mechanism in the remaining mutases.

4.12.3 Does Y160 contribute to Co–C bond homolysis in OAM?

We have demonstrated that the interaction between the phenolic hydroxyl group of Y160 and the α-carboxylate group of the substrate (Figure 4.10) plays an important role in OAM catalysis. Even though D-ornithine is secured within the OAM active site by a bidentate ionic interaction with the guanidinium side-chain of Arg297, a salt-bridge interaction with Glu81, and a hydrogen bond with His182 (Figure 2.15), removal of the phenolic hydroxyl group in Y160F resulted in a 130-fold reduction in OAM turnover. Pre-steady-state kinetic analysis revealed a 3-fold decrease in the rate constant for transimination, suggesting that Y160 (like Y187) is involved in positioning the substrate relative to the PLP cofactor for efficient external aldimine formation. Anaerobic UV-visible spectroscopy revealed limited homolysis of the Co–C bond in Y160F with both D-ornithine and DL-2,4-diaminobutyrate, and no detectable cob(II)alamin build-up (Figure 4.11), suggesting that the equilibrium constant for homolysis is shifted in favor of the intact cofactor. This is consistent with the reduced susceptibility of the variant to inactivation by molecular oxygen. Furthermore, Y160F exhibited elevated deuterium kinetic isotope effects on k_{cat} and k_{cat}/K_m, indicating that the barrier to hydrogen atom abstraction and/or homolysis is increased and therefore more rate-determining in the catalytic mechanism.

A comparison of the KIE obtained for wild-type OAM, Y160F, and the E338D variant from Chapter 3 provides additional insight into the role of Y160 in OAM catalysis. As demonstrated in Chapter 2, substrate binds to the active site of wild-type OAM with a relatively tight binding affinity. As such, the rate of substrate release is slow relative to

product formation, which consequently suppresses the value of $^{D}k_{cat}/K_m$ relative to $^{D}k_{cat}$. Mutation of E338 to an aspartate results in differential effects on $^{D}k_{cat}$ and $^{D}k_{cat}/K_m$. Specifically, the value of $^{D}k_{cat}/K_m$ increases ~2.5-fold compared to wild-type OAM, while the value of $^{D}k_{cat}$ remains the same. The increase in only $^{D}k_{cat}/K_m$ indicates that the mutation slows the rate of product formation by increasing the energy barrier for one or more steps of the mechanism prior to product release. Combined with additional spectroscopic evidence, this step was determined to be homolysis of the Co–C bond. Like E338D, substitution of Y160 with a phenylalanine also results in differential effects on $^{D}k_{cat}$ and $^{D}k_{cat}/K_m$. However, in the case of Y160F, $^{D}k_{cat}$ increases 2-fold, while $^{D}k_{cat}/K_m$ increases 3.4-fold. The fact that $^{D}k_{cat}/K_m$ increases by a greater amount than $^{D}k_{cat}$ suggests that, in addition to an increased barrier to hydrogen transfer, other steps of the mechanism are also affected by the mutation. These steps could include transimination and homolysis, as both showed slower rate constants relative to the native enzyme, as well as isomerization. However, given that homolysis is 'gated' by transimination in OAM, the reduced rate constant for homolysis is likely in part due to the reduced rate constant for transimination, rather than a true increase in the barrier for homolysis.

Replacement of the active site tyrosine residue with a phenylalanine produces markedly different results in OAM than it does in MCM. Mutation of Y89 in MCM results in a more pronounced decrease in catalytic activity (580-fold) compared to mutation of Y160 in OAM (130-fold). Moreover, in contrast to Y160F, the Y89F variant exhibits a 4-fold decrease in the value of $^{D}k_{cat}$ compared to native MCM, indicating that hydrogen transfer is no longer rate-limiting in the mechanism. Y89F displays no detectable homolysis under both pre-steady-state and steady-state conditions which, in combination with the reduced value of $^{D}k_{cat}$, indicates that homolysis is rate-determining in the variant. Thus, the presence of Y89 in the MCM active site accounts for ~10^3 of the $10^{12\pm1}$-fold rate acceleration of the Co–C bond homolysis step.[136] In comparison, not only is homolysis detected in the OAM variant (albeit limited), the rate of Co–C bond homolysis in Y160F is only 2-fold slower than native OAM. Thus, it appears from these data that Y160 contributes less to homolysis in OAM than does Y89 in MCM, and that PCET mediated by Y160 is an unlikely contributor to activation of the Co–C bond.

4.12.4 Concluding remarks

In summary, we have shown through mutagenesis and isotope studies that the π-stacking interaction between Y187 and the pyridine ring not only optimally positions the PLP cofactor for formation of the external aldimine, but is also essential for positioning the substrate relative to the adenosyl radical for effective hydrogen atom abstraction in OAM. In addition, the differential effects observed in OAM and 5,6-LAM upon mutation of the conserved tyrosine residue provide further support for tighter substrate binding interactions in OAM, which lead to increased substrate specificity and more controlled radical chemistry compared to 5,6-LAM. We also provide additional evidence to support kinetic gating of Co–C bond homolysis by the preceding transimination step, as slower rates of transimination in the Y187 and Y160 variants are reflected in the slower rates of homolysis. Finally, mutation of Y160 to a phenylalanine residue minimally affects homolysis suggesting that PCET does not contribute to labilization of the Co–C bond in OAM.

4.13 Experimental procedures

4.13.1 Materials

AdoCbl, PLP, D-ornithine, L-ornithine, and DL-2,4-diaminobutyric acid were obtained from Sigma. L-ornithine-3,3,4,4,5,5-d_6 hydrochloride was obtained from C/D/N Isotopes Inc. DL-ornithine-3,3,4,4,5,5-d_6 was prepared as described in section 2.9.6. The Ni^{2+}-nitrilotriacetic acid (Ni-NTA) column and Q-sepharose High Performance resins were from GE Biosciences. Restriction endonucleases were from New England Biolabs, *Pfu* Turbo DNA polymerase was from Agilent Technologies and Rosetta(DE3)pLysS competent cells were purchased from EMD Biosciences. All other chemicals were purchased from Fisher Scientific and were of the highest grade available.

4.13.2 Construction of OAM variants

The Y187F, Y187A, and Y160F single-point mutations were introduced into the pOAMH2 vector[64] using the QuikChange site-directed mutagenesis kit (Agilent Technologies, Mississauga, ON). The forward and reverse primers for the Y187F variant are 5'-GCT CAC CAA GAT CCA CAA TTC AAC GTA CTA TAC AGA AAT ATT AAT ATG-3' and 5'-CAT ATT AAT ATT TCT GTA TAG TAC GTT GAA TTG TGG ATC TTG GTG AGC-3', respectively. The complementary primers for the Y187A variant are 5'-GCT CAC CAA GAT CCA CAA GCC AAC GTA CTA TAC AGA AAT ATT AAT ATG-3' and 5'-CAT ATT AAT ATT TCT GTA TAG TAC GTT GGC TTG TGG ATC TTG GTG AGC-3'. The forward and reverse primers for the Y160F variant are 5'-CCA ATT AAC TAT CAT TCA TTT GTT TCT GGA GTT GCA GG-3' and 5'-CC TGC AAC TCC AGA AAC AAA TGA ATG ATA GTT AAT TGG-3'. The NAPS DNA Sequencing Laboratory at University of British Columbia, Vancouver, Canada confirmed the presence of the mutations and the absence of any other PCR-induced errors.

4.13.3 Enzyme purification

The OAM variants and wild-type DAPDH were purified as previously described in section 2.10.5.

4.13.4 Coupled enzyme assays

The activity of the OAM variants towards DL-ornithine and DL-ornithine-3,3,4,4,5,5-d_6 was measured using a coupled spectrophotometric assay with DAPDH, as previously described in section 2.10.7.

4.13.5 Aerobic and Anaerobic UV-visible spectroscopy

Aerobic and anaerobic spectral studies were performed as previously described in sections 2.10.9 and 2.10.10.

4.13.6 Stopped-flow spectroscopy

Pre-steady-state kinetic analysis following Co–C bond homolysis (decrease at 528 nm) and transimination (decrease at 416 nm) was carried out as described in section 2.10.11.

4.13.7 EPR spectroscopy

The EPR samples containing 600 μM holoY187F and holoY187A were prepared as described for wild-type OAM in section 2.10.12. EPR spectra were recorded at a frequency of 9.379 GHz, microwave power of 2.0 mW, time constant of 40.96 ms, and modulation amplitude of 6 G. Five two minute scans were averaged for each sample.

Chapter 5 : Importance of the Protonation State of the Imino and Pyridine Nitrogens of Pyridoxal 5'-Phosphate in Ornithine 4,5-aminomutase Catalysis.

5.1 Chapter summary

Pyridoxal 5'-phosphate (PLP), in the active site of ornithine 4,5-aminomutase (OAM), forms a Schiff base with terminal amino group of the D-ornithine side-chain and facilitates interconversion of the amino acid to (2R,4S) 2,4-diaminopentanoic acid *via* a radical-based mechanism. The crystal structure of OAM reveals that His225 is within hydrogen bond distance to the PLP phenolic oxygen, and may influence the pK_a of the Schiff base during radical rearrangement. To evaluate the role of His225 in radical stabilization and catalysis, the residue was substituted with a glutamine or an alanine. The H225Q and H225A variants have a 3- and 10-fold reduction in catalytic turnover, respectively, and a decrease in catalytic efficiency (7-fold for both variants). Diminished catalytic performance is not linked to an increase in radical-based side reactions leading to enzyme inactivation. pH-dependence studies show that k_{cat} increases with the ionization of a functional group, but it is not attributed to His225. Binding of 2,4-diaminobutyrate to native OAM leads to formation of an overstabilized 2,4-diaminobutyryl-PLP radical. In the H225A and H225Q variants, the radical forms and then decays, as evidenced by accumulation of cob(III)alamin. From these data, we propose that His225 enhances radical stability by acting as a hydrogen bond acceptor to the phenolic oxygen, which favors the deprotonated state of the imino nitrogen and leads to greater resonance stabilization of the 2,4-diaminobutyryl-PLP radical intermediate. Recent studies of PLP-dependent enzymes have highlighted the importance of the protonation state of the pyridine nitrogen and its ability to control reaction specificity in traditional PLP-dependent enzymes.[98] Computational studies have also shown that the protonation state of the pyridine nitrogen may be important in stabilizing and lowering the barrier to formation of the proposed azacyclopropylcarbinyl radical intermediate during OAM catalysis. Here we have mutated Ser162, which forms a hydrogen bond with the pyridine nitrogen, to an alanine and an aspartate to evaluate its role in OAM catalysis. Additionally, the effect of methylating the pyridine nitrogen was assessed by reconstituting

OAM with the PLP analogue N-methyl-PLP. The S162A and S162D variants have a 50- and 1450-fold decrease in catalytic activity. Pre-steady-state kinetic analysis of S162A reveals diminished rate constants for both transimination and homolysis, which may in part account for the reduced activity of the variant. Additionally, deuterium kinetic isotope effects indicate that a step in the mechanism, other than hydrogen transfer, is more rate-limiting in S162A. Both variants exhibit minimal homolysis of the Co–C bond and are less susceptible to oxygen inactivation. Replacement of Ser162 with an aspartate, thereby promoting protonation of the pyridine nitrogen, shifts the tautomeric equilibrium of the external aldimine towards the hydrogen-bonded iminium zwitterion form, which likely destabilizes potential radical intermediates. Substitution of the native PLP cofactor with the N-methyl-PLP analogue results in an 88-fold decrease in k_{cat}, and produces similar isotope effects to those observed with S162A. The reduced catalytic activity is not attributed to weaker binding of N-methyl-PLP within the OAM active site, but could be explained by impaired transimination and homolysis of the Co–C bond. The potential role of His225 and Ser162, as well as the protonation states of the imino and pyridine nitrogens in lowering the activation energy barrier to mediate PLP-dependent radical rearrangements is discussed.

5.2 Interaction of H225 with phenolic oxygen of PLP

The crystal structure of OAM extends the profile for enzymatic control of radical catalysis beyond that of the PLP cofactor, revealing residues directly coordinated to the cofactor and their potential role in facilitating radical rearrangement of the PLP-bound substrate. In the previous chapter, we showed that tyrosine 187, which forms a π-stacking interaction with the pyridine ring of PLP, participates in formation of the external aldimine species as well as stabilization of radical intermediates during catalysis. Here we have turned our attention to His225, which forms a hydrogen bond to the PLP phenolic oxygen (Figure 5.1). Given that the imidazole side chain can act as both a hydrogen bond donor and a hydrogen bond acceptor to the phenolic oxygen, the active site residue can potentially influence the pK_a of the Schiff base of the PLP external aldimine. Thus, the location of His225 suggests a possible role in catalysis and/or radical stabilization by direct participation

in proton transfer to the PLP aldimine in one or more steps of the catalytic mechanism of OAM. As such, His225 was substituted with an alanine (H225A) and a glutamine (H225Q) to investigate its role in catalysis as a proton donor or acceptor to the phenolic oxygen.

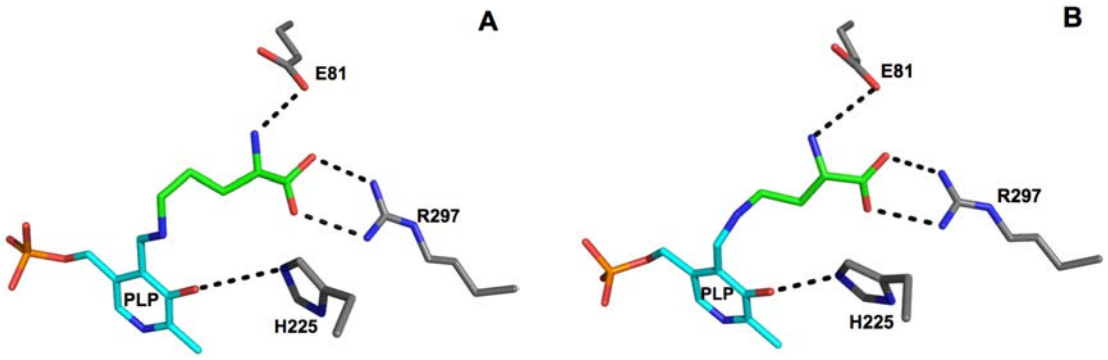

Figure 5.1 Active site of OAM complexed with the natural substrate D-ornithine and the substrate analogue DL-2,4-diaminobutyrate. (A) The natural substrate D-ornithine (green) and (B) the substrate analogue DL-2,4-diaminobutyrate form a covalent imine linkage with the PLP cofactor (cyan). Shown in gray is His225 which hydrogen bonds to the phenolic oxygen of PLP, as well as Arg297 and Glu81, which interact with the substrate. PDB ID: 3KOZ (A) and 3KOX (B).

5.3 Steady-state kinetic parameters for the H225 variants

The steady-state kinetic parameters for the H225A and H225Q variants were determined using the aforementioned coupled-enzyme assay. The turnover number for wild-type OAM was 2.9 ± 0.1 s^{-1}. Substitution of His225 with a glutamine resulted in a 3-fold reduction in k_{cat} (Table 5.1). Removal of the imidazole moiety and disruption of hydrogen bonding to the phenolic group of PLP achieved in the H225A variant had a more substantial effect on the turnover rate, decreasing it 10-fold. The K_m for D-ornithine is 453 ± 34 μM and 140 ± 5 μM for the H225Q and H225A variants, respectively. Consequently, the catalytic efficiency (k_{cat}/K_m) decreases by the same magnitude (7-fold) in both variants (2.2 x 10^3 $M^{-1}s^{-1}$) compared to the native enzyme (15.2 x 10^3 $M^{-1}s^{-1}$). The inhibition constant, K_i, for DABA also increased the same magnitude in both the H225A (95 ± 25 μM) and

H225Q (98 ± 17 μM) variants compared to wild-type (5 ± 1 μM), indicating that H225 contributes to inhibitor binding. Additionally, H225A showed a $^{D}k_{cat}$ value of 9.8 ± 0.4 and a $^{D}k_{cat}/K_m$ value of 5.8 ± 0.6, which are respectively 1.3- and 2.3-fold greater than the values obtained for wild-type OAM. The elevated deuterium isotope effects indicate that hydrogen transfer is more rate-limiting in the H225A variant.

Table 5.1 Summary of steady-state kinetic parameters for wild-type OAM and the H225Q and H225A variants.

Enzyme	k_{cat} (s^{-1})	K_m (D-orn) μM	K_i (DABA) μM	k_{cat}/K_m (D-orn) × 10^3 $M^{-1}s^{-1}$
Wild-type	2.9 ± 0.1	190 ± 13	4.6 ± 0.6	15.2 ± 1.2
H225Q	1.0 ± 0.1	453 ± 34	98 ± 17	2.2 ± 0.2
H225A	0.3 ± 0.1	140 ± 5	95 ± 25	2.2 ± 0.1

5.4 pH dependence on k_{cat} for wild-type OAM and the H225 variants

Given that the steady-state kinetic assays were performed at pH 8.5, it is likely that the imidazole ring of His225 is neutral given that the pK_a of the imidazole side chain is ~6.5. In this ionization state, the residue may be acting as a general base to the phenolic group, increasing the pK$_a$ of the imino nitrogen. As His225 was shown to affect OAM turnover, the pH dependence of k_{cat} was measured to determine if the protonation state of the imidazole ring influences the steady-state kinetic parameters. For wild-type OAM and the His225 variants, k_{cat} increased at higher pH and plots of log k_{cat} versus pH (Figure 5.2) had a limiting slope of 1 on the acidic limb, indicating that for each variant of OAM, one ionizable group limits turnover. A fit of equation 5.2 (section 5.16.1) to the data produced pK$_a$ values of 7.1 ± 0.1, 7.6 ± 0.1, and 7.4 ± 0.2 for wild-type, H225A, and H225Q, respectively. The protonation

state of His225 does not limit steady-state catalysis, as the pH profiles and calculated pK_a values are similar between the three forms of OAM.

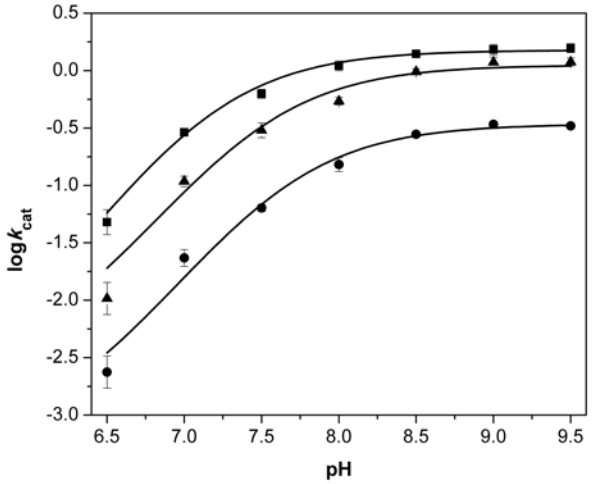

Figure 5.2 pH dependence profile for turnover of wild-type OAM and the His225 variants. The data for wild-type OAM (squares), H225Q (triangles), and H225A (circles) were fit to equation 5.2. Similar pK_a values of 7.1 ± 0.1, 7.6 ± 0.1, and 7.4 ± 0.2 were obtained for wild-type OAM, H225A, and H225Q, respectively.

5.5 Anaerobic UV-visible spectroscopic assays for H225A and H225Q

As detailed in section 2.2, the binding of D-ornithine to holoOAM induces UV-visible absorbance changes, including a decrease in absorbance at 416 nm caused by the formation of the external aldimine and a small reduction in absorbance at 528 nm demonstrating homolysis of the Co–C bond (Figure 2.7). In addition, OAM is susceptible to suicide inactivation whereby the undetectable cob(II)alamin intermediate is converted to cob(III)alamin. The rate constant for cob(III)alamin formation in the native enzyme under anaerobic conditions is 0.08 min^{-1} (Figure 5.3). Spectral perturbations upon the addition of D-ornithine to H225Q and H225A are similar to that of wild-type OAM, as all three show a decrease at 416 nm indicating binding of substrate to PLP and an increase in absorbance at 358 nm, representing formation of cob(III)alamin at the rate of ~0.06 min^{-1} (Figures 5.4A and 5.4C). The fact that the rate of cob(III)alamin formation is similar between the OAM variants indicates that the His225 variants are not more susceptible to enzyme inactivation compared

to the native enzyme. It is interesting to note that upon addition of D-ornithine to H225A, the absorbance change at 528 nm (Figure 5.4C) is negligible, indicating that homolysis of the Co–C bond is catalytically restricted in this variant.

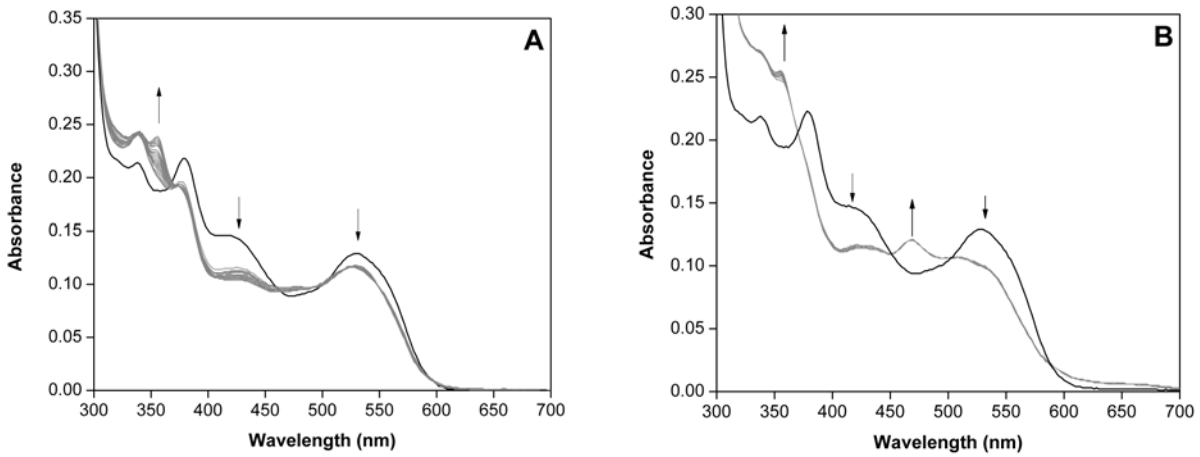

Figure 5.3 Anaerobic inactivation of wild-type OAM upon addition of D-ornithine and DL-2,4-diaminobutyrate. The holoenzyme solution contained 15 μM apoOAM, 15 μM PLP, and 15 μM AdoCbl in 100 mM NH_4^+EPPS buffer, pH 8.5. UV-visible spectra were recorded from 300 to 700 nm before (black line) and every minute for 30 minutes following the addition of (A) 2.5 mM D-ornithine and (B) 2.5 mM DL-2,4-diaminobutyrate. Only representative spectra are shown.

Binding of the substrate analogue, DL-2,4-diaminobutyrate, to wild-type OAM leads to formation of an external aldimine species (absorbance decrease at 416 nm; Figures 5.3B, 5.4B and 5.4D). However, in contrast to the natural substrate, binding of DABA also leads to an absorbance peak at 470 nm in native OAM, representing detectable cob(II)alamin formation (Figure 5.3B). The stable nature of the 2,4-diaminobutyryl-PLP radical intermediate, which is tightly coupled to the cob(II)alamin species, is emphasized by minimal formation of cob(III)alamin during the 30 minute time course of the reaction (Figure 5.3B). UV-visible absorbance changes following the addition of DABA to the H225Q and H225A variants are distinctive from wild-type. As for the native enzyme, binding of the inhibitor leads to a decrease at 416 nm indicating formation of the external aldimine. There is also a peak at 470 nm, but unlike the wild-type enzyme both variants exhibit a relatively rapid increase in absorbance at 358 nm, suggesting that the biradical state of the enzyme is

unstable as cob(II)alamin loses an electron to form cob(III)alamin by a pathway that is independent of O_2. Comparison of the UV-visible absorbance spectra between the two His225 variants in Figures 5.4B and 5.4D reveals that there is less AdoCbl homolysis and cob(II)alamin in H225A compared to H225Q. The rate of cob(III)alamin formation is also slower in H225A (0.10 min^{-1}) compared to H225Q (0.23 min^{-1}), supporting the observation that there is less overall radical formation for this variant. Less efficient AdoCbl homolysis may also account for slower steady-state turnover by the OAM H225A variant.

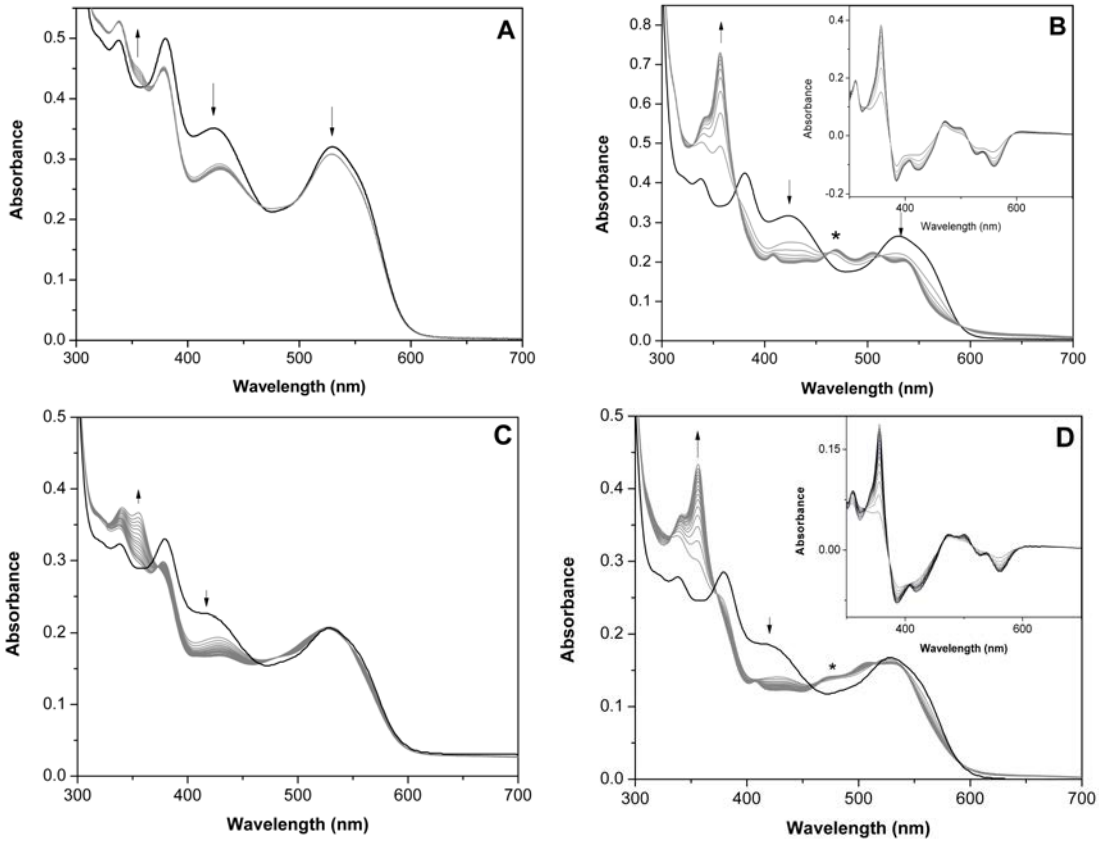

Figure 5.4 Anaerobic UV-visible spectral changes of holoOAM H225Q and H225A variants following the addition of D-ornithine and DL-2,4-diaminobutyrate. The holoenzyme solution contained 15 μM apoOAM, 15 μM PLP, and 15 μM AdoCbl in 100 mM NH_4^+EPPS buffer, pH 8.5. Spectral changes in H225Q (A and B) and H225A (C and D) were recorded before (black line) and after (gray lines) the addition of 2.5 mM D-ornithine (A and C) and DL-2,4-diaminobutyrate (B and D). Spectra were recorded every 2 minutes for 30 minutes. Only representative spectra are shown.

5.6 Aerobic UV-visible spectroscopic assays for H225A and H225Q

To determine if the His225 mutations make the enzyme more susceptible to O_2 inactivation (causing oxidation of cob(II)alamin to cob(III)alamin), the UV-visible absorbance assays were repeated under aerobic conditions (Figure 5.5). Mutation of His225 to a glutamine or alanine decreases the sensitivity of the enzyme to O_2 inactivation with D-ornithine and DL-2,4-diaminobutyrate with respect to the wild-type enzyme (0.4 min^{-1}). The rate constants for cob(III)alamin formation with D-ornithine are 0.13 and 0.07 min^{-1} for H225A and H225Q (Figures 5.5A and 5.5C), respectively, while the corresponding rate constants for the two variants with DABA are 0.15 and 0.33 min^{-1} (Figures 5.5B and 5.5D).

The overall reduced sensitivity of the variant enzymes to O_2 suggests that less cob(II)alamin exists in the active site following binding of the substrate or inhibitor compared to the wild-type enzyme. This may arise from less efficient AdoCbl Co–C bond homolysis leading to slower cob(II)alamin formation, as has been suggested from the anaerobic UV-visible spectral assays involving H225A. As shown in Chapter 2, the rate of aerobic inactivation of wild-type OAM is 4-fold greater in the presence of DL-2,4-diaminobutyrate (1.6 min^{-1}) than with D-ornithine (0.4 min^{-1}). Even though H225Q presents with reduced sensitivity to O_2 compared to wild-type, the rate of inactivation is still faster with DABA (0.33 min^{-1}) than with D-ornithine (0.07 min^{-1}). In contrast, H225A shows similar rates of inactivation with D-ornithine (0.13 min^{-1}) and DABA (0.15 min^{-1}), indicating that the H225A variant is in fact more sensitive to molecular oxygen.

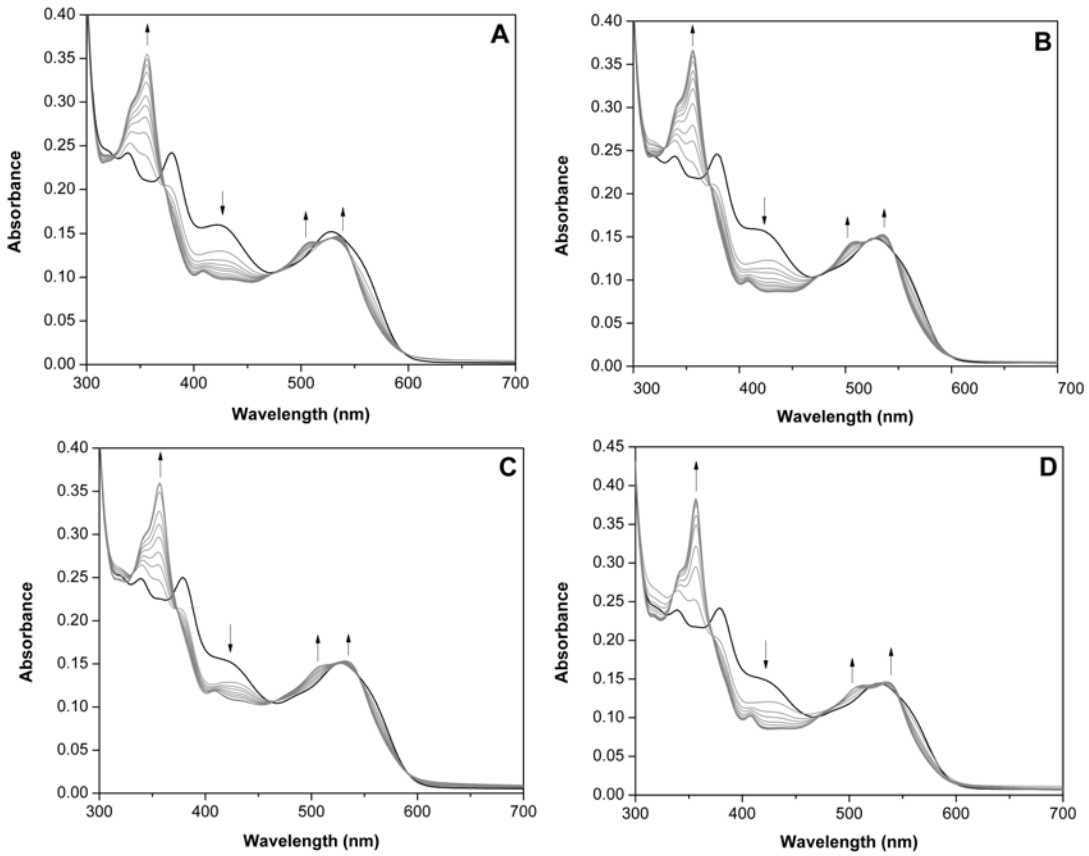

Figure 5.5 Aerobic UV-visible spectral changes of holoOAM H225Q and H225A variants following the addition of D-ornithine and DL-2,4-diaminobutyrate. The holoenzyme solution contained 15 μM apoOAM, 15 μM PLP, and 15 μM AdoCbl in 100 mM NH_4^+EPPS buffer, pH 8.5. Spectral changes in H225A (A and B) and H225Q (C and D) were recorded before (black line) and after (gray lines) the addition of 2.5 mM D-ornithine (A and C) and DL-2,4-diaminobutyrate (B and D). Spectra were recorded every 2 minutes for 30 minutes. Only representative spectra are shown.

5.7 Spectroscopic properties of PLP-bound OAM and the H225 variants

UV-visible spectroscopy was also used to determine if the His225 variants perturb the protonation state of the Schiff base of the external aldimine with either D-ornithine or DABA bound to the enzyme. As shown in Figure 5.6, the two PLP tautomers of the external aldimine arise from internal proton transfer between the imino nitrogen and the 3-oxo anion of the pyridine ring. A hydrogen-bonded iminium zwitterion (A) forms upon protonation of the Schiff base; this tautomer has an absorption maximum between 401 nm and 425 nm. Internal proton transfer to the phenolic oxygen generates a hydrogen-bonded imine (B1),

with an absorption maximum between 325 nm and 340 nm.[142] If His225 acts as a hydrogen-bond acceptor to the phenolic oxygen, it may shift the equilibrium towards the hydrogen-bonded imine state of the cofactor, by favoring the B2 intermediate of Figure 5.6.

To observe a change in the equilibrium distribution of the PLP tautomers, absorbance spectra were recorded for OAM with only PLP bound to the enzyme (referred to as PLP-OAM), as the absorbance spectrum of AdoCbl partially masks that of PLP. Figure 5.7A shows that the D-ornithinyl-PLP external aldimine is a mixture of the hydrogen-bonded imine (absorbance shoulder at 330 nm) and hydrogen-bonded iminium zwitterion (absorbance peak at 415 nm) with the major species being the latter form. This indicates that the imino nitrogen is predominantly protonated in the D-ornithinyl-PLP-OAM complex (without AdoCbl). In contrast, loading of DABA onto PLP-OAM results in a shift of the tautomeric distribution towards the hydrogen-bonded imine (Figure5.7B). The UV-visible spectra of the D-ornithinyl-PLP and DL-2,4-diaminobutyryl-PLP aldimines in both of the His225 variants are similar to wild-type OAM in that the predominant species is the iminium zwitterion (A in Figure 5.6) with the natural substrate, whereas binding of DABA shifts the equilibrium towards the imine state (B in Figure 5.6). These data suggest that direct hydrogen bonding between the imidazole of His225 and the phenolic group does not significantly influence the protonation state of the Schiff base upon non-enzymatic condensation of the cofactor with the substrate or inhibitor in PLP-OAM. However, there still remains the possibility that His225 influences the pK_a of the Schiff base in the holoenzyme at different steps of the catalytic cycle.

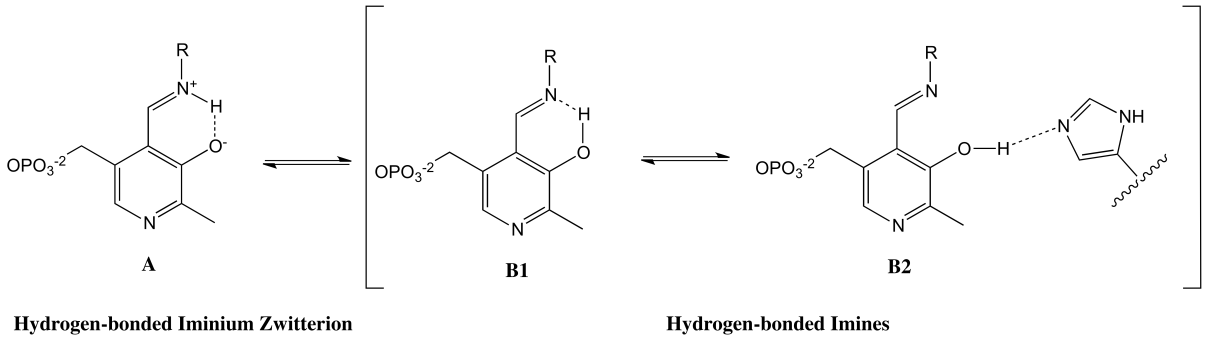

Figure 5.6 Tautomers of the PLP external aldimine species. Internal proton transfer occurs between the imino nitrogen and the 3-oxo anion of the pyridine ring such that two tautomeric species of the PLP external aldimine are detected spectroscopically. The (A) hydrogen-bonded iminium zwitterion and (B) hydrogen-bonded imine respectively absorb at 401–425 nm and 325–340 nm.

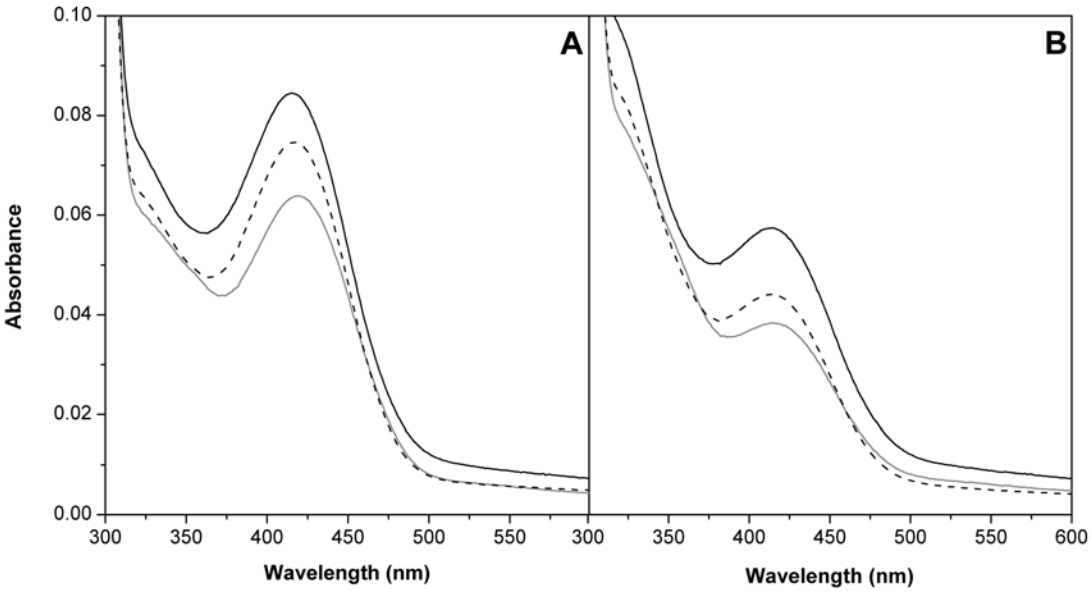

Figure 5.7 Spectroscopic characterization of PLP external aldimine tautomers. The distribution of (A) D-ornithinyl-PLP external aldimine and (B) DL-2,4-diaminobutyrl-PLP external aldimine tautomers in wild-type OAM (black), H225Q (dashed), and H225A (gray). An equimolar mixture of apoOAM (15 μM) and PLP (15 μM) in 100 mM NH_4^+EPPS (pH 8.5) was incubated for 5 minutes following the addition of (A) 2.5 mM D-ornithine and (B) 2.5 mM DL-2,4-diaminobutyrate. Spectra were recorded from 300 to 600 nm.

5.8 Interaction of S162 with the pyridine nitrogen of PLP

Traditionally, pyridoxal 5'-phosphate participates in the stabilization of a carbanion intermediate, which is central to the mechanism of PLP-dependent enzymes. The cofactor is often referred to as an "electron-sink" because the negative charge on the α-carbon of the amino acid substrate becomes delocalized through the extended π-system of the Schiff base and pyridine ring. Recently, experimental studies have revealed the importance of the protonation state of the pyridine nitrogen in controlling reaction specificity of PLP-dependent enzymes, which catalyze a diverse array of transformations despite all initially proceeding through a carbanion intermediate. Specific active site residues coordinated to the pyridine nitrogen, which vary in the different PLP-dependent enzymes, were shown to affect the protonation state of the pyridine nitrogen, and therefore its electrophilicity during catalysis.[98] Modulation of the electrophilic strength of the pyridine ring was in turn found to participate in controlling the reaction specificity of these enzymes.[98, 143]

The same chemical properties that allow the PLP cofactor to stabilize the carbanion intermediate in traditional PLP-dependent enzymes also allow it to facilitate radical rearrangements in the adenosylcobalamin-dependent aminomutases. Computational studies have indicated that protonation of the pyridine nitrogen is important in stabilizing radical intermediates, such as the proposed azacyclopropylcarbinyl radical species, in the catalytic cycle of AdoCbl-dependent aminomutases. However, the coordination of a serine residue (pK_a~9) within the active sites of ornithine 4,5-aminomutase and lysine 5,6-aminomutase suggests that the pyridine nitrogen exists in the deprotonated state. As such, it is unclear to what extent the protonation state of the pyridine ring actually participates in the stabilization of radical intermediates within these enzymes. Here we have mutated Ser162 to an alanine and aspartate residue to determine the role of the hydrogen bond interaction with the pyridine nitrogen. In addition, we have reconstituted the wild-type enzyme with N-methyl-PLP (N-MePLP), a cofactor analogue in which the pyridine nitrogen is methylated and therefore bears a formal positive charge.

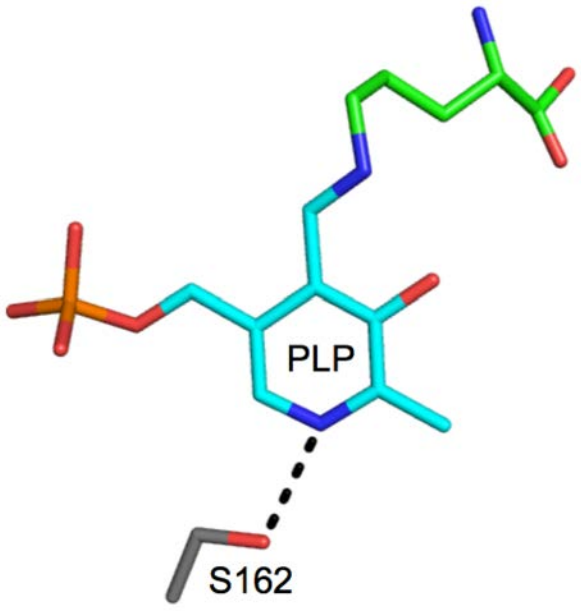

Figure 5.8 Active site of OAM complexed with D-ornithine showing the relative position of S162 with respect to PLP. Active site residue Ser162 forms a hydrogen bond with the pyridine nitrogen of the PLP cofactor and therefore likely controls the protonation state of the nitrogen atom.

5.9 Steady-state kinetic parameters of the S162 variants

The steady-state kinetic parameters for the two Ser162 variants, as well as the wild-type enzyme reconstituted with N-MePLP, are summarized in Table 5.2. Removal of the hydroxyl group of S162, in S162A, resulted in a 50-fold decrease in k_{cat} and a 5-fold decrease in k_{cat}/K_m. In comparison, replacement of the hydroxyl group with a carboxylate group, in S162D, resulted in a more drastic 1450-fold reduction in k_{cat} and a 155-fold reduction in k_{cat}/K_m. In the case of the cofactor analogue, methylation of the pyridine nitrogen reduced the catalytic activity and overall catalytic efficiency of wild-type OAM 88- and 8-fold, respectively.

Deuterium kinetic isotope effect studies were also conducted to further investigate the effects of mutating Ser162 and replacing the native PLP cofactor with the N-MePLP analogue. The S162A variant exhibited a 2.2-fold decrease in $^{D}k_{cat}$ and a 1.5-fold increase in $^{D}k_{cat}/K_m$. Similarly, the wild-type enzyme showed a 1.3-fold decrease in $^{D}k_{cat}$ and a 1.5-fold increase in $^{D}k_{cat}/K_m$ when reconstituted with N-MePLP. These results suggest that in both cases a step other than hydrogen transfer is more rate-limiting in the catalytic mechanism.

Table 5.2 Summary of steady-state kinetic parameters for wild type OAM and the Ser162 variants with substrate DL-ornithine and the observed deuterium kinetic isotope effects upon reaction with DL-ornithine-3,3,4,4,5,5-d_6.

Enzyme (Cofactor)	k_{cat} (s^{-1})	K_m (μM)	k_{cat}/K_m ($M^{-1}s^{-1}$)	$^{D}k_{cat}$	$^{D}k_{cat}/K_m$
Wild type (PLP)	2.9 ± 0.1	567 ± 45	5120 ± 410	7.6 ± 0.5	2.5 ± 0.4
Wild type (N-MePLP)	$3.3 \times 10^{-2} \pm 0.1 \times 10^{-2}$	54 ± 3	610 ± 44	5.8 ± 0.2	3.9 ± 0.5
S162A (PLP)	$5.7 \times 10^{-2} \pm 0.1 \times 10^{-2}$	52 ± 3	1100 ± 93	3.4 ± 0.3	3.8 ± 0.7
S162D (PLP)	$2.0 \times 10^{-3} \pm 0.1 \times 10^{-3}$	61 ± 2	33 ± 3	ND	ND

5.10 Anaerobic and aerobic spectroscopic characterization of S162 variants

Following steady-state kinetic characterization of the S162 variants, anaerobic and aerobic spectral studies were conducted to assess whether substrate binding, Co–C bond homolysis, and/or the stability of radical intermediates had been affected in S162A and S162D. Binding of both D-ornithine (Figure 5.9A) and DL-2,4-diaminobutyrate (Figure 5.9B) to S162A results in an absorbance decrease at 416 nm, reflecting formation of the external aldimine, similar to that observed for wild-type OAM (Figure 2.7A). However, substrate-induced cleavage of the Co–C bond (absorbance decrease at 528 nm) is limited in the S162A variant and, in contrast to wild-type, binding of DABA does not induce a greater percentage of the enzyme to undergo homolysis. It is unclear from the absorbance spectrum shown in Figure 5.9B whether the persistent PLP-DABA radical still forms in S162A, but the small increase in absorbance at 470 nm suggests that a minor amount of the cob(II)alamin species may have accumulated.

The anaerobic binding spectra of the S162D variant (Figures 5.9C and 5.9D) exhibit even more notable differences from those of the wild-type enzyme. Figure 5.9C reveals that formation of the external aldimine species is greatly impaired in the variant; even though the absorbance peak did shift from 416 nm to 425 nm upon the addition of D-ornithine to the holoenzyme, no absorbance decrease at 416 nm was detected. Similarly, a greatly reduced transimination signal was observed upon addition of DL-2,4-diaminobutyrate (Figure 5.9D). As for the S162A variant, homolysis is greatly impaired in S162D as evidenced by the minor absorbance decreases at 528 nm in both the D-ornithine and DABA cases. Impaired transimination and Co–C bond homolysis, or decreased stability of the PLP-DABA derived radical, could account for the inability to detect the cob(II)alamin species in S162D.

The aerobic binding spectra for S162A (Figure 5.10) are similar to those of wild-type OAM (Figure 2.11). Addition of D-ornithine (Figure 5.10A) to the holoenzyme results in a rapid build-up of cob(III)alamin (absorbance increase at 358 nm) at a rate of 0.07 min^{-1}. As for the wild-type enzyme, the rate of inactivation is faster in the presence of DL-2,4-diaminobutyrate (0.16 min^{-1}; Figure 5.10B), suggesting that the overstabilized PLP-DABA derived radical is still coupled to the oxygen-sensitive cob(II)alamin species. Overall, the inactivation rates for D-ornithine and DL-2,4-diaminobutyrate are 6- and 10-fold slower than

those for wild-type OAM; however, these results are consistent with the reduced level of homolysis and cob(II)alamin build-up detected under anaerobic conditions.

Like the anaerobic binding spectra, the aerobic binding spectra of S162D (Figures 5.10C and 5.10D) are notably different from those of wild-type OAM and the S162A variant. In particular, the rapid build-up of cob(III)alamin upon the addition of substrate to the holoenzyme is absent. Interestingly, although transimination appears to be more greatly impaired with the natural substrate D-ornithine, a small amount of cob(III)alamin build-up is still detected during the 60-minute time course of the reaction (Figure 5.10C). In contrast, no cob(III)alamin is detected upon DABA binding (Figure 5.10D), which could be attributed to weaker coupling of the PLP-DABA derived radical and cob(II)alamin species.

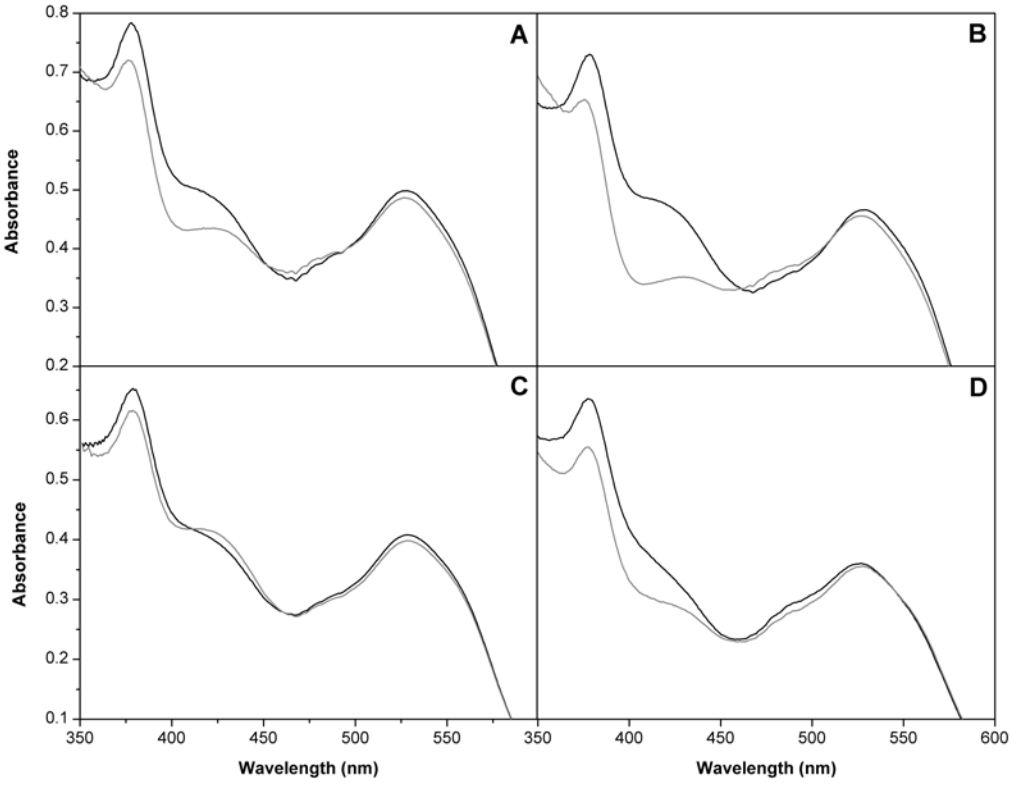

Figure 5.9 Anaerobic binding spectra for the S162 variants. The holoenzyme solution contained an equimolar (40 μM) amount of apoOAM, PLP, and AdoCbl in 100 mM NH_4^+EPPS pH 8.5. Spectral changes for S162A (A and B) and S162D (C and D) were recorded before (black line) and 10 minutes after (gray line) the addition of 2.5 mM D-ornithine (A and C) and the substrate analogue DL-2,4-diaminobutyrate (B and D).

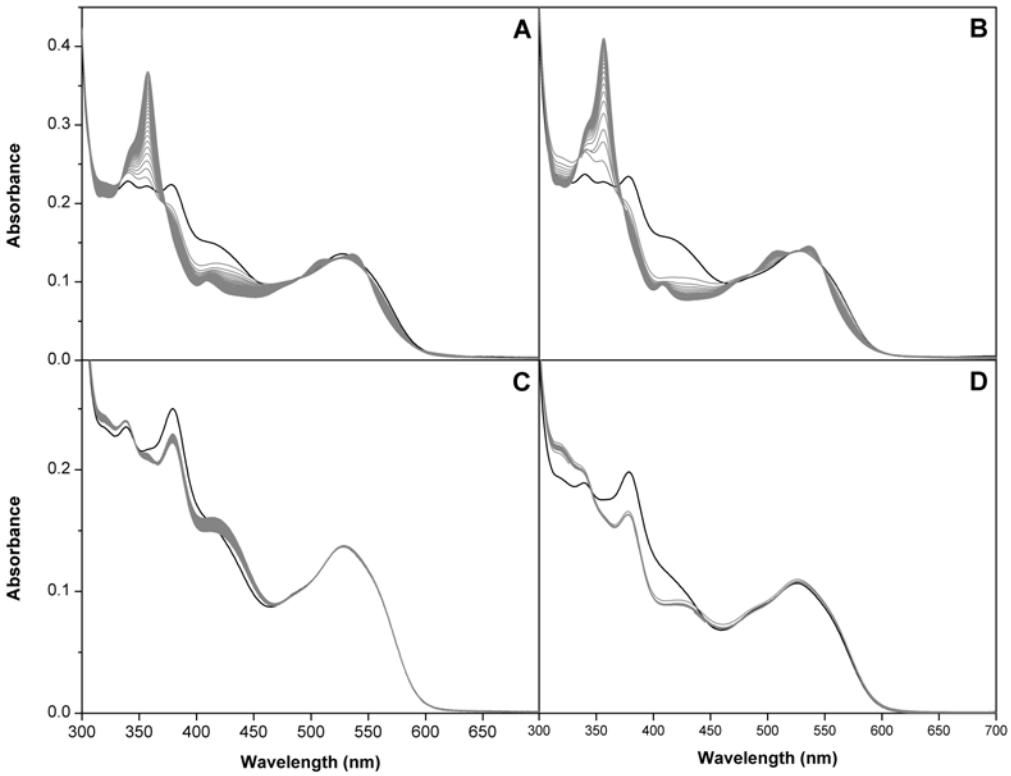

Figure 5.10 Aerobic binding spectra for the S162 variants. The holoenzyme solution contained 15 μM apoOAM, 15 μM PLP, and 15 μM AdoCbl in 100 mM NH_4^+EPPS pH 8.5. Spectral changes for S162A (A and B) and S162D (C and D) were recorded prior to the addition of substrate (black line) and then every minute for 60 minutes following the addition of 2.5 mM D-ornithine (A and C) and 2.5 mM DL-2,4-diaminobutyrate (B and D).

5.11 Spectroscopic properties of PLP-bound OAM and the S162 variants

Previous experimental and computational studies have indicated that protonation of the pyridine nitrogen shifts the tautomeric equilibrium towards the hydrogen-bonded iminium zwitterion form of the PLP external aldimine (A in Figure 5.6).[99, 144-146] UV-visible spectral studies, in which only PLP was added to the apoenzyme, were therefore performed to examine the equilibrium distribution of the PLP external aldimine tautomers in S162A and S162D. Figure 5.11 shows that the positions of the absorbance maxima representing the hydrogen-bonded iminium zwitterion (401 to 425 nm) and hydrogen-bonded imine (325 to 340 nm) forms of the PLP external aldimines are shifted slightly in S162A and S162D

compared to wild-type OAM. Even so, the relative ratio of the tautomeric species in the S162A variant is similar to that of wild-type, suggesting that substitution of S162 with an alanine does not significantly influence the protonation state of the imino nitrogen in both the D-ornithinyl-PLP- and DL-2,4-diaminobutyryl-PLP-OAM complexes.

The PLP binding spectra of the S162D variant differ significantly from those of both wild-type OAM and the S162A variant. As shown in Figure 5.11A, the height of the single peak at 415 nm relative to the corresponding peak in wild-type and S162A suggests that a minimal amount of the D-ornithinyl-PLP external aldimine species forms in S162D. This is consistent with the holoenzyme binding spectra obtained upon reaction with D-ornithine (Figure 5.9C and 5.10C). In addition, no peak representing the hydrogen-bonded imine is detected in the 325 to 340 nm range. As such, the peak at 415 nm likely represents the dominant hydrogen-bonded iminium zwitterion form of the internal or the external aldimine species.

In contrast to D-ornithine, binding of the substrate analogue DL-2,4-diaminobutyrate to S162D was shown to cause a greater absorbance decrease at 415 nm (Figures 5.9D and 5.10D), suggesting that a DL-2,4-diaminobutyryl-PLP external aldimine species does form to a detectable level in the variant. Moreover, Figure 5.11B reveals two absorbance maxima (one at 323 nm and one at 415 nm) indicating that the tautomeric equilibrium between the hydrogen-bonded iminium zwitterion and hydrogen-bonded imine exists. The relative ratio of two tautomeric species still favors formation of the hydrogen-bonded imine, however not to the same degree as for the wild-type enzyme. This difference in the tautomeric equilibrium constant could be attributed to protonation of the pyridine nitrogen due to the close proximity of the aspartate residue, which would shift the equilibrium towards the hydrogen-bonded iminium zwitterion. Alternatively, given that transimination is impaired in the variant, the apparent equilibrium shift could also be due to a greater percentage of the internal aldimine species over the external aldimine within the enzyme.

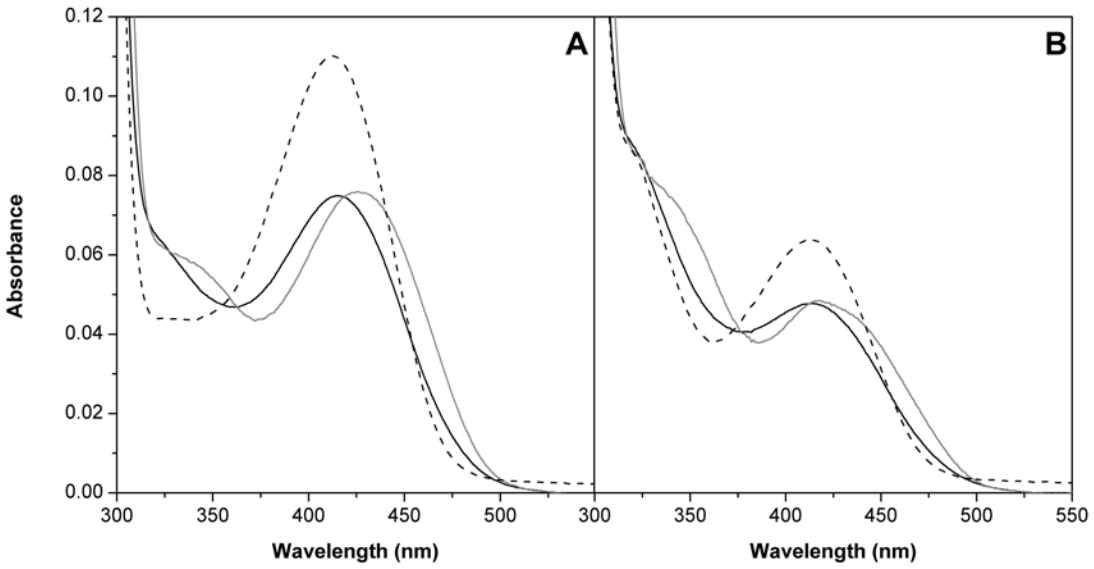

Figure 5.11 Equilibrium distribution of external aldimine tautomeric species in wild-type OAM and the S162 variants. The reaction mixture contained 15 μM apoOAM and 15 μM PLP in 100 mM NH_4^+EPPS, pH 8.5. Spectra were recorded from 300 to 550 nm following the addition of (A) D-ornithine and (B) DL-2,4-diaminobutyrate to wild-type OAM (solid black line), S162A (solid gray line), and S162D (black dashes). The hydrogen-bonded iminium zwitterion and hydrogen-bonded imine external aldimine species absorb at 401–425 nm and 325–340 nm, respectively.

5.12 Stopped-flow analysis of S162A

Rapid stopped-flow studies were performed to determine the effects of mutating S162 to an alanine on the pre-steady-state rate constants for transimination and Co–C bond homolysis. Figure 5.12A reveals that the rate constant for transimination (60 ± 1 s^{-1}) is ~8-fold slower than that of wild-type OAM (464 ± 36 s^{-1}), indicating that the mutation does affect the initial formation of the PLP-DABA external aldimine species. The rate constant for homolysis (51 ± 4 s^{-1}) in Figure 5.12B was also found to be slower than that of wild-type (980 ± 88 s^{-1}), but on the same order of magnitude as the rate constant for transimination for the variant.

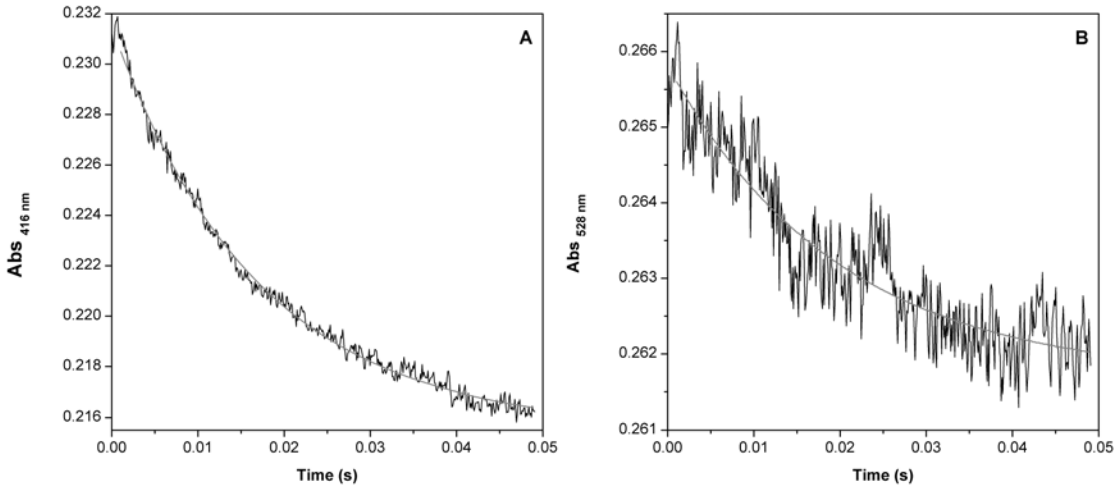

Figure 5.12 Stopped-flow absorbance changes following transimination and Co–C bond homolysis in S162A. Formation of (A) the external aldimine and (B) homolysis of the Co–C bond were followed at 416 nm and 528 nm, respectively. The absorbance changes were monitored over 20 ms following rapid mixing of 50 μM holoenzyme with 5 mM DL-2,4-diaminobutyrate. An average of 8–10 traces were fit to a monoexponential equation to obtain the observed rate constants for transimination (60 ± 1 s^{-1}) and homolysis (51 ± 4 s^{-1}).

5.13 Spectroscopic characterization of wild-type OAM with N-methyl-PLP

The wild-type enzyme reconstituted with N-MePLP was shown to be active (section 5.9), albeit 88-fold slower than the native PLP-bound form of OAM. To determine the origin of this reduced catalytic activity, anaerobic and aerobic UV-visible studies were used to examine the effect of the methylated pyridine nitrogen on formation of the external aldimine, homolysis of the Co–C bond, and the stability of any radical intermediates formed during the catalytic cycle. The anaerobic binding spectra in Figure 5.13 show an absorbance decrease at 415 nm, suggesting that the external aldimine species forms upon addition of D-ornithine (Figure 5.13A) and DL-2,4-diaminobutyrate (Figure 5.13B) to the N-MePLP bound holoenzyme. The spectra also reveal that homolysis is restricted, because no absorbance decrease at 528 nm is detected in the case of D-ornithine and only a minor decrease is seen with DABA. Additionally, the lack of formation of an absorbance peak at 470 nm indicates that the cob(II)alamin intermediate does not accumulate to a detectable level.

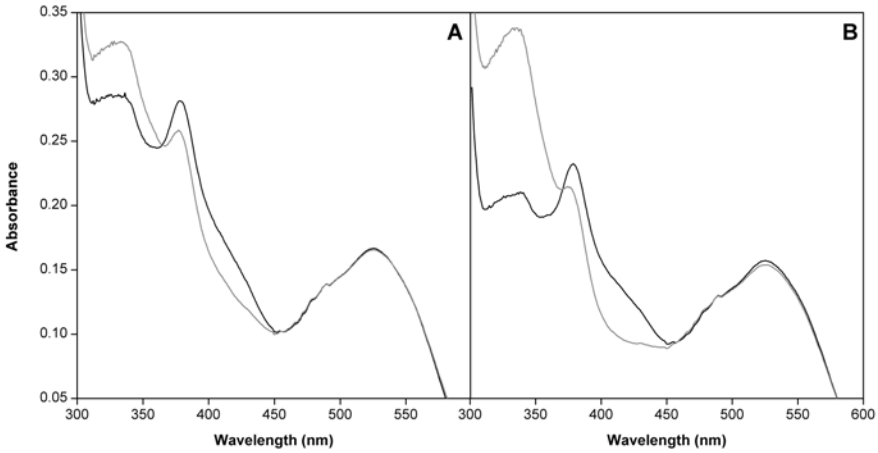

Figure 5.13 Changes in the anaerobic UV-visible absorbance spectra of wild-type OAM reconstituted with N-MePLP upon substrate binding. The holoenzyme reaction mixture contained 15 μM apoOAM, 15 μM N-MePLP, and 15 μM AdoCbl in 100 mM NH_4^+EPPS buffer, pH 8.5. Spectral changes were recorded before (black line) and 10 minutes after (gray line) the addition of (A) 2.5 mM D-ornithine and (B) 2.5 mM DL-2,4-diaminobutyrate.

The spectral changes observed under aerobic conditions (Figure 5.14) are significantly different from those of PLP-bound holoOAM (Figure 2.11). Typically the native enzyme shows a rapid increase at 358 nm, signifying a build-up of cob(III)alamin, due to interception of the cob(II)alamin species by molecular oxygen. In the case of N-MePLP-bound holoOAM, however, no increase in absorbance at 358 nm is observed with either substrate, suggesting that the enzyme is not susceptible to oxygen inactivation. This is consistent with the absence of detectable cob(II)alamin under anaerobic conditions. The binding spectra instead show an increase in absorbance at 338 nm, which occurs at the same rate as the absorbance decrease seen at 415 nm. Given that these absorbance changes are linked, they likely both reflect formation of the external aldimine species, where the increase in absorbance at 338 nm represents the hydrogen-bonded imine tautomer. It should be noted that due to the potential overlap of these absorbance changes with those monitored at 340 nm during the coupled-enzyme assay, control experiments were run to ensure that the turnover rate measured was indeed due to production of 2,4-diaminopentanoate by OAM. This was confirmed in Figure 5.15 as no significant increase in absorbance at 340 nm was detected in the absence of the coupling enzyme DAPDH or when NAD^+ was excluded from the reaction mixture.

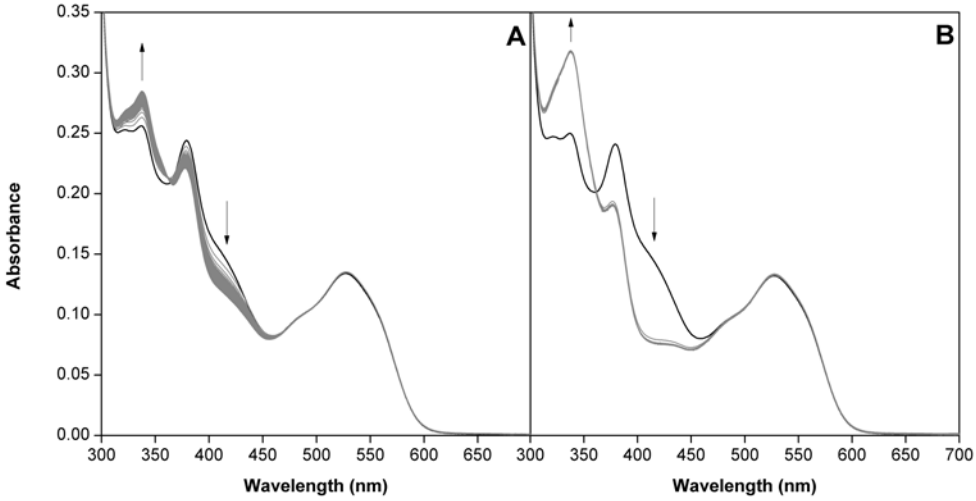

Figure 5.14 Changes in the aerobic UV-visible spectra of wild-type OAM reconstituted with N-MePLP following substrate binding. The holoenzyme solution contained 15 μM apoOAM, 15 μM N-MePLP, and 15 μM AdoCbl in 100 mM NH_4^+EPPS buffer, pH 8.5. Spectral changes were recorded prior to the addition of substrate (black line) and then every minute for 60 minutes (gray lines) following the addition of (A) 2.5 mM D-ornithine and (B) 2.5 mM DL-2,4-diaminobutyrate.

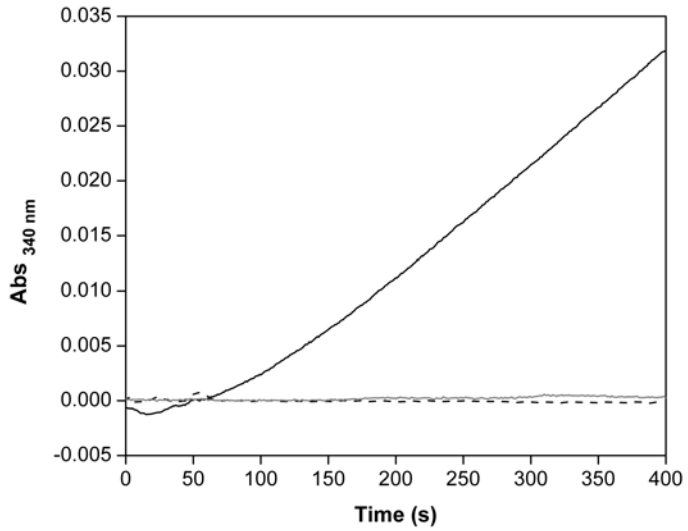

Figure 5.15 Coupled-enzyme assay showing the rate of OAM turnover when reconstituted with N-MePLP. Absorbance data were collected at 340 nm for three different scenarios: the black dashes show the absorbance trace in the absence of DAPDH, the gray line shows the absorbance trace in the absence of NAD^+, and the black line shows the absorbance trace where all components of the coupled-assay were present.

As protonation of the pyridine ring has been shown to affect the protonation state of the Schiff base, spectral studies were performed with N-MePLP-bound OAM (no AdoCbl added) to assess whether methylation of the pyridine ring would produce similar results. As for the holoenzyme binding studies, a decrease in absorbance is observed at 415 nm followed by an absorbance increase at 338 nm (Figure 5.16). These spectral changes suggest that upon formation of the external aldimine species the imino nitrogen becomes deprotonated (i.e. neutral) in favor of formation of the hydrogen-bonded imine tautomer. This proton transfer occurs more slowly in the case of D-ornithine (Figure 5.16A) than it does with the substrate analogue DL-2,4-diaminobutyrate (Figure 5.16B). Similar to PLP-bound OAM, the imino nitrogen is predominantly deprotonated in the DL-2,4-diaminobutyryl-N-MePLP-OAM complex, although to an even greater degree. Following the 60-minute time course of the reaction, the D-ornithinyl-N-MePLP-OAM complex also exists predominantly as the hydrogen-bonded imine tautomer. As such, it appears from these data that methylation of the pyridine ring actually shifts the equilibrium away from the hydrogen-bonded iminium zwitterion species rather than towards it. Similar spectral changes were also found to occur upon mixing of N-MePLP and the substrate in the absence of OAM.

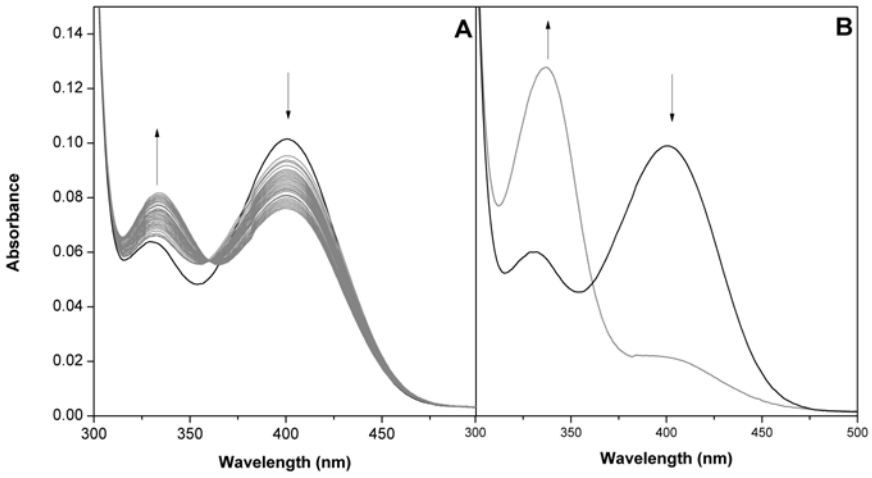

Figure 5.16 Spectral changes resulting from the addition of D-ornithine and DL-2,4-diaminobutyrate to N-MePLP bound OAM. The reaction mixture contained 15 μM apoOAM and 15 μM N-MePLP in 100 mM NH_4^+EPPS buffer, pH 8.5, and was maintained at 25 °C by a circulating water bath. In the case of (A) D-ornithine the observed spectral changes were slow and as such formation of the D-ornithinyl-PLP external aldimine was followed over the time course of 60 minutes. Only representative spectra are shown. (B) Binding of DL-2,4-diaminobutyrate results in a rapid absorbance decrease at 415 nm and simultaneous increase at 338 nm.

5.14 Determination of the equilibrium binding constants for PLP and N-MePLP

A fluorescence binding assay was used to assess the binding of PLP and the methylated cofactor analogue, N-MePLP, to the OAM active site. Binding of PLP and N-MePLP was shown to result in a quenching of the intrinsic tryptophan fluorescence of the enzyme. The decrease in fluorescence emission at 340 nm was graphed as a function of added cofactor concentration (Figure 5.17) and the data were fit to the quadratic binding isotherm (Eq. 5.3). The apparent K_d for PLP was determined to be 122 ± 19 nM, which is similar to the value previously determined using equilibrium dialysis.[147] The apparent K_d for the cofactor analogue (123 ± 19 nM) was found to be similar to that for PLP, suggesting that methylation of the pyridine nitrogen does not significantly affect binding of the cofactor to the OAM active site.

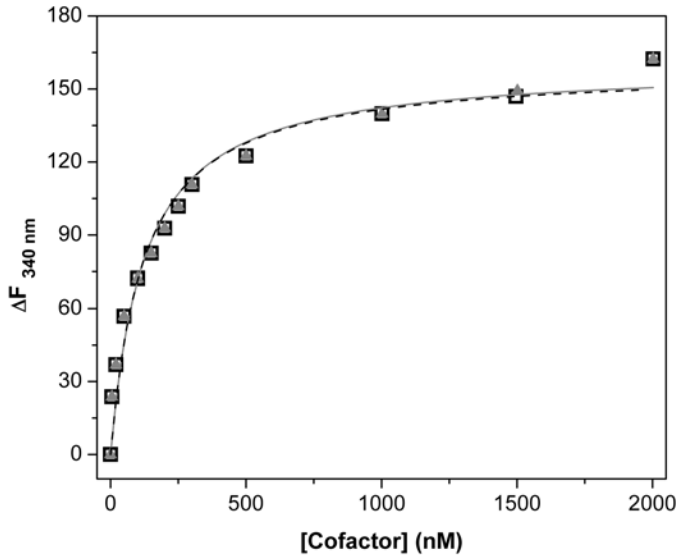

Figure 5.17 Determination of the equilibrium dissociation constants for PLP and N-MePLP for wild-type OAM. Wild-type OAM (0.268 μM) was titrated with 5–2000 nM PLP (black boxes) or N-MePLP (gray triangles) at 25 °C in 100 mM NH_4^+EPPS buffer, pH 8.5. The change in fluorescence at 340 nm was plotted against total concentration of added cofactor and the data were fit to Eq 5.3 (solid and dashed lines) keeping the total enzyme concentration fixed at 0.268 μM. The K_d was determined to be 122 ± 19 nM for PLP and 123 ± 19 nM for N-MePLP.

5.15 Discussion

PLP-dependent enzymes catalyze a diverse array of biological transformations of amino acids and other amine-containing substrates, including transaminations, racemizations, decarboxylations, and β- and γ-eliminations and replacements. For each of these reactions, PLP facilitates catalysis by stabilizing an α-carbanion catalytic intermediate by electronic delocalization through the conjugated π-system of the pyridine ring and Schiff base. Computational and experimental work has highlighted the importance of ionizable groups of the cofactor (i.e. phenolic oxygen, imino nitrogen, and pyridine nitrogen) in mediating resonance stabilization of polar intermediates.[132, 148] Moreover, external hydrogen bond donors and acceptors to the PLP phenolic oxygen and pyridine nitrogen have been shown to finely tune the catalytic role of the PLP cofactor.[99, 149]

However, little is known how corresponding residues in PLP-dependent aminomutases participate in catalysis. For this group of enzymes, which includes lysine 2,3-aminomutase, lysine 5,6-aminomutase, arginine 2,3-aminomutase, and glutamate 2,3-aminomutase, PLP assumes an unusual role in catalysis: the stabilization and isomerization of nonpolar radical intermediates. Here in this study we chose to investigate the roles of His225 and Ser162 as they are within hydrogen bond distance to the phenolic oxygen and pyridine nitrogen of PLP, respectively, and therefore in a position to participate in catalysis by influencing the protonation state of the imino and pyridine nitrogens. In addition, the PLP cofactor analogue, N-methylPLP, was used to further probe the role of the pyridine nitrogen in stabilizing radical intermediates.

5.15.1 Role of His225 and the protonation state of the imino nitrogen in OAM catalysis

The steady-state kinetic experiments show that His225 participates in catalysis. The fact that replacement of His225 with an alanine results in a larger reduction in turnover compared to the H225Q variant suggests that a glutamine side-chain can partially substitute for the histidine imidazole moiety, perhaps through formation of a hydrogen bond to the PLP phenolic oxygen or by maintaining a modestly bulky side-chain in the active site. The pH studies show that the rate of catalysis is dependent on the deprotonation of an ionizable

group, but the residue is not His225 as each of the three OAM forms tested show similar pH profiles and pK_a values. The ionizable group may be the internal or external aldimine, known to have pK_a values within this range.[150] If this were the case, then it suggests that aldiminium ionization limits catalysis. Alternatively, the ionizable group may be another active site residue in OAM or the coupling enzyme DAPDH.

In the presence of O_2, the rate of cob(III)alamin formation is much greater in the presence of DABA compared to D-ornithine due to the lingering presence of the metallo-paramagnetic species in the active site. The susceptibility of the enzyme to O_2 in the presence of D-ornithine and DL-2,4-diaminobutyrate is diminished in both H225Q and to a greater extent in H225A, presumably because of the shortened lifetime of cob(II)alamin in the active site. Interestingly, the rate of inactivation of H225A with D-ornithine (0.13 min^{-1}) approximates the rate observed with DABA (0.15 min^{-1}). This suggests that even though H225A is less susceptible to O_2 inactivation compared to wild-type, radical intermediates formed upon reaction with D-ornithine may in fact be more susceptible to the presence of oxygen, and points to an important role for His225 in stabilizing radical intermediates. With the H225A variant, AdoCbl homolysis is also noticeably reduced (not detectable by UV-visible spectroscopy), which likely explains the impaired catalytic turnover and attenuated side reactions with O_2.

The inability to spectrally detect homolysis also suggests that the equilibrium constant for the homolysis step is shifted in favor of the intact cofactor. In addition, elevated deuterium isotope effects indicate that the variant has an increased barrier to hydrogen atom transfer. The greater increase in ${}^{D}k_{cat}/K_m$ (2.3-fold) compared to ${}^{D}k_{cat}$ (1.3-fold) further suggests that the barriers to other steps of the mechanism have also increased. This could include formation of the azacylopropylcarbinyl radical intermediate as computational studies have shown that protonation of the imino nitrogen, which is more likely to occur in the absence of His225 acting as an external hydrogen bond acceptor to the phenolic group, increases the barrier to ring closure.[96] The increase in the barrier to hydrogen transfer, which is coupled to the homolysis event,[67] likely accounts for the reduced level of AdoCbl homolysis seen in H225A. Alternatively, AdoCbl homolysis may also be tightly coupled to steps further along the catalytic cycle, i.e. formation of the azacyclopropylcarbinyl radical. If

the energy barriers were elevated for these downstream catalytic steps, one would also expect attenuation of Co–C bond cleavage.

For the H225Q variant, UV-visible spectroscopy clearly shows that AdoCbl homolysis occurs as for wild-type OAM. However, the cob(II)alamin that does form upon loading of the enzyme with DABA collapses to form cob(III)alamin by a mechanism that is independent of O_2. This is also observed with H225A, albeit to a lesser degree. To rationalize why cob(II)alamin, which is presumably coupled to the 2,4-diaminobutyryl-PLP derived radical, is less stable in the H225 variants compared to wild-type, the crystal structures of OAM with DABA and D-ornithine were closely investigated (Figure 5.1). D-ornithine is secured within the active site by electrostatic/polar interactions between the α-carboxylate and the side-chain of Arg297 and between the α-amino group and the carboxylate group of Glu81. As a result of these interactions, the D-ornithinyl-PLP aldimine is positioned such that the p-orbitals of the Schiff base and pyridine nitrogen are aligned for optimal electronic delocalization of ensuing radical intermediates.

The crystal structure of the OAM-DABA complex also shows that the α-carboxylate of the inhibitor forms a salt-bridge with Arg297, despite being one carbon atom shorter than the natural substrate. As a consequence, the p-orbitals of the Schiff base of the external aldimine are not optimally aligned with the pyridine ring. This suggests that upon abstraction of the C4 hydrogen atom by the 5'-deoxyadenosyl radical from the 2,4-diaminobutyryl-PLP aldimine, the radical localized to the C4 atom is principally stabilized through resonance stabilization involving the imino group and not the conjugated π-system of the pyridine ring. If this is indeed the case, then a deprotonated imino nitrogen likely leads to greater resonance stabilization of the C4 radical. For wild-type OAM, His225 may be acting as a general base to the phenolic oxygen, which would favor the deprotonated state of the imino nitrogen (B2 in Figure 5.6). As such, mutation of His225 would likely shift the position of the bridging proton towards the imino nitrogen, which could account for the collapse of the organic radical.

Steady-state inhibition studies reveal that His225 contributes to the binding of 2,4-diaminobutyrate. Although the crystal structure of the OAM-DABA complex does not reveal direct hydrogen bonding between the His225 imidazole side-chain and the PLP-bound

inhibitor, the two moieties are within van der Waals contact, and therefore this weak noncovalent interaction may partially contribute to the binding affinity of the inhibitor.

From UV-visible spectral studies, it is evident that the D-ornithinyl-PLP aldimine is predominantly in the hydrogen-bonded iminium zwitterion state without AdoCbl bound to the enzyme. However, the protonation state of the external aldimine prior to hydrogen abstraction from the substrate is unknown as factors such as the substituent on the imino group and the localized polar environment can shift the tautomeric equilibrium of the Schiff base.[146, 151] For example, upon formation of the catalytically closed complex in the holoenzyme, a prerequisite for PLP-mediated radical rearrangement, the solvent polarity around the PLP external aldimine is expected to change, and this likely shifts the position of the bridging proton between the phenolic oxygen and the imino nitrogen.

Following abstraction of the C4 hydrogen atom from the substrate, the next step in the proposed catalytic cycle involves formation of an azacyclopropylcarbinyl radical. This cyclic intermediate arises from reversible radical addition involving unpairing of the π electrons of the imino group. Deprotonation of the imino nitrogen, possibly facilitated by proton abstraction by His225, lowers the energy barrier for ring closure. Computational calculations by Wetmore et al. revealed that the N–H–O intramolecular bridge of PLP was integral in preventing overstabilization of the cyclic radical intermediate by disrupting optimal alignment of p-orbitals and minimizing captodative stabilization of the radical intermediate.[96] Thus, ring opening may involve partial proton transfer back to the phenolic oxygen, again possibly facilitated by H225, to avoid deep energy wells along the reaction coordinate, a key goal in catalysis. Thus, His225 may finely tune radical rearrangement by participating in partial proton transfer with PLP, thereby lowering the energy barrier for ring closure and opening. *Ab initio* calculations have previously alluded to the importance of protonation or partial protonation of the migrating group being critical for facilitating 1,2-shifts in other AdoCbl-dependent enzymes.[82, 85, 152, 153]

5.15.2 Role of Ser162 and the protonation state of the pyridine nitrogen in OAM catalysis

The protonation states of the Schiff base and pyridine nitrogen of PLP have been shown to play a significant role in controlling reaction specificity in PLP-dependent enzymes.[98, 99, 143] Likewise, computational studies have indicated that the protonation state of these ionizable groups contributes to the stabilization of radical intermediates in the rearrangement mechanisms of the PLP-dependent aminomutases. Notably, protonation of the pyridine nitrogen not only lowers the barrier to ring closure, but also stabilizes the proposed azacyclopropylcarbinyl radical to a greater extent than the neutral pyridine ring.[96] In addition, protonation of the imino nitrogen by the phenolic group was found to destabilize the cyclic intermediate, thereby preventing it from becoming trapped in a local energy minimum.[96] As such, the tautomeric equilibrium established through internal proton transfer between the imino nitrogen and phenolic group is thought to play an important role in OAM catalysis. The crystal structure of OAM reveals a serine residue (Ser162), which forms a hydrogen bond to the pyridine nitrogen of PLP. The relatively high pK_a of this residue (pK_a~9) compared to that of the pyridine nitrogen (pK_a~6) suggests that the pyridine ring exists in a deprotonated state within the active site. As such, it is unclear to what extent protonation or partial protonation of the pyridine ring contributes to radical catalysis.

To determine the role of Ser162 in OAM, we have mutated the residue to an alanine and an aspartate. The S162A variant severs hydrogen bond contact to the pyridine nitrogen, while replacement of the serine with an aspartate residue promotes protonation of the pyridine nitrogen. The S162A and S162D variants respectively show a 50- and 1450-fold decrease in catalytic activity compared to the native enzyme, indicating that the residue does in fact play a significant role in OAM catalysis.

In contrast to the H225A variant, in which hydrogen transfer was shown to become more rate-limiting, the value of $^{D}k_{cat}$ decreases in S162A. Therefore a step (or steps) other than hydrogen transfer has become more rate-limiting in the mechanism. The increase in the value of $^{D}k_{cat}/K_m$ further points to slower product formation relative to substrate release in the variant. Consistent with these results, pre-steady-state kinetic analysis revealed diminished rate constants for transimination and homolysis in S162A. The rate constant for

transimination was 8-fold slower than that of wild-type, and the rate of homolysis, which is kinetically gated by formation of the external aldimine, was found to be on the same order of magnitude as the rate of transimination. Moreover, UV-visible spectroscopy showed limited homolysis in both variants, indicating that the equilibrium constant for homolysis favors reformation of the Co–C bond. However, attenuated homolysis could also be linked to impaired formation of the azacyclopropylcarbinyl radical, which is thought to be stabilized by protonation or partial protonation of the pyridine nitrogen.

Full protonation of the pyridine nitrogen may actually be detrimental, rather than beneficial, to OAM catalysis. Mutation of S162 to an aspartate results in a more profound decrease in catalytic activity compared to removal of the hydrogen bond in S162A. In addition to limited homolysis, no cob(II)alamin intermediate is detected in the S162D variant, which is consistent with its lack of susceptibility to oxygen. In comparison, a small amount of cob(II)alamin is still detectable in the S162A variant, and the rate of inactivation in the presence of oxygen is only slightly diminished compared to wild-type OAM. UV-visible spectral studies indicate that the equilibrium distribution of external aldimine tautomers is unchanged in the S162A variant compared to wild-type. In contrast, the hydrogen-bonded iminium zwitterion state seems to dominate in S162D. These results are consistent with the finding that protonation of the pyridine ring sways the tautomeric equilibrium constant towards the hydrogen-bonded iminium zwitterion state in traditional PLP-dependent enzymes.[145]

However, we know from computational studies that protonation of the imino nitrogen destabilizes ensuing radical intermediates.[96] It could be the case that partial protonation, provided by the serine hydrogen bond donor, is enough to sufficiently lower the barrier to ring closure and stabilize the cyclic intermediate. And while full protonation would further stabilize the cyclic intermediate, it also affects the protonation state of the imino nitrogen. Thus, the destabilizing effects of the protonated imino nitrogen may outweigh the stabilizing effects of the protonated pyridine nitrogen. We cannot, however, rule out the possibility that the large reduction in S162D activity is simply due to an inability of the D-ornithinyl-PLP external aldimine to form within the active site.

In addition to mutagenesis studies, cofactor analogues have been used to provide further insight into the role of particular functional groups in PLP-dependent catalysis.[98] Here

in this study, N-methylPLP, in which the pyridine nitrogen is methylated, was used to further explore the role of electrophilic strength of the pyridine ring in OAM radical catalysis. The wild-type enzyme was found to be 88-fold slower when reconstituted with N-MePLP, suggesting that the analogue is a poor substitute for the native PLP cofactor. The reduced activity is not attributed to weaker cofactor binding, as the equilibrium dissociation constant for N-MePLP is the same as that for PLP. Similar to the S162A variant, N-MePLP-OAM also exhibits a decreased value of $^{D}k_{cat}$ and an increased value of $^{D}k_{cat}/K_{m}$, indicating that another catalytic step (or steps) is more rate-limiting than hydrogen transfer. UV-visible spectral studies show that formation of the D-ornithinyl-PLP external aldimine may be impaired or slower and that homolysis is restricted, which could explain the reduced activity of the enzyme. The lack of observable homolysis and the cob(II)alamin species likely accounts for the absence of cob(III)alamin buildup under aerobic conditions.

Unlike protonation of the pyridine nitrogen, methylation does not shift the external aldimine tautomeric equilibrium towards the hydrogen-bonded iminium zwitterion form; in fact, it shifts it further towards the hydrogen-bonded imine state for both the D-ornithinyl- and DL-2,4-diaminobutyryl-N-MePLP complexes. Protonation of the pyridine nitrogen is thought to stabilize the phenolate anion of the zwitterion state by increasing the inductive stabilizing effects of the pyridine ring.[99] It is therefore unclear why the same stabilization of the hydrogen-bonded iminium zwitterion state does not occur upon methylation of the pyridine ring, but it may be due to the increased electron-donating capability of the methyl group compared to a hydrogen atom. Additional studies, including analogous studies with 1-deaza-pyridoxal 5'-phosphate, a PLP analogue lacking the pyridine nitrogen, are currently underway to further elucidate the role of the pyridine nitrogen in OAM catalysis.

5.15.3 Concluding remarks

In conclusion, our data indicate that His225 plays a role in catalysis; *via* its interaction with the phenolic oxygen, the imidazole side-chain may serve as a site for partial proton transfer during catalysis, enabling efficient intramolecular cyclization. Mutation of the residue does not appreciably increase the enzyme's susceptibility to uncontrolled catalysis

during turnover with D-ornithine, suggesting that trajectories and stability of radical intermediates are preserved. His225 does, however, contribute to the overstabilization of the DL-2,4-diaminobutyryl-PLP radical species by acting as a general base to the phenolic oxygen, lowering the pK_a of the imino nitrogen, which in turn favors resonance stabilization of the unpaired electron through the Schiff base. We have also shown that Ser162 plays an important role in OAM catalysis through its interaction with the pyridine nitrogen. Much like His225, Ser162 may also serve as a site for partial proton transfer to the pyridine nitrogen, thereby lowering the activation barrier to ring closure and stabilizing the azacyclopropylcarbinyl radical intermediate. It remains unclear how full protonation of the pyridine nitrogen affects OAM catalysis.

5.16 Experimental procedures

5.16.1 Materials

AdoCbl, PLP, D-ornithine, L-ornithine, and DL-2,4-diaminobutyric acid were obtained from Sigma. L-ornithine-3,3,4,4,5,5-d_6 hydrochloride were obtained from C/D/N Isotopes Inc. DL-ornithine-3,3,4,4,5,5-d_6 was prepared as described in section 2.9.6. The Ni^{2+}-nitrilotriacetic acid (Ni-NTA) column and Q-sepharose High Performance resins were from GE Biosciences. Restriction endonucleases were from New England Biolabs, *Pfu* Turbo DNA polymerase was from Agilent Technologies and Rosetta(DE3)pLysS competent cells were purchased from EMD Biosciences. All other chemicals were purchased from Fisher Scientific and were of the highest grade available.

5.16.2 Synthesis of N-methyl-PLP

N-methyl-PLP was synthesized using the method described by Pfeuffer et al.[154] Briefly, about 53 mg of PLP was dissolved in 10 mL of dH_2O. The pH was adjusted to 12–13 with NaOH. Dimethyl sulfate (20 μL) was then added to the mixture, which was left to stir at room temperature for 2 hrs. The N-methyl-PLP product was then purified from unreacted

starting material using anion exchange chromatography. The solution was loaded onto the column with 0.1 M sodium bicarbonate (pH 8.5) and eluted with 0.25 M sodium bicarbonate (pH 8.5). The presence of the methylated pyridine nitrogen was confirmed by ^{1}H-NMR, which revealed a 3H singlet at 4.25 ppm. The compound also showed the previously described UV-visible absorbance maxima at 330 and 400 nm.

5.16.3 Construction of the H225 variants

The H225A, H225Q, S162A, and S162D mutations were introduced into the pOAMH2 vector[64] harboring the C-terminal hexahistidine tagged OAM from *C. sticklandii* using the QuikChange site-directed mutagenesis kit (Agilent Technologies, Mississauga, ON). The complementary primers for the H225A variant are 5'-CAG ATA GAT GGA GCG GCT AAT GCA AAC GCT ACA G-3' and 5'-CTG TAG CGT TTG CAT TAC GCG CTC CAT CTA TCT G-3'. The sense and the antisense oligonucleotides for the H225Q variant are 5'-CAG ATA GAT GGA GCG CAG AAT GCA AAC GCT ACA G-3' and 5'-CTG TAG CGT TTG CAT TCT GCG CTC CAT CTA TCT G-3', respectively. The forward and reverse primers for the S162A variant are 5'-C TAT CAT TCA TAT GTT GCT GGA GTT GCA GGT CCA G-3' and 5'-C TGG ACC TGC AAC TCC GAC AAC ATA TGA ATG ATA G-3', respectively. Finally, the complementary primers for S162D are 5'-C TAT CAT TCA TAT GTT GAT GGA GTT GCA GGT CCA G-3' and 5'-C TGG ACC TGC AAC TCC ATC AAC ATA TGA ATG ATA G-3'. The NAPS DNA Sequencing Laboratory at University of British Columbia, Vancouver, Canada confirmed the presence of the mutations and the absence of any other PCR-induced errors.

5.16.4 Enzyme purification

The OAM variants and wild-type DAPDH were purified as previously described in section 2.10.5.

5.16.5 Coupled enzyme assays

The activity of wild-type OAM and the H225 variants towards D-ornithine was measured using the coupled spectrophotometric assay as described in section 2.10.7. For inhibition assays, the reaction mixture contained 100 mM NH_4^+EPPS, pH 8.5, 100 nM holoOAM, 100 nM DAPDH, 0.5 mM NAD^+ and variable concentrations of D-ornithine and DL-2,4-diaminobutyric acid. Reactions were performed under dim light and were initiated with the addition of D-ornithine. Data for the inhibition studies were fitted to the equation for competitive inhibition (Eq. 5.1) by non-linear least-squares regression analysis using the program Origin, version 8.5 (MicroCal Software Inc.).

$$\upsilon_i = \frac{VA}{K_m\left(1+\frac{I}{K_i}\right)+A} \qquad \text{Eq. 5.1}$$

where υ_i is the initial velocity, V is the maximal velocity, A is the concentration of D-ornithine, K_m is the Michaelis constant for D-ornithine, I is the inhibitor concentration and K_i is the inhibition constant.

The pH dependence assays were measured in a triple-component buffer (25 mM CHES, 25 mM HEPES, and 25 mM MES) in a 1 mL reaction containing 100 nM holo-OAM, 100 nM DAPDH, 0.5 mM NAD^+, and 2.5 mM D-ornithine. The pH titration data were fitted to the following equation (Eq. 5.2), where the protonation of an ionizable group leads to an increase in activity.

$$Y = \frac{Y_{max}-Y_{min}}{1+10^{pK-pH}+Y_{min}} \qquad \text{Eq. 5.2}$$

where Y is the observed turnover rate and Y_{max} and Y_{min} are the maximal and minimal turnover rates at high and low pH, respectively.

5.16.6 Anaerobic UV-visible spectroscopy

The anaerobic spectral studies were conducted as described in section 2.10.9.

5.16.7 Aerobic UV-visible spectroscopy

Aerobic UV-visible spectral assays were performed on a Perkin Elmer Lambda 25 spectrophotometer at 25 °C. The 1 mL reaction contained 15 μM apoOAM, 15 μM PLP or N-MePLP, and 15 μM AdoCbl in 100 mM NH_4^+EPPS, pH 8.5. The reaction was initiated with the addition of 2.5 mM D-ornithine or 2.5 mM DL-2,4-diaminobutyric acid, and the spectra were recorded every minute for 30 to 60 minutes. UV-visible spectral studies with the PLP-bound form of the enzyme contained 15 μM apoOAM and 15 μM PLP or N-MePLP in 100 mM NH_4^+EPPS, pH 8.5 in 1 mL. The spectra of PLP-bound OAM was recorded from 700 to 300 nm before and 5 minutes after the addition of 2.5 mM D-ornithine or DL-2,4-diaminobutyric acid.

5.16.8 PLP and N-MePLP equilibrium binding assays

Fluorescence spectroscopy was used to determine the equilibrium dissociation constants for PLP and N-MePLP. The assays were performed on a Perkin Elmer LS45 fluorescence spectrometer with excitation and emission slit widths of 10.0 nm. The temperature was maintained at 25 °C with a PTP-1 temperature control circulating water bath. PLP or N-MePLP was sequentially added to a fluorescence cuvette containing 0.268 μM apoOAM, achieving PLP or N-MePLP concentrations ranging from 5–2000 nM. The titration was carried out in 100 mM NH_4^+EPPS buffer, pH 8.5. After each addition of cofactor, the mixture was allowed to stir and incubate for 15 minutes at 25 °C. The tryptophan residues of the enzyme were excited at 280 nm and fluorescence emission was detected between 300 and 450 nm. Note that no fluorescence signal was detected in this range from the PLP cofactor in the absence of enzyme. Five scans (600 nm/min) at each concentration of cofactor were averaged. The change in the fluorescence emission at 340 nm was fitted to the quadratic binding isotherm (Eq 5.3).

$$\Delta F = \left(\frac{\Delta F_{\max}}{2E_o}\right)\left\{E_o + L_o + K_d - \left[\left(E_o + L_o + K_d\right)^2 - 4E_oL_o\right]^{1/2}\right\} \qquad \text{Eq. 5.3}$$

where L_o is total AdoCbl concentration; E_o is total enzyme concentration; ΔF is the change in fluorescence, ΔF_{max} is the maximum change in fluorescence emission; and K_d is the dissociation constant for the cofactor-OAM complex.

Chapter 6 : Conclusion

Understanding how enzymes control the generation, stability, and trajectory of high-energy radical intermediates is of fundamental importance and will certainly aid in their development as biocatalysts. Here, using adenosylcobalamin- and pyridoxal 5'-phosphate-dependent ornithine 4,5-aminomutase as a model system, we have made several advances toward this end. Through comparisons between ornithine 4,5-aminomutase and its structural homologue lysine 5,6-aminomutase, we have shown that fewer and weaker substrate binding interactions likely contribute to the increased substrate promiscuity of 5,6-LAM. However, the ability of 5,6-LAM to accept multiple substrates leads to an increased susceptibility of the enzyme to uncontrolled radical side reactions, which ultimately lead to its rapid rate of inactivation. The OAM active site exhibits tighter substrate binding interactions and thereby limits its substrate preferences to just D-ornithine. As such, OAM is less susceptible to inactivation than 5,6-LAM.

A long outstanding question in bioinorganic chemistry has been the mechanism by which AdoCbl-dependent enzymes are able to activate the Co–C bond to such a great extent ($10^{12\pm1}$-fold) within the active site. Recent computational studies have indicated that this catalytic effect may be due to electrostatic stabilization of the transition state during the bond-breaking process. In Chapter 3 we were able to identify a conserved glutamate residue within the class I mutases and the class III aminomutases that forms electrostatic contact with the hydroxyl groups of the adenosyl ribose moiety only once substrate binds to the enzyme. Through mutagenesis studies we highlighted the importance of this electrostatic interaction to substrate-induced homolysis of the Co–C bond. Specifically, the single glutamate residue potentially accounts for half of the observed decrease in activation energy achieved upon binding of the cofactor to the enzyme. Moreover, this mechanism for Co–C bond activation appears to be conserved in both the class I mutases and the class III aminomutases. Displacement of the residue from the ribose moiety in the resting state affords these enzymes additional control over the timing of radical generation and thereby safeguards them against spurious radical generation and enzyme inactivation in the absence of substrate.

A feature that distinguishes the class III aminomutases from the class I mutases is the requirement of pyridoxal 5'-phosphate to facilitate the radical 1,2-rearrangement. We have shown that an important consequence of this additional cofactor requirement is kinetic gating of the Co–C bond homolysis step by the preceding (and slower) formation of the external aldimine species. As such, not only is Co–C bond homolysis coupled to hydrogen atom abstraction but it is also coupled to transimination, and therefore mutations that affect the rate of transimination in OAM also result in slower rates of homolysis of the Co–C bond. Thus, it will be important to know which steps in the catalytic mechanism are coupled when trying to modify the functional behaviour of a radical-based enzyme.

Recent computational and experimental studies have revealed the importance of ionizable groups of the PLP cofactor (i.e. phenolic oxygen, imino nitrogen, and pyridine nitrogen) in the mechanisms of traditional PLP-dependent enzymes. Through mutagenesis and the use of a PLP cofactor analogue, we have demonstrated that partial proton transfer mediated by residues proximal to the PLP cofactor plays an essential role in lowering the activation energy barrier to isomerization in OAM. Specifically, His225 acts as a general base to the phenolic oxygen, thus lowering the pK_a of the imino nitrogen to promote its existence in a deprotonated state. Similarly, Ser162 likely serves as a partial proton donor to the pyridine nitrogen thereby stabilizing formation of the azacyclopropylcarbinyl radical intermediate. Knowledge of how the various ionizable groups of PLP contribute to the stabilization of radical intermediates could lead to the development of PLP analogues that are able to trap the proposed radical intermediates, to lend support for the catalytic mechanism. These PLP analogues may also lead to optimized activity of radical enzymes.

Taken together, the research described herein constitutes a stepping-stone towards the development of radical-based enzymes as biocatalysts. Expanding our knowledge of enzyme-driven radical chemistry is more important than ever due to the rapid increase in the number of radical enzymes shown to exist in recent years. The diversity and complexity of the reactions carried out by the handful of these enzymes that have thus far been characterized truly is remarkable. Harnessing the catalytic power of these enzymes would certainly open many doors in the areas of pharmaceutical, agrochemical, and specialty chemical production.

One of the long-term goals of this research is to develop ornithine 4,5-aminomutase as a biocatalyst. OAM has the potential to produce chiral diamines and β-amino acids, which

are used as precursors in synthetic chemistry. However, preliminary attempts to increase the substrate promiscuity of OAM were deleterious to enzyme activity, suggesting that OAM may not be an easy target for development as a biocatalyst using rational design. Instead, techniques such as directed evolution combined with protein immobilization might prove to be more successful in re-engineering OAM to accept different substrates. Future work should also investigate whether the substrate specificity of structural homologue 5,6-LAM can be increased, such that it accepts fewer substrates, and whether this results in more controlled radical chemistry. If this is the case, the correlation between substrate specificity and controlled radical chemistry will be an important factor to consider when tailoring radical enzymes for biocatalytic purposes.

References

1. Turner, N. J. (2009) Directed evolution drives the next generation of biocatalysts, *Nature chemical biology 5*, 567-573.
2. Turner, N. J. (2011) Ammonia lyases and aminomutases as biocatalysts for the synthesis of alpha-amino and beta-amino acids, *Current Opinion in Chemical Biology 15*, 234-240.
3. Weiner, B., Szymanski, W., Janssen, D. B., Minnaard, A. J., and Feringa, B. L. (2010) Recent advances in the catalytic asymmetric synthesis of beta-amino acids, *Chemical Society Reviews 39*, 1656-1691.
4. Donato, L., Figoli, A., and Drioli, E. (2005) Novel composite poly(4-vinylpyridine)/polypropylene membranes with recognition properties for (S)-naproxen, *Journal of Pharmaceutical and Biomedical Analysis 37*, 1003-1008.
5. Abrahamson, M. J., Vazquez-Figueroa, E., Woodall, N. B., Moore, J. C., and Bommarius, A. S. (2012) Development of an amine dehydrogenase for synthesis of chiral amines, *Angewandte Chemie 51*, 3969-3972.
6. Chowdari, N. S., Ahmad, M., Albertshofer, K., Tanaka, F., and Barbas, C. F., 3rd. (2006) Expedient synthesis of chiral 1,2- and 1,4-diamines: protecting group dependent regioselectivity in direct organocatalytic asymmetric Mannich reactions, *Organic Letters 8*, 2839-2842.
7. Bornscheuer, U. T., Huisman, G. W., Kazlauskas, R. J., Lutz, S., Moore, J. C., and Robins, K. (2012) Engineering the third wave of biocatalysis, *Nature 485*, 185-194.
8. Savile, C. K., Janey, J. M., Mundorff, E. C., Moore, J. C., Tam, S., Jarvis, W. R., Colbeck, J. C., Krebber, A., Fleitz, F. J., Brands, J., Devine, P. N., Huisman, G. W., and Hughes, G. J. (2010) Biocatalytic asymmetric synthesis of chiral amines from ketones applied to sitagliptin manufacture, *Science 329*, 305-309.
9. Nestl, B. M., Nebel, B. A., and Hauer, B. (2011) Recent progress in industrial biocatalysis, *Current Opinion in Chemical Biology 15*, 187-193.
10. Frey, P. A., Hegeman, A. D., and Ruzicka, F. J. (2008) The Radical SAM Superfamily, *Critical Reviews in Biochemistry and Molecular Biology 43*, 63-88.

11. Sofia, H. J., Chen, G., Hetzler, B. G., Reyes-Spindola, J. F., and Miller, N. E. (2001) Radical SAM, a novel protein superfamily linking unresolved steps in familiar biosynthetic pathways with radical mechanisms: functional characterization using new analysis and information visualization methods, *Nucleic Acids Research 29*, 1097-1106.
12. Ehrenber.A, and Reichard, P. (1972) Electron-Spin Resonance of Iron-Containing Protein-B2 from Ribonucleotide Reductase, *Journal of Biological Chemistry 247*, 3485-3488.
13. Atkin, C. L., Thelander, L., Reichard, P., and Lang, G. (1973) Iron and free radical in ribonucleotide reductase. Exchange of iron and Mossbauer spectroscopy of the protein B2 subunit of the Escherichia coli enzyme, *Journal of Biological Chemistry 248*, 7464-7472.
14. Reichard, P., and Ehrenberg, A. (1983) Ribonucleotide Reductase - a Radical Enzyme, *Science 221*, 514-519.
15. Nordlund, P., Sjoberg, B. M., and Eklund, H. (1990) 3-Dimensional Structure of the Free-Radical Protein of Ribonucleotide Reductase, *Nature 345*, 593-598.
16. Voegtli, W. C., Sommerhalter, M., Saleh, L., Baldwin, J., Bollinger, J. M., and Rosenzweig, A. C. (2003) Variable coordination geometries at the diiron(II) active site of ribonucleotide reductase R2, *Journal of the American Chemical Society 125*, 15822-15830.
17. Sjoberg, B. M., Reichard, P., Graslund, A., and Ehrenberg, A. (1978) Tyrosine Free-Radical in Ribonucleotide Reductase from Escherichia-Coli, *Journal of Biological Chemistry 253*, 6863-6865.
18. Sjoberg, B. M., Reichard, P., Graslund, A., and Ehrenberg, A. (1977) Nature of Free-Radical in Ribonucleotide Reductase from Escherichia-Coli, *Journal of Biological Chemistry 252*, 536-541.
19. Larsson, A., and Sjoberg, B. M. (1986) Identification of the Stable Free-Radical Tyrosine Residue in Ribonucleotide Reductase, *EMBO Journal 5*, 2037-2040.
20. Mao, S. S., Holler, T. P., Bollinger, J. M., Jr., Yu, G. X., Johnston, M. I., and Stubbe, J. (1992) Interaction of C225SR1 mutant subunit of ribonucleotide reductase with R2 and nucleoside diphosphates: tales of a suicidal enzyme, *Biochemistry 31*, 9744-9751.

21. Uhlin, U., and Eklund, H. (1994) Structure of ribonucleotide reductase protein R1, *Nature 370*, 533-539.
22. Stubbe, J., and van Der Donk, W. A. (1998) Protein Radicals in Enzyme Catalysis, *Chemical Reviews 98*, 705-762.
23. Stubbe, J., Nocera, D. G., Yee, C. S., and Chang, M. C. (2003) Radical initiation in the class I ribonucleotide reductase: long-range proton-coupled electron transfer?, *Chemical Reviews 103*, 2167-2201.
24. Mao, S. S., Holler, T. P., Yu, G. X., Bollinger, J. M., Jr., Booker, S., Johnston, M. I., and Stubbe, J. (1992) A model for the role of multiple cysteine residues involved in ribonucleotide reduction: amazing and still confusing, *Biochemistry 31*, 9733-9743.
25. Unkrig, V., Neugebauer, F. A., and Knappe, J. (1989) The free radical of pyruvate formate-lyase. Characterization by EPR spectroscopy and involvement in catalysis as studied with the substrate-analogue hypophosphite, *European Journal of Biochemistry 184*, 723-728.
26. Fontecave, M., Eliasson, R., and Reichard, P. (1989) Oxygen-sensitive ribonucleoside triphosphate reductase is present in anaerobic Escherichia coli, *Proceedings of the National Academy of Sciences 86*, 2147-2151.
27. Eliasson, R., Fontecave, M., Jornvall, H., Krook, M., Pontis, E., and Reichard, P. (1990) The anaerobic ribonucleoside triphosphate reductase from Escherichia coli requires S-adenosylmethionine as a cofactor, *Proceedings of the National Academy of Sciences 87*, 3314-3318.
28. Mulliez, E., Fontecave, M., Gaillard, J., and Reichard, P. (1993) An iron-sulfur center and a free radical in the active anaerobic ribonucleotide reductase of Escherichia coli, *Journal of Biological Chemistry 268*, 2296-2299.
29. Sun, X., Ollagnier, S., Schmidt, P. P., Atta, M., Mulliez, E., Lepape, L., Eliasson, R., Graslund, A., Fontecave, M., Reichard, P., and Sjoberg, B. M. (1996) The free radical of the anaerobic ribonucleotide reductase from Escherichia coli is at glycine 681, *Journal of Biological Chemistry 271*, 6827-6831.
30. Sun, X., Harder, J., Krook, M., Jornvall, H., Sjoberg, B. M., and Reichard, P. (1993) A possible glycine radical in anaerobic ribonucleotide reductase from Escherichia

coli: nucleotide sequence of the cloned nrdD gene, *Proceedings of the National Academy of Sciences 90*, 577-581.

31. Licht, S., Gerfen, G. J., and Stubbe, J. (1996) Thiyl radicals in ribonucleotide reductases, *Science 271*, 477-481.
32. Booker, S., Licht, S., Broderick, J., and Stubbe, J. (1994) Coenzyme B12-dependent ribonucleotide reductase: evidence for the participation of five cysteine residues in ribonucleotide reduction, *Biochemistry 33*, 12676-12685.
33. Baron, A. J., Stevens, C., Wilmot, C., Seneviratne, K. D., Blakeley, V., Dooley, D. M., Phillips, S. E., Knowles, P. F., and McPherson, M. J. (1994) Structure and mechanism of galactose oxidase. The free radical site, *Journal of Biological Chemistry 269*, 25095-25105.
34. Ito, N., Phillips, S. E., Yadav, K. D., and Knowles, P. F. (1994) Crystal structure of a free radical enzyme, galactose oxidase, *Journal of Molecular Biology 238*, 794-814.
35. Boal, A. K., Cotruvo, J. A., Jr., Stubbe, J., and Rosenzweig, A. C. (2010) Structural basis for activation of class Ib ribonucleotide reductase, *Science 329*, 1526-1530.
36. Knappe, J., Neugebauer, F. A., Blaschkowski, H. P., and Ganzler, M. (1984) Post-translational activation introduces a free radical into pyruvate formate-lyase, *Proceedings of the National Academy of Sciences 81*, 1332-1335.
37. Knappe, J., and Schmitt, T. (1976) A novel reaction of S-adenosyl-L-methionine correlated with the activation of pyruvate formate-lyase, *Biochemical and Biophysical Research Communications 71*, 1110-1117.
38. Frey, M., Rothe, M., Wagner, A. F., and Knappe, J. (1994) Adenosylmethionine-dependent synthesis of the glycyl radical in pyruvate formate-lyase by abstraction of the glycine C-2 pro-S hydrogen atom. Studies of [2H]glycine-substituted enzyme and peptides homologous to the glycine 734 site, *Journal of Biological Chemistry 269*, 12432-12437.
39. Wagner, A. F., Frey, M., Neugebauer, F. A., Schafer, W., and Knappe, J. (1992) The free radical in pyruvate formate-lyase is located on glycine-734, *Proceedings of the National Academy* of Sciences *89*, 996-1000.

40. Magnusson, O. T., Reed, G. H., and Frey, P. A. (2001) Characterization of an allylic analogue of the 5'-deoxyadenosyl radical: an intermediate in the reaction of lysine 2,3-aminomutase, *Biochemistry 40*, 7773-7782.
41. Magnusson, O. T., Reed, G. H., and Frey, P. A. (1999) Spectroscopic Evidence for the Participation of an Allylic Analogue of the 5‘-Deoxyadenosyl Radical in the Reaction of Lysine 2,3-Aminomutase, *Journal of the American Chemical Society 121*, 9764-9765.
42. Kulzer, R., Pils, T., Kappl, R., Huttermann, J., and Knappe, J. (1998) Reconstitution and characterization of the polynuclear iron-sulfur cluster in pyruvate formate-lyase-activating enzyme. Molecular properties of the holoenzyme form, *Journal of Biological Chemistry 273*, 4897-4903.
43. Krebs, C., Broderick, W. E., Henshaw, T. F., Broderick, J. B., and Huynh, B. H. (2002) Coordination of adenosylmethionine to a unique iron site of the [4Fe-4S] of pyruvate formate-lyase activating enzyme: a Mossbauer spectroscopic study, *Journal of the American Chemical Society 124*, 912-913.
44. Jarrett, J. T. (2003) The generation of 5'-deoxyadenosyl radicals by adenosylmethionine-dependent radical enzymes, *Current Opinion in Chemical Biology 7*, 174-182.
45. Hodgkin, D. C., Kamper, J., Mackay, M., Pickworth, J., Trueblood, K. N., and White, J. G. (1956) Structure of vitamin B12, *Nature 178*, 64-66.
46. Randaccio, L., Geremia, S., and Wuerges, J. (2007) Crystallography of vitamin B12 proteins, *Journal of Organometallic Chemistry 692*, 1198-1215.
47. Banerjee, R., and Ragsdale, S. W. (2003) The many faces of vitamin B12: catalysis by cobalamin-dependent enzymes, *Annual Review of Biochemistry 72*, 209-247.
48. Padovani, D., and Banerjee, R. (2009) Coenzyme B12-Catalyzed Radical Isomerizations, In *Tetrapyrroles*, pp 330-342, Springer New York.
49. Jensen, K. P., and Ryde, U. (2009) Cobalamins uncovered by modern electronic structure calculations, *Coordination Chemistry Reviews 253*, 769-778.
50. Sandala, G. M., Smith, D. M., and Radow, L. (2010) Modeling the Reactions Catalyzed by Coenzyme B-12-Dependent Enzymes, *Accounts of Chemical Research 43*, 642-651.

51. Banerjee, R. (2003) Radical carbon skeleton rearrangements: catalysis by coenzyme B12-dependent mutases, *Chemical Reviews 103*, 2083-2094.
52. Gruber, K., and Kratky, C. (2002) Coenzyme B(12) dependent glutamate mutase, *Current Opinion in Chemical Biology 6*, 598-603.
53. Schwartz, P. A., and Frey, P. A. (2007) Dioldehydrase: an essential role for potassium ion in the homolytic cleavage of the cobalt-carbon bond in adenosylcobalamin, *Biochemistry 46*, 7293-7301.
54. Jensen, K. P., and Ryde, U. (2005) How the Co-C bond is cleaved in coenzyme B12 enzymes: a theoretical study, *Journal of the American Chemical Society 127*, 9117-9128.
55. Padmakumar, R., Taoka, S., Padmakumar, R., and Banerjee, R. (1995) Coenzyme B12 Is Coordinated by Histidine and Not Dimethylbenzimidazole on Methylmalonyl-CoA Mutase, *Journal of the American Chemical Society 117*, 7033-7034.
56. Zelder, O., Beatrix, B., Kroll, F., and Buckel, W. (1995) Coordination of a histidine residue of the protein-component S to the cobalt atom in coenzyme B12-dependent glutamate mutase from Clostridium cochlearium, *FEBS Letters 369*, 252-254.
57. Chang, C. H., and Frey, P. A. (2000) Cloning, sequencing, heterologous expression, purification, and characterization of adenosylcobalamin-dependent D-lysine 5,6-aminomutase from Clostridium sticklandii, *Journal of Biological Chemistry 275*, 106-114.
58. Yamanishi, M., Yamada, S., Muguruma, H., Murakami, Y., Tobimatsu, T., Ishida, A., Yamauchi, J., and Toraya, T. (1998) Evidence for axial coordination of 5,6-dimethylbenzimidazole to the cobalt atom of adenosylcobalamin bound to diol dehydratase, *Biochemistry 37*, 4799-4803.
59. Makins, C., Pickering, A. V., Mariani, C., and Wolthers, K. R. (2013) Mutagenesis of a conserved glutamate reveals the contribution of electrostatic energy to adenosylcobalamin co-C bond homolysis in ornithine 4,5-aminomutase and methylmalonyl-CoA mutase, *Biochemistry 52*, 878-888.
60. Sharma, P. K., Chu, Z. T., Olsson, M. H., and Warshel, A. (2007) A new paradigm for electrostatic catalysis of radical reactions in vitamin B12 enzymes, *Proceedings of the National Academy of Sciences 104*, 9661-9666.

61. Durbeej, B., Sandala, G. M., Bucher, D., Smith, D. M., and Radom, L. (2009) On the importance of ribose orientation in the substrate activation of the coenzyme B12-dependent mutases, *Chemistry 15*, 8578-8585.
62. Marsh, E. N. G., and Melendez, G. D. R. (2012) Adenosylcobalamin enzymes: Theory and experiment begin to converge, *Biochimica et Biophysica Acta-Proteins and Proteomics 1824*, 1154-1164.
63. Hay, B. P., and Finke, R. G. (1986) Thermolysis of the Co-C Bond of Adenosylcobalamin .2. Products, Kinetics, and Co-C Bond-Dissociation Energy in Aqueous-Solution, *Journal of the American Chemical Society 108*, 4820-4829.
64. Wolthers, K. R., Rigby, S. E., and Scrutton, N. S. (2008) Mechanism of radical-based catalysis in the reaction catalyzed by adenosylcobalamin-dependent ornithine 4,5-aminomutase, *Journal of Biological Chemistry 283*, 34615-34625.
65. Padmakumar, R., Padmakumar, R., and Banerjee, R. (1997) Evidence that cobalt-carbon bond homolysis is coupled to hydrogen atom abstraction from substrate in methylmalonyl-CoA mutase, *Biochemistry 36*, 3713-3718.
66. Marsh, E. N., and Ballou, D. P. (1998) Coupling of cobalt-carbon bond homolysis and hydrogen atom abstraction in adenosylcobalamin-dependent glutamate mutase, *Biochemistry 37*, 11864-11872.
67. Padmakumar, R., and Banerjee, R. (1997) Evidence that cobalt-carbon bond homolysis is coupled to hydrogen atom abstraction from substrate in methylmalonyl-CoA mutase, *Biochemistry 36*, 3713-3718.
68. Bucher, D., Sandala, G. M., Durbeej, B., Radom, L., and Smith, D. M. (2012) The Elusive 5'-Deoxyadenosyl Radical in Coenzyme-B(12)-Mediated Reactions, *Journal of the American Chemical Society 34*, 1591-1599.
69. Kozlowski, P. M., Kamachi, T., Toraya, T., and Yoshizawa, K. (2007) Does Cob(II)alamin act as a conductor in coenzyme B12 dependent mutases?, *Angewandte Chemie 46*, 980-983.
70. Finke, R. G., and Martin, B. D. (1990) Coenzyme AdoB12 vs AdoB12.-homolytic Co-C cleavage following electron transfer: a rate enhancement greater than or equal to 10(12), *Journal of Inorganic Biochemistry 40*, 19-22.

71. Toraya, T. (2003) Radical catalysis in coenzyme B12-dependent isomerization (eliminating) reactions, *Chemical Reviews 103*, 2095-2127.

72. Halpern, J. (1985) Mechanisms of coenzyme B12-dependent rearrangements, *Science 227*, 869-875.

73. Dong, S. L., Padmakumar, R., Banerjee, R., and Spiro, T. G. (1999) Co-C bond activation in B-12-dependent enzymes: Cryogenic resonance Raman studies of methylmalonyl-coenzyme A mutase, *Journal of the American Chemical Society 121*, 7063-7070.

74. Huhta, M. S., Chen, H. P., Hemann, C., Hille, C. R., and Marsh, E. N. (2001) Protein-coenzyme interactions in adenosylcobalamin-dependent glutamate mutase, *Biochemical Journal 355*, 131-137.

75. Berkovitch, F., Behshad, E., Tang, K. H., Enns, E. A., Frey, P. A., and Drennan, C. L. (2004) A locking mechanism preventing radical damage in the absence of substrate, as revealed by the x-ray structure of lysine 5,6-aminomutase, *Proceedings of the National Acadamy of Sciences 101*, 15870-15875.

76. Wolthers, K. R., Levy, C., Scrutton, N. S., and Leys, D. (2010) Large-scale domain dynamics and adenosylcobalamin reorientation orchestrate radical catalysis in ornithine 4,5-aminomutase, *Journal of Biological Chemistry 285*, 13942-13950.

77. Mancia, F., Keep, N. H., Nakagawa, A., Leadlay, P. F., McSweeney, S., Rasmussen, B., Bosecke, P., Diat, O., and Evans, P. R. (1996) How coenzyme B12 radicals are generated: the crystal structure of methylmalonyl-coenzyme A mutase at 2 A resolution, *Structure 4*, 339-350.

78. Reitzer, R., Gruber, K., Jogl, G., Wagner, U. G., Bothe, H., Buckel, W., and Kratky, C. (1999) Glutamate mutase from Clostridium cochlearium: the structure of a coenzyme B12-dependent enzyme provides new mechanistic insights, *Structure 7*, 891-902.

79. Shibata, N., Nakanishi, Y., Fukuoka, M., Yamanishi, M., Yasuoka, N., and Toraya, T. (2003) Structural rationalization for the lack of stereospecificity in coenzyme B12-dependent diol dehydratase, *Journal of Biological Chemistry 278*, 22717-22725.

80. Abend, A., Bandarian, V., Reed, G. H., and Frey, P. A. (2000) Identification of cis-ethanesemidione as the organic radical derived from glycolaldehyde in the suicide

inactivation of dioldehydrase and of ethanolamine ammonia-lyase, *Biochemistry 39*, 6250-6257.

81. Masuda, J., Shibata, N., Morimoto, Y., Toraya, T., and Yasuoka, N. (2000) How a protein generates a catalytic radical from coenzyme B(12): X-ray structure of a diol-dehydratase-adeninylpentylcobalamin complex, *Structure 8*, 775-788.
82. Smith, D. M., Golding, B. T., and Radom, L. (2001) Understanding the mechanism of B(12)-dependent diol dehydratase: a synergistic retro-push--pull proposal, *Journal of the American Chemical Society 123*, 1664-1675.
83. Gruber, K., Reitzer, R., and Kratky, C. (2001) Radical Shuttling in a Protein: Ribose Pseudorotation Controls Alkyl-Radical Transfer in the Coenzyme B(12) Dependent Enzyme Glutamate Mutase, *Angewandte Chemie 40*, 3377-3380.
84. Chih, H.-W., and Marsh, E. N. G. (2000) Mechanism of Glutamate Mutase: Identification and Kinetic Competence of Acrylate and Glycyl Radical as Intermediates in the Rearrangement of Glutamate to Methylaspartate, *Journal of the American Chemical Society 122*, 10732-10733.
85. Wetmore, S. D., Smith, D. M., Golding, B. T., and Radom, L. (2001) Interconversion of (S)-glutamate and (2S,3S)-3-methylaspartate: a distinctive B(12)-dependent carbon-skeleton rearrangement, *Journal of the American Chemical Society 123*, 7963-7972.
86. Fonknechten, N., Chaussonnerie, S., Tricot, S., Lajus, A., Andreesen, J. R., Perchat, N., Pelletier, E., Gouyvenoux, M., Barbe, V., Salanoubat, M., Le Paslier, D., Weissenbach, J., Cohen, G. N., and Kreimeyer, A. (2010) Clostridium sticklandii, a specialist in amino acid degradation:revisiting its metabolism through its genome sequence, *BMC Genomics 11*, 555.
87. Baker, J. J., Vanderdr.C, and Stadtman, T. C. (1973) Purification and Properties of Beta-Lysine Mutase, a Pyridoxal-Phosphate and B-12 Coenzyme Dependent Enzyme, *Biochemistry 12*, 1054-1063.
88. Chang, C. H., and Frey, P. A. (2000) Cloning, sequencing, heterologous expression, purification, and characterization of adenosylcobalamin-dependent D-lysine 5, 6-aminomutase from Clostridium sticklandii, *Journal of Biological Chemistry 275*, 106-114.

89. Chen, H. P., Wu, S. H., Lin, Y. L., Chen, C. M., and Tsay, S. S. (2001) Cloning, sequencing, heterologous expression, purification, and characterization of adenosylcobalamin-dependent D-ornithine aminomutase from Clostridium sticklandii, *Journal of Biological Chemistry 276*, 44744-44750.

90. Dowling, D. P., Croft, A. K., and Drennan, C. L. (2012) Radical Use of Rossmann and TIM Barrel Architectures for Controlling Coenzyme B-12 Chemistry, *Annual Review of Biophysics 41*, 403-427.

91. Maity, A. N., Hsieh, C. P., Huang, M. H., Chen, Y. H., Tang, K. H., Behshad, E., Frey, P. A., and Ke, S. C. (2009) Evidence for conformational movement and radical mechanism in the reaction of 4-thia-L-lysine with lysine 5,6-aminomutase, *Journal of Physical Chemistry B 113*, 12161-12163.

92. Ballinger, M. D., Frey, P. A., and Reed, G. H. (1992) Structure of a substrate radical intermediate in the reaction of lysine 2,3-aminomutase, *Biochemistry 31*, 10782-10789.

93. Ballinger, M. D., Frey, P. A., Reed, G. H., and LoBrutto, R. (1995) Pulsed electron paramagnetic resonance studies of the lysine 2,3-aminomutase substrate radical: evidence for participation of pyridoxal 5'-phosphate in a radical rearrangement, *Biochemistry 34*, 10086-10093.

94. Wu, W., Lieder, K. W., Reed, G. H., and Frey, P. A. (1995) Observation of a second substrate radical intermediate in the reaction of lysine 2,3-aminomutase: a radical centered on the beta-carbon of the alternative substrate, 4-thia-L-lysine, *Biochemistry 34*, 10532-10537.

95. Miller, J., Bandarian, V., Reed, G. H., and Frey, P. A. (2001) Inhibition of lysine 2,3-aminomutase by the alternative substrate 4-thialysine and characterization of the 4-thialysyl radical intermediate, *Archives of Biochemistry and Biophysics 387*, 281-288.

96. Wetmore, S. D., Smith, D. M., and Radom, L. (2001) Enzyme catalysis of 1,2-amino shifts: the cooperative action of B6, B12, and aminomutases, *Journal of the American Chemical Society 123*, 8678-8689.

97. Tang, K. H., Mansoorabadi, S. O., Reed, G. H., and Frey, P. A. (2009) Radical Triplets and Suicide Inhibition in Reactions of 4-Thia-D- and 4-Thia-L-lysine with Lysine 5,6-Aminomutase, *Biochemistry 48*, 8151-8160.

98. Griswold, W. R., and Toney, M. D. (2011) Role of the pyridine nitrogen in pyridoxal 5'-phosphate catalysis: activity of three classes of PLP enzymes reconstituted with deazapyridoxal 5'-phosphate, *Journal of the American Chemical Society 133*, 14823-14830.

99. Lin, Y. L., and Gao, J. L. (2010) Internal Proton Transfer in the External Pyridoxal 5'-Phosphate Schiff Base in Dopa Decarboxylase, *Biochemistry 49*, 84-94.

100. Tang, K. H., Casarez, A. D., Wu, W., and Frey, P. A. (2003) Kinetic and biochemical analysis of the mechanism of action of lysine 5,6-aminomutase, *Archives of Biochemistry and Biophysics 418*, 49-54.

101. Tang, K. H., Chang, C. H., and Frey, P. A. (2001) Electron transfer in the substrate-dependent suicide inactivation of lysine 5,6-aminomutase, *Biochemistry 40*, 5190-5199.

102. Chen, Y. H., Maity, A. N., Frey, P. A., and Ke, S. C. (2013) Mechanism-based Inhibition Reveals Transitions between Two Conformational States in the Action of Lysine 5,6-Aminomutase: A Combination of Electron Paramagnetic Resonance Spectroscopy, Electron Nuclear Double Resonance Spectroscopy, and Density Functional Theory Study, *Journal of the American Chemical Society 135*, 788-794.

103. Fonknechten, N., Perret, A., Perchat, N., Tricot, S., Lechaplais, C., Vallenet, D., Vergne, C., Zaparucha, A., Le Paslier, D., Weissenbach, J., and Salanoubat, M. (2009) A Conserved Gene Cluster Rules Anaerobic Oxidative Degradation of L-Ornithine, *Journal of Bacteriology 191*, 3162-3167.

104. Bothe, H., Darley, D. J., Albracht, S. P., Gerfen, G. J., Golding, B. T., and Buckel, W. (1998) Identification of the 4-glutamyl radical as an intermediate in the carbon skeleton rearrangement catalyzed by coenzyme B12-dependent glutamate mutase from Clostridium cochlearium, *Biochemistry 37*, 4105-4113.

105. Jones, A. R., Hay, S., Woodward, J. R., and Scrutton, N. S. (2007) Magnetic field effect studies indicate reduced geminate recombination of the radical pair in substrate-bound adenosylcobalamin-dependent ethanolamine ammonia lyase, *Journal of the American Chemical Society 129*, 15718-15727.

106. Cheng, M. C., and Marsh, E. N. (2005) Isotope effects for deuterium transfer between substrate and coenzyme in adenosylcobalamin-dependent glutamate mutase, *Biochemistry 44*, 2686-2691.

107. Yoon, M., Kalli, A., Lee, H. Y., Hakansson, K., and Marsh, E. N. (2007) Intrinsic deuterium kinetic isotope effects in glutamate mutase measured by an intramolecular competition experiment, *Angewandte Chemie 46*, 8455-8459.

108. Makins, C., Miros, F. N., Scrutton, N. S., and Wolthers, K. R. (2011) Role of histidine 225 in adenosylcobalamin-dependent ornithine 4,5-aminomutase, *Bioorganic Chemistry 40*, 39-47.

109. Northrop, D. B. (1975) Steady-State Analysis of Kinetic Isotope-Effects in Enzymic Reactions, *Biochemistry 14*, 2644-2651.

110. Northrop, D. B. (1998) On the meaning of K-m and V/K in enzyme kinetics, *Journal of Chemical Education 75*, 1153-1157.

111. Maity, A. N., Hsieh, C. P., Huang, M. H., Chen, Y. H., Tang, K. H., Behshad, E., Frey, P. A., and Ke, S. C. (2009) Evidence for Conformational Movement and Radical Mechanism in the Reaction of 4-Thia-L-lysine with Lysine 5,6-Aminomutase, *Journal of Physical Chemistry B 113*, 12161-12163.

112. Pang, J. Y., Li, X., Morokuma, K., Scrutton, N. S., and Sutcliffe, M. J. (2012) Large-Scale Domain Conformational Change Is Coupled to the Activation of the Co-C Bond in the B-12-Dependent Enzyme Ornithine 4,5-Aminomutase: A Computational Study, *Journal of the American Chemical Society 134*, 2367-2377.

113. Mancia, F., and Evans, P. R. (1998) Conformational changes on substrate binding to methylmalonyl CoA mutase and new insights into the free radical mechanism, *Structure 6*, 711-720.

114. Froese, D. S., Kochan, G., Muniz, J. R., Wu, X., Gileadi, C., Ugochukwu, E., Krysztofinska, E., Gravel, R. A., Oppermann, U., and Yue, W. W. (2010) Structures of the human GTPase MMAA and vitamin B12-dependent methylmalonyl-CoA mutase and insight into their complex formation, *Journal of Biological Chemistry 285*, 38204-38213.

115. Taoka, S., Padmakumar, R., Lai, M. T., Liu, H. W., and Banerjee, R. (1994) Inhibition of the human methylmalonyl-CoA mutase by various CoA-esters, *Journal of Biological Chemistry 269*, 31630-31634.
116. McKie, N., Keep, N. H., Patchett, M. L., and Leadlay, P. F. (1990) Adenosylcobalamin-dependent methylmalonyl-CoA mutase from Propionibacterium shermanii. Active holoenzyme produced from Escherichia coli, *Biochemical Journal 269*, 293-298.
117. Chowdhury, S., and Banerjee, R. (1999) Role of the dimethylbenzimidazole tail in the reaction catalyzed by coenzyme B12-dependent methylmalonyl-CoA mutase, *Biochemistry 38*, 15287-15294.
118. Calafat, A. M., Taoka, S., Puckett, J. M., Jr., Semerad, C., Yan, H., Luo, L., Chen, H., Banerjee, R., and Marzilli, L. G. (1995) Structural and electronic similarity but functional difference in methylmalonyl-CoA mutase between coenzyme B12 and the analog 2',5'-dideoxyadenosylcobalamin, *Biochemistry 34*, 14125-14130.
119. Roman-Melendez, G. D., von Glehn, P., Harvey, J. N., Mulholland, A. J., and Marsh, E. N. (2014) Role of active site residues in promoting cobalt-carbon bond homolysis in adenosylcobalamin-dependent mutases revealed through experiment and computation, *Biochemistry 53*, 169-177.
120. Toraya, T., and Fukui, S. (1977) Immunochemical evidence for the difference between coenzyme-B12-dependent diol dehydratase and glycerol dehydratase, *European Journal of Biochemistry 76*, 285-289.
121. Bandarian, V., and Reed, G. H. (2002) Analysis of the electron paramagnetic resonance spectrum of a radical intermediate in the coenzyme B-12-dependent ethanolamine ammonia-lyase catalyzed reaction of S-2-aminopropanol, *Biochemistry 41*, 8580-8588.
122. Abend, A., Bandarian, V., Reed, G. H., and Frey, P. A. (2000) Identification of cis-ethanesemidione as the organic radical derived from glycolaldehyde in the suicide inactivation of dioldehydrase and of ethanolamine ammonia-lyase, *Biochemistry 39*, 6250-6257.

123. Mansoorabadi, S. O., Magnusson, O. T., Poyner, R. R., Frey, P. A., and Reed, G. H. (2006) Analysis of the cob(II)alamin-5 '-deoxy-3 ',4 '-anhydroadenosyl radical triplet spin system in the active site of diol dehydrase, *Biochemistry 45*, 14362-14370.

124. Warncke, K., and Utada, A. S. (2001) Interaction of the substrate radical and the 5 '-deoxyadenosine-5 '-methyl group in vitamin B-12 coenzyme-dependent ethanolamine deaminase, *Journal of the American Chemical Society 123*, 8564-8572.

125. Makins, C., Miros, F. N., Scrutton, N. S., and Wolthers, K. R. (2012) Role of histidine 225 in adenosylcobalamin-dependent ornithine 4,5-aminomutase, *Bioorganic Chemistry 40*, 39-47.

126. Taoka, S., Padmakumar, R., Lai, M. T., Liu, H. W., and Banerjee, R. (1994) Inhibition of the human methylmalonyl-CoA mutase by various CoA-esters, *Journal of Biological Chemistry 269*, 31630-31634.

127. Chen, Y. H., Maity, A. N., Pan, Y. C., Frey, P. A., and Ke, S. C. (2011) Radical Stabilization Is Crucial in the Mechanism of Action of Lysine 5,6-Aminomutase: Role of Tyrosine-263 alpha As Revealed by Electron Paramagnetic Resonance Spectroscopy, *Journal of the American Chemical Society 133*, 17152-17155.

128. Kumar, M., and Kozlowski, P. M. (2009) Role of tyrosine residue in the activation of Co-C bond in coenzyme B12-dependent enzymes: another case of proton-coupled electron transfer?, *Journal of Physical Chemistry. B 113*, 9050-9054.

129. Kozlowski, P. M., Kamachi, T., Kumar, M., Nakayama, T., and Yoshizawa, K. (2010) Theoretical analysis of the diradical nature of adenosylcobalamin cofactor-tyrosine complex in B12-dependent mutases: inspiring PCET-driven enzymatic catalysis, *Journal of Physical Chemistry. B 114*, 5928-5939.

130. Kozlowski, P. M., Kamachi, T., Kumar, M., and Yoshizawa, K. (2012) Initial step of B12-dependent enzymatic catalysis: energetic implications regarding involvement of the one-electron-reduced form of adenosylcobalamin cofactor, *Journal of Biological Inorganic Chemistry 17*, 293-300.

131. Kumar, N., Liu, S., and Kozlowski, P. M. (2012) Charge Separation Propensity of the Coenzyme B12–Tyrosine Complex in Adenosylcobalamin-Dependent Methylmalonyl–CoA Mutase Enzyme, *The Journal of Physical Chemistry Letters 3*, 1035-1038.

132. Toney, M. D. (2005) Reaction specificity in pyridoxal phosphate enzymes, *Archives of Biochemistry and Biophysics 433*, 279-287.

133. Yoon, M., Song, H. T., Hakansson, K., and Marsh, E. N. G. (2010) Hydrogen Tunneling in Adenosylcobalamin-Dependent Glutamate Mutase: Evidence from Intrinsic Kinetic Isotope Effects Measured by Intramolecular Competition, *Biochemistry 49*, 3168-3173.

134. Chowdhury, S., and Banerjee, R. (2000) Evidence for quantum mechanical tunneling in the coupled cobalt-carbon bond homolysis-substrate radical generation reaction catalyzed by methylmalonyl-CoA mutase, *Journal of the American Chemical Society 122*, 5417-5418.

135. Thoma, N. H., Meier, T. W., Evans, P. R., and Leadlay, P. F. (1998) Stabilization of radical intermediates by an active-site tyrosine residue in methylmalonyl-CoA mutase, *Biochemistry 37*, 14386-14393.

136. Vlasie, M. D., and Banerjee, R. (2003) Tyrosine 89 accelerates Co-carbon bond homolysis in methylmalonyl-CoA mutase, *Journal of the American Chemical Society 125*, 5431-5435.

137. Kim, M.-H., and Birke, R. L. (1983) Electrochemical reduction of methylcobalamin and 5′-deoxyadenosylcobalamin on mercury in basic medium, *Journal of Electroanalytical Chemistry and Interfacial Electrochemistry 144*, 331-350.

138. Martin, B. D., and Finke, R. G. (1992) Methylcobalamin's full- vs. "half"-strength cobalt-carbon sigma bonds and bond dissociation enthalpies: A >10(15) Co-CH3 homolysis rate enhancement following one-antibonding-electron reduction of methlycobalamin, *Journal of the American Chemical Society 114*, 585-592.

139. Vass, I., and Styring, S. (1991) pH-dependent charge equilibria between tyrosine-D and the S states in photosystem II. Estimation of relative midpoint redox potentials, *Biochemistry 30*, 830-839.

140. Mansoorabadi, S. O., Padmakumar, R., Fazliddinova, N., Vlasie, M., Banerjee, R., and Reed, G. H. (2005) Characterization of a succinyl-CoA radical-cob(II)alamin spin triplet intermediate in the reaction catalyzed by adenosylcobalamin-dependent methylmalonyl-CoA mutase, *Biochemistry 44*, 3153-3158.

141. Leutbecher, U., Albracht, S. P., and Buckel, W. (1992) Identification of a paramagnetic species as an early intermediate in the coenzyme B12-dependent glutamate mutase reaction. A cob(II)amide?, *FEBS Letters 307*, 144-146.

142. Robitaille, P. M., Scott, R. D., Wang, J., and Metzler, D. E. (1989) Schiff bases and geminal diamines derived from pyridoxal 5'-phosphate and diamines, *Journal of the American Chemical Society 111*, 3034-3040.

143. Toney, M. D. (2011) Controlling reaction specificity in pyridoxal phosphate enzymes, *Biochimica et Biophysica Acta 1814*, 1407-1418.

144. Limbach, H. H., Chan-Huot, M., Sharif, S., Tolstoy, P. M., and Toney, M. D. (2010) NMR Studies of the Stability, Protonation States, and Tautomerism of (13)C- and (15)N-Labeled Aldimines of the Coenzyme Pyridoxal 5'-Phosphate in Water, *Biochemistry 49*, 10818-10830.

145. Limbach, H. H., Chan-Huot, M., Sharif, S., Tolstoy, P. M., Shenderovich, I. G., Denisov, G. S., and Toney, M. D. (2011) Critical hydrogen bonds and protonation states of pyridoxal 5'-phosphate revealed by NMR, *Biochimica et Biophysica Acta 1814*, 1426-1437.

146. Sharif, S., Schagen, D., Toney, M. D., and Limbach, H. H. (2007) Coupling of functional hydrogen bonds in pyridoxal-5'-phosphate-enzyme model systems observed by solid-state NMR spectroscopy, *Journal of the American Chemical Society 129*, 4440-4455.

147. Chen, H. P., Hsui, F. C., Lin, L. Y., Ren, C. T., and Wu, S. H. (2004) Coexpression, purification and characterization of the E and S subunits of coenzyme B(12) and B(6) dependent Clostridium sticklandii D-ornithine aminomutase in Escherichia coli, *European Journal of Biochemistry 271*, 4293-4297.

148. Casasnovas, R., Salva, A., Frau, J., Donoso, J., and Munoz, F. (2009) Theoretical study on the distribution of atomic charges in the Schiff bases of 3-hydroxypyridine-4-aldehyde and alanine. The effect of the protonation state of the pyridine and imine nitrogen atoms, *Chemical Physics 355*, 149-156.

149. Shiraiwa, Y., Ikushiro, H., and Hayashi, H. (2009) Multifunctional Role of His(159) in the Catalytic Reaction of Serine Palmitoyltransferase, *Journal of Biological Chemistry 284*, 15487-15495.

150. Limbach, H. H., Chan-Huot, M., Niether, C., Sharif, S., Tolstoy, P. M., and Toney, M. D. (2010) NMR studies of the protonation states of pyridoxal-5'-phosphate in water, *Journal of Molecular Structure 976*, 282-289.

151. Sharif, S., Denisov, G. S., Toney, M. D., and Limbach, H. H. (2007) NMR studies of coupled low- and high-barrier hydrogen bonds in pyridoxal-5'-phosphate model systems in polar solution, *Journal of the American Chemical Society 129*, 6313-6327.

152. Smith, D. M., Golding, B. T., and Radom, L. (1999) Facilitation of enzyme-catalyzed reactions by partial proton transfer: Application to coenzyme-B-12-dependent methylmalonyl-CoA mutase, *Journal of the American Chemical Society 121*, 1383-1384.

153. Smith, D. M., Golding, B. T., and Radom, L. (1999) Understanding the mechanism of B-12-dependent methylmalonyl-CoA mutase: Partial proton transfer in action, *Journal of the American Chemical Society 121*, 9388-9399.

154. Pfeuffer, T., Helmreic.E, and Ehrlich, J. (1972) Role of Pyridoxal 5'-Phosphate in Glycogen-Phosphorylase .1. Synthesis of 3'-O-Methylpyridoxal 5'-Phosphate N-Oxide and Pyridoxal 5'-Phosphate Monomethyl Ester and Conversion of N-Oxide to Pyridoxal 5'-Phosphate by Apophosphorylase B from Rabbit Skeletal-Muscle, *Biochemistry 11*, 2125-2136.